2e(mix)

THE NIMBUS 5 USER'S GUIDE

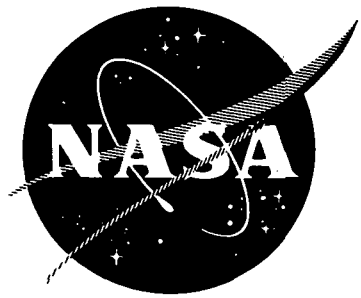

PRICES SUBJECT TO CHANGE

GODDARD SPACE FLIGHT CENTER

GREENBELT, MARYLAND

THE NIMBUS 5 USER'S GUIDE

Prepared By

The ERTS/Nimbus Project
Goddard Space Flight Center
National Aeronautics and Space Administration

Edited By

Romeo R. Sabatini
Allied Research Associates, Inc.
Baltimore, Maryland

November, 1972

THE NIMBUS 5 USER'S GUIDE

FOREWORD

This document has been prepared to provide potential data users with background information on the Nimbus 5 spacecraft and experiments as a basis for selecting, obtaining and utilizing Nimbus 5 data in research studies.

The basic spacecraft system operation and the objectives of the Nimbus 5 flight are outlined, followed by a detailed discussion of each of the experiments. The format, archiving, and access to the data are also described. Finally, the contents and format of the Nimbus 5 Data Catalogs are described. These catalogs will be issued periodically. They will contain THIR pictorial data obtained during each period as well as information on the collection and availability of all Nimbus 5 data.

The individual sections on the meteorological experiments were prepared by the respective experimenters. The assembly and editing of this publication was accomplished by Allied Research Associates, Inc. (ARA), under Contract No. NAS 5-21617 with the Goddard Space Flight Center, NASA, Greenbelt, Maryland.

Stanley Weiland
ERTS/Nimbus Project Manager
Goddard Space Flight Center

TABLE OF CONTENTS

TABLE OF CONTENTS (Continued)

TABLE OF CONTENTS (Continued)

TABLE OF CONTENTS (Continued)

LIST OF FIGURES

LIST OF FIGURES (Continued)

LIST OF FIGURES (Continued)

LIST OF TABLES

SECTION 1

THE NIMBUS 5 SPACECRAFT SYSTEM

by
Staff Members, ERTS/Nimbus Project
National Aeronautics and Space Administration
Goddard Space Flight Center

The purpose of this section is to outline the component subsystems of the Nimbus 5 spacecraft (Figure 1-1) and the objectives of the Nimbus 5 flight.

1.1 The Nimbus 5 Objectives

The Nimbus 5 mission has two major objectives:

- Fulfill the central role in meeting the expanding objectives of NASA's meteorological program
- Initiate satellite studies in the applications areas, particularly the development of advanced sensors for the exploration of natural resources and geophysical phenomena

The meteorological program calls for the application of space technology to increase understanding of the atmosphere and efficiency in making global meteorological observations. The Nimbus 5 mission will provide a versatile orbital platform for a variety of meteorological experiments to accomplish two balanced objectives:

- To observe atmospheric conditions and processes whose bearing on weather prediction is not yet fully understood
- To develop techniques for measuring, on a global scale, those parameters required for the mathematical modeling of the atmospheric circulation

The Nimbus 5 mission affords an opportunity to sound the atmosphere with advanced techniques, extending and refining the capability for sounding and atmospheric structure measurement first demonstrated on Nimbus 3 and 4. In addition, new techniques involving microwave radiometry will explore the capability for sounding through clouds. The Nimbus 5 mission will provide an

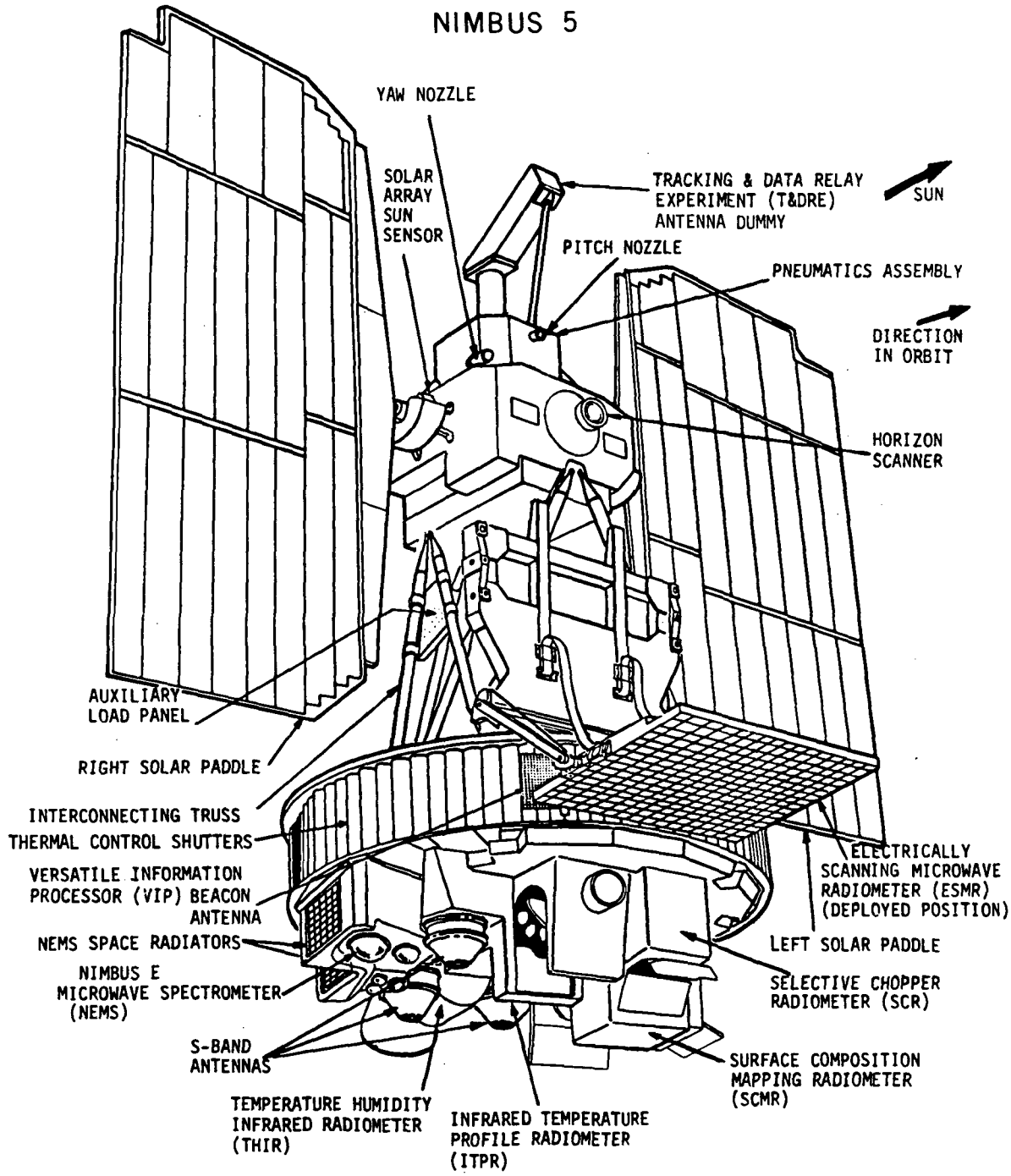

Figure 1-1. Nimbus 5 Spacecraft.

opportunity to assess instrument operation in the space environment and to collect a sizable body of data with the global and seasonal coverage needed for support of meteorological experiments.

As part of the Global Atmospheric Research Program (GARP), a number of large-scale meteorological experiments employing conventional (ground-based and balloon) observation platforms are now planned for the period when Nimbus 5 will be operating. Observations of clouds, moisture patterns, and vertical temperature structure of the atmosphere from Nimbus 5 will be used by NOAA and Goddard Institute for Space Studies (GISS) in the GARP Data System Test.

The Nimbus 5 experiments are listed in Table 1-1.

1.2 Orbit

The Nimbus 5 orbit was selected to satisfy the diverse experiment, power, and data retrieval requirements. Nimbus 5 is intended to be placed in an orbit which is circular at 1112 kilometers (600 nautical miles), sun-synchronous, having a local noon (ascending) and midnight (descending) equator crossing, and an 81 degree retrograde inclination. Successive orbits cross the equator at 27 degrees of longitude separation. The period for this orbit is about 107 minutes. Nimbus 5 is scheduled to be launched in the fourth quarter of 1972 from the Western Test Range in California. The launch vehicle is a Delta 0900.

1.3 Spacecraft Attitude

Attitude stabilization for the Nimbus 5 is provided by the same improved attitude control system flown on Nimbus 4, and developed from the attitude system successfully utilized on previous Nimbus spacecraft. The primary functions of the attitude control system are to stabilize the spacecraft with respect to the earth and orbital plane, with the yaw axis pointing normal to the earth and the roll axis aligned with the spacecraft velocity vector, and to orient the solar paddles with respect to the sun (see Figure 1-2). The improved attitude control system of Nimbus 5 will permit fine control of ±1 degree in pitch and ±0.5 degree in roll and yaw.

1.4 Spacecraft Data Systems

The spacecraft data are stored and transmitted via three data systems on the spacecraft:

Table 1-1
Nimbus 5 Experiments

Experiment	Spectral Bands	Main Purpose	Experimenter
Temperature Humidity Infrared Radiometer (THIR)	10.5-12.5 μm 6.5-7.0 μm	Daytime and nighttime surface and cloud top temperatures Cloud mapping Atmospheric water vapor mapping	A. Mc Culloch, NASA/GSFC Greenbelt, Maryland 20771
Surface Composition Mapping Radiometer (SCMR)	8.3-9.3 μm 10.2-11.2 μm 0.8-1.1 μm	Distinguish acidic from basic rocks Map surface temperatures Map surface features	W. Hovis, NASA/GSFC Greenbelt, Maryland 20771
Electrically scanning Microwave Radiometer (ESMR)	19.225-19.475 GHz	Map surface features even in the presence of clouds Map distribution of polar ice Map precipitating clouds over ocean areas	T. Wilheit, NASA/GSFC Greenbelt, Maryland 20771
Infrared Temperature Profile Radiometer (ITPR)	3.8 μm 11 μm 15 μm (4 bands) 20 μm	Vertical temperature profile of the atmosphere	W. L. Smith, NESS/NOAA Suite 300, 3737 Branch Avenue Hillcrest Heights, Maryland 20031
Selective Chopper Radiometer (SCR)	2.08 μm 2.59 μm 2.65 μm 3.5 μm 11.1 μm 13.8-14.8 μm (4 bands) 15 μm (4 bands) 18.6 μm 46.5 μm 100 μm	Vertical temperature profile of the atmosphere Water vapor distribution in the atmosphere Density of ice particles in cirrus clouds	J. T. Houghton, Oxford University Oxford, England S. D. Smith, Heriot-Watt University Edinburg, Scotland
Nimbus E Microwave Spectrometer (NEMS)	27.23 GHz 31.4 GHz 53.65 GHz 54.90 GHz 58.80 GHz	Vertical temperature profile of the atmosphere even in presence of clouds Atmospheric water vapor	D. H. Staelin, MIT Cambridge, Massachusetts 02139

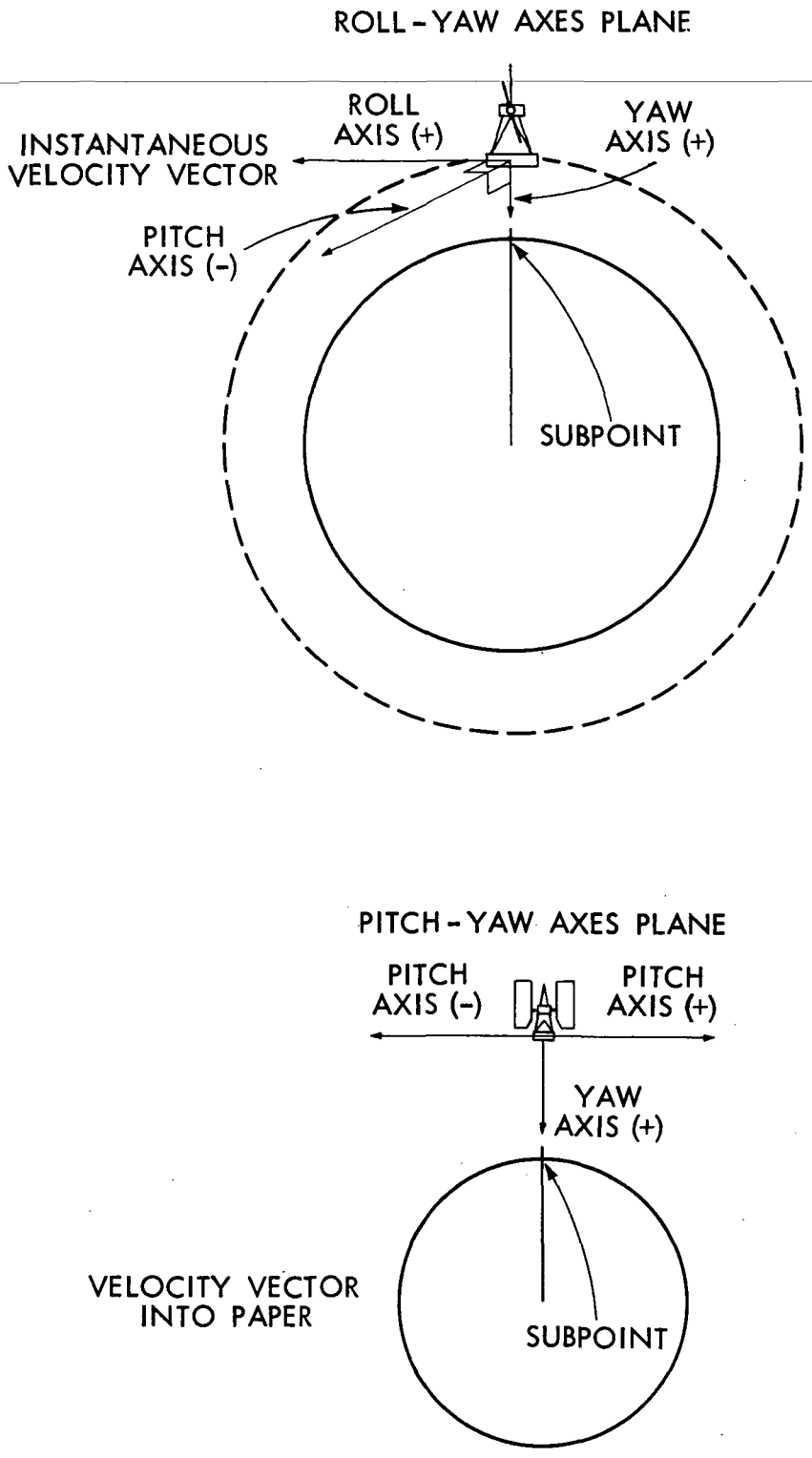

Figure 1-2. Nimbus Attitude Axes

- The Versatile Information Processor (VIP) including real-time telemetry
- The High Data Rate Storage System (HDRSS)
- The Surface Composition Mapping Radiometer (SCMR) Data System

A simplified block diagram of the Nimbus data system is shown in Figure 1-3.

1.4.1 The Versatile Information Processor (VIP)

The VIP samples approximately 1000 outputs from spacecraft systems. The sensor data are digitized (where necessary), time-multiplexed, and formatted into a 4-kilobits per second (kbs) serial bit stream. The serial bit stream can be recorded in biphase on the HDRSS tape recorder and simultaneously transmitted over the Pulse Code Modulation (PCM) 136.5 MHz beacon transmission link.

Data transmitted in the VIP mode include spacecraft subsystem and experiment housekeeping telemetry such as temperature of components, calibration signals and voltages, plus the output of four experiments: NEMS, ESMR, ITPR, and SCR. Switching is provided in the VIP so that, when commanded, the standard NASA time code format data (100-bps, pulse duration modulation) are substituted for the VIP data.

1.4.2 High Data Rate Storage System (HDRSS)

The HDRSS consists of a 5-channel tape recorder and the associated recording and playback electronics for collecting and storing data from the THIR, VIP subsystems, and the time code. For purposes of redundancy and extending useful data capacity, there are two parallel and independent HDRSS on Nimbus 5. Each HDRSS can record 134 minutes of data. The recorders can record in parallel or can be programmed to record sequentially for more complete coverage. Included with this system is the S-band transmitter used to send the data to the ground. Each HDRSS operates into a 4-watt solid-state transmitter. The transmitters operate at 1702.5 MHz and 1707.5 MHz. Normal operation will use only one transmitter, with the capability of switching should one transmitter fail.

1.4.3 The Surface Composition Mapping Radiometer (SCMR) Data System

The primary objective of the SCMR data system is to transfer the data from the SCMR experiment to the S-Band transmitter with a minimum of signal

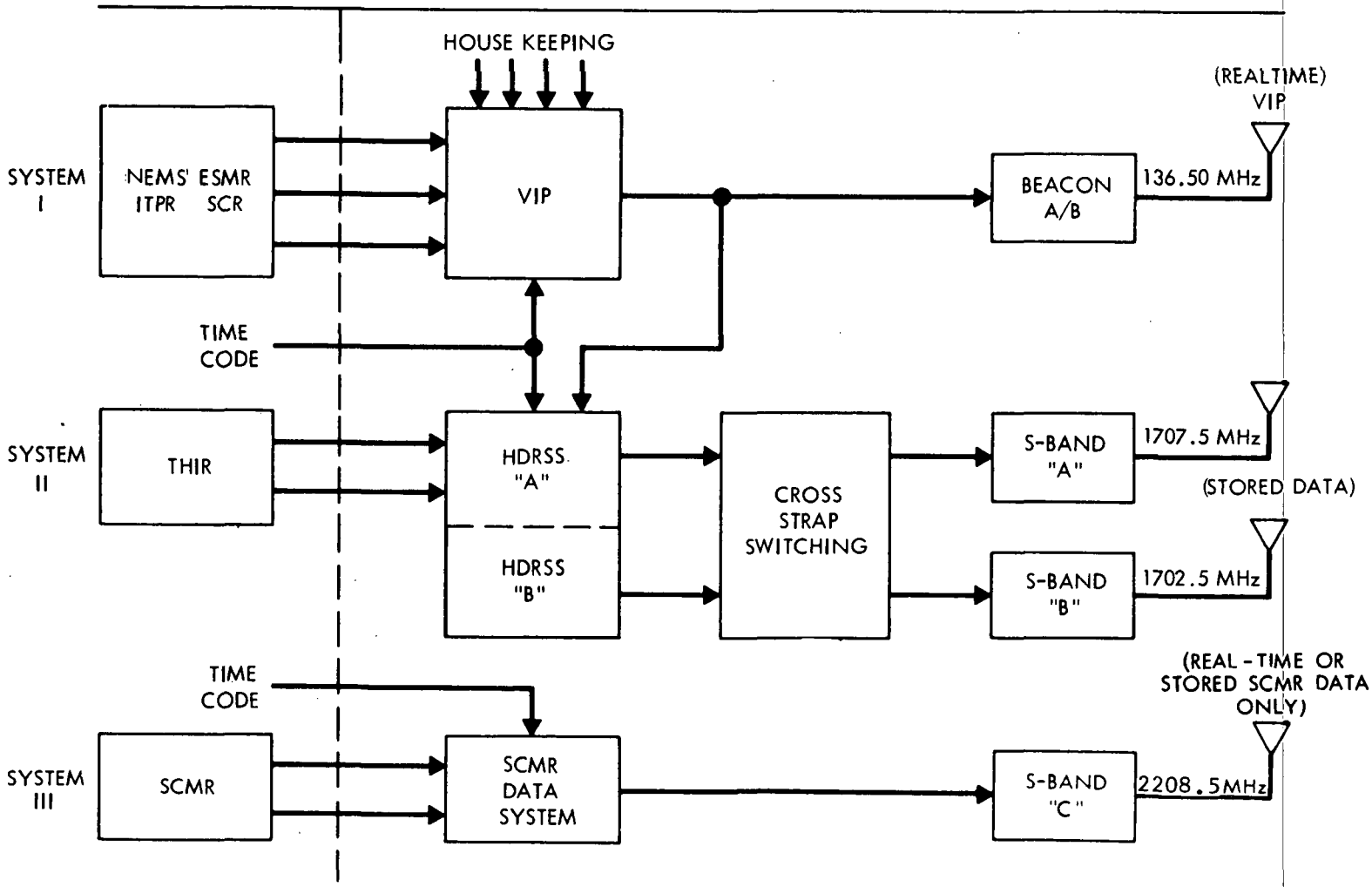

Figure 1-3. Nimbus 5 Data Systems

degradation. Two of the three data channels from the SCMR experiment, plus the time code and a fixed frequency for tape speed compensation, will be recorded for about eight minutes per orbit and transmitted when the satellite is in contact with a Spaceflight Tracking and Data Network (STDN) ground station. The two data channels and time code are frequency multiplexed before transmission.

SCMR data can also be transmitted in real-time when the satellite is in view of a STDN station.

1.5 Ground Station Complex

Data from the HDRSS are received at the two STDN stations located near Fairbanks, Alaska, and Rosman, North Carolina. The HDRSS data acquired at Alaska are recorded on pass and then transmitted over a microwave link at reduced rates to the Meteorological Data Handling System (MDHS) at GSFC. HDRSS data acquired at Rosman are relayed directly to GSFC over a wideband data link. PCM data acquired at either Alaska, Rosman or other STDN sites are relayed by data link to GSFC as they are received from the spacecraft.

At present five STDN stations are equipped to receive SCMR data. They are at Rosman, North Carolina; Goldstone, California; Fairbanks, Alaska; Honeysuckle Creek, Australia; and Madrid, Spain. Only data collected at Rosman can be transmitted by a wideband data link to GSFC for immediate processing. Because of data link noise, this data will not be of archival quality. Therefore, all data will be taped at the acquisition sites and mailed to GSFC for archival processing.

Alaska acquires the spacecraft 10 orbits each day (of the 13 to 14 orbits per day). Rosman acquires two orbits per day missed by Alaska. Other STDN stations acquire real-time PCM data for orbits missed by Rosman and Alaska.

All spacecraft data are processed in the MDHS at GSFC. Photographic images of SCMR, ESMR, and THIR data, generated by MDHS, are processed through the Nimbus/ATS Data Utilization Center (NADUC). Digitized magnetic tape recordings of SCMR, THIR, NEMS, and ESMR experiment data are distributed by NADUC to the respective experimenters for further data reduction. ITPR data, extracted and formatted in the MDHS, are transmitted over landline in near real-time to the National Oceanic and Atmospheric Administration (NOAA). SCR data, with associated housekeeping and extracted corollary THIR data, are stripped from the data stream, formatted, and transmitted by data link to the experimenter at Clarendon Laboratories, Oxford University, England.

1.6 Nimbus/ATS Data Utilization Center (NADUC)

The NADUC performs the following functions:

- Accounts for and distributes all experiment data processed by the MDHS
- Processes and reproduces all photographic data through to archival products
- Generates periodic data catalogs (in a format as outlined in Section 8) to provide information about all experiment data collected and their availability
- Provides special technical services to the experimenters and data users
- Maintains a complete photographic data reference file

1.7 Archival and Dissemination of Nimbus 5 Data

The nature and format of the data to be available from each experiment are explained in detail in the respective sections of this guide. The data will be archived and available as described below:

- Photographic data from THIR and ESMR will be archived and available through the National Space Science Data Center (NSSDC), Goddard Space Flight Center, Code 601, Greenbelt, Maryland 20771.
- Digital data tapes from THIR, SCR, ESMR and NEMS will be archived and available through the NSSDC.
- Availability of photographic and digital SCMR data will only be through the experimenter, Dr. Warren Hovis, Code 652, Goddard Space Flight Center, Greenbelt, Maryland 20771.
- ITPR digital data tapes will be available in three different formats from three different agencies:

    1. Archival tapes containing the calibrated, located radiances, and a minimum of auxiliary information will be available from NSSDC.

2. Archival tapes containing atmospheric temperature profiles and the corresponding radiances and earth locations will be at the National Oceanic and Atmospheric Administration (NOAA), National Environmental Satellite Service (NESS), FOB4, Suitland, Maryland 20023.

3. Archival tapes containing the ITPR derived temperature profiles used in the National Meteorological Center's (NMC) operational forecasts will be available from the National Climatic Center (NCC), NOAA, Federal Building, Asheville, North Carolina 28801.

ITPR data will be available from the NCC at cost. Limited quantities of all other data will be furnished to qualified investigators, by the NSSDC, without charge. A charge for production and dissemination costs may be established by NSSDC if a large volume of data is requested. Whenever it is determined that a charge is required, a cost estimate will be provided to the user prior to filling his data request.

All requests from foreign researchers for Nimbus 5 data archived and available through NSSDC must be specifically addressed to:

Director, World Data Center A for Rockets and Satellites
Code 601, Goddard Space Flight Center
Greenbelt, Maryland 20771, U.S.A.

When ordering data from either the NSSDC or the World Data Center, a user should specify why the data are needed, the subject of his work, the name of the organization with which he is connected, and any government contracts he may have for performing his study.

When a user requests data on magnetic tapes, he should provide additional information concerning his plans for using the data, e.g., what computers and operating systems will be used. In this context, the NSSDC is compiling a library of routines which can unpack or transform the contents of many of the data sets into formats which are more appropriate for the user's computer. NSSDC will provide, upon request, information concerning its services.

When requesting data on magnetic tape, the user must specify whether he will:

- Supply new tapes prior to the processing, or
- Return the original NSSDC tapes after the data have been copied

SECTION 2

THE TEMPERATURE-HUMIDITY INFRARED RADIOMETER (THIR) SUBSYSTEM

by
Andrew W. McCulloch
National Aeronautics and Space Administration
Goddard Space Flight Center

2.1 Introduction

The THIR is a two channel high resolution scanning radiometer designed to perform two major functions. First, a 10.5-12.5 μm (11.5 μm) window channel will provide both day and night cloud top or surface temperatures. Second, a water vapor channel at 6.5-7.0 μm (6.7 μm) will give information on the moisture content of the upper troposphere and stratosphere and the location of jet streams and frontal systems. The ground resolution at the subpoint is 8 km for the window channel and 22 km for the water vapor channel. Both channels will operate continuously to provide day and night global coverage.

2.2 Instrumentation

2.2.1 Radiometer

The THIR radiometer consists of an optical scanner (shown in Figure 2-1) and an electronic module (not shown). The blackened collar seen near the scan mirror is a sun shield whose function is to prevent sunlight contamination during spacecraft sunrise and sunset. The other side of the sun shield is painted white. The end of the scanner opposite the sun shield contains the optical system and preamplifiers.

The optical system (shown in Figure 2-2) consists of a scan mirror, a telescope (comprised of primary and secondary mirrors) and a dichroic beam-splitter. The scan mirror, inclined at 45° to the optical axis, rotates at 48 rpm, and scans in a plane perpendicular to the direction of the motion of the satellite. The scan mirror rotation is such that, when combined with the velocity vector of the satellite, a right-hand spiral results. Therefore, the field of view scans across the earth from east to west in daytime and west to east at night, when the satellite is traveling northward and southward respectively.

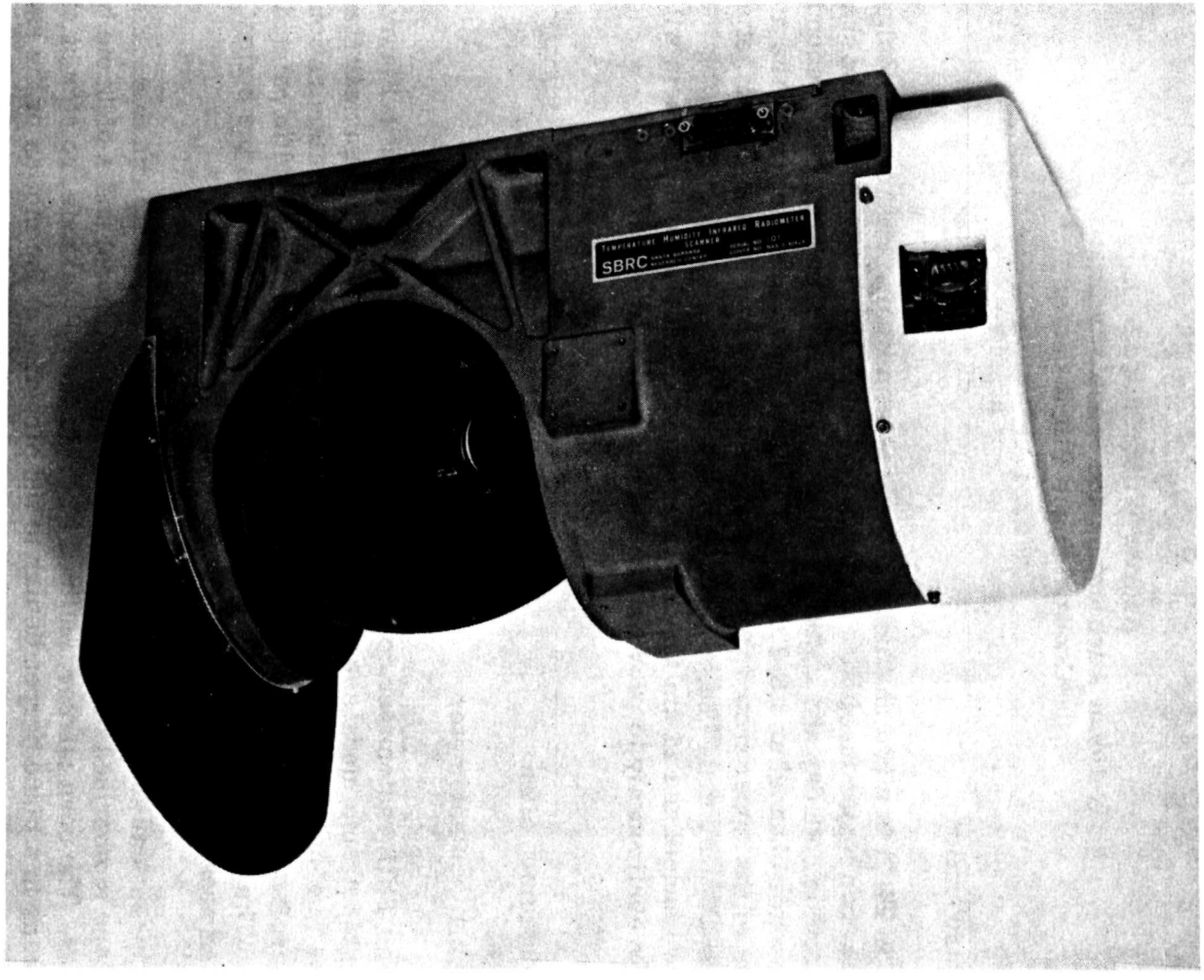

Figure 2-1. The Temperature Humidity Infrared Radiometer

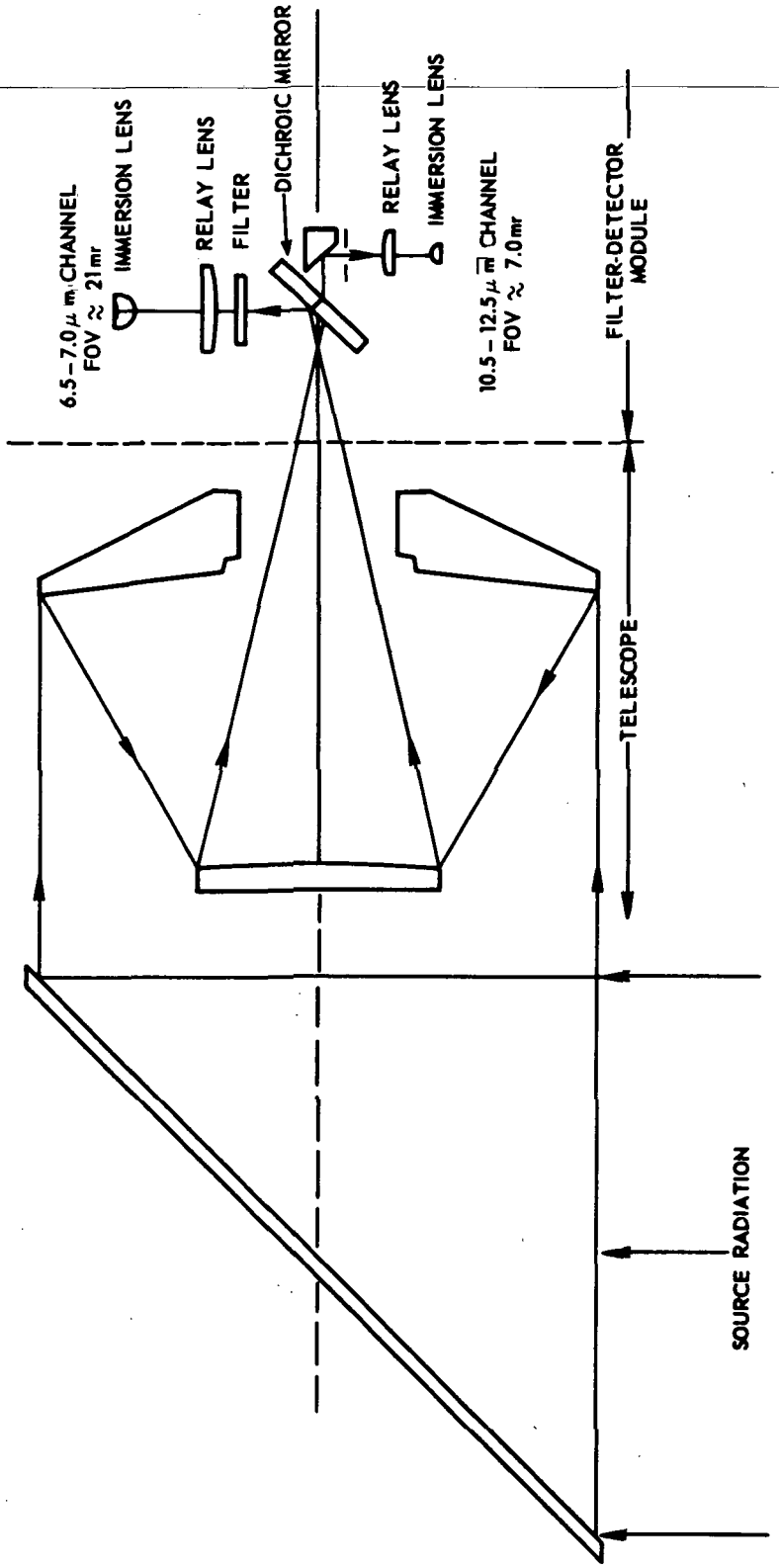

Figure 2-2. THIR Optical Schematic

The telescope focuses the energy at the dichroic beamsplitter which divides the energy spectrally and spatially into two channels. A 21 milliradian channel detects energy in the 6.7 μm band and consists of a passband filter germanium relay lens, baffles, and germanium immersed thermistor bolometer. A 7.0 milliradian channel detects energy in the 11.5 μm band. It consists of a bandpass filter (transmission portion of the dichroic), an Itran-2 relay lens which also serves as a long wavelength blocking filter, a folding mirror, and a germanium immersed thermistor bolometer.

The signals from the detectors are capacitively coupled to the preamplifiers, amplified and sent to the electronic module. In the electronic module, the signals are further amplified and corrected for detector time constant to provide the overall frequency response as required by the subsystem optical resolution. The signals are processed out of the electronic module through buffer amplifiers. The 6.7 μm channel output is available on a full time basis as the shifted level channel. The offset of the shifted level channel is provided in the buffer of that channel. A second video output selects either the 6.7 μm or the 11.5 μm channel by means of a command relay. In addition to the two video output signals, there are fourteen telemetry channels, ten analog and four digital.

The actual fields of view for both channels are shown in Figures 2-3 and 2-4. The tabulated values of the relative spectral response are shown in Table 2-1, while Figures 2-5 and 2-6 illustrate the data graphically.

The instantaneous field of view (IFOV) of the window channel is approximately 7 milliradians. At an altitude of 1112 kilometers (600 nautical miles), this results in a subsatellite ground resolution of 7.67 kilometers (4.1 nautical miles). The scan rate of 48 rpm produces contiguous coverage along the subsatellite track. Due to the earth-scan geometry of the THIR, as nadir angle increases, overlapping occurs between consecutive scans, reaching 350 percent overlap at the horizons, and resulting in a loss of ground resolution in the direction of the satellite motion. Even greater loss of resolution occurs along the scan line (perpendicular to the line of motion of the satellite) because of the expansion, with increasing nadir angle, of the target area viewed.

Figure 2-7b shows graphically, for the window channel, the relationship between nadir angle and ground resolution element size along the path of the satellite and perpendicular to it. Pictorially this is represented in Figure 2-7a. The numbers under each resolution element are nadir angle (in degrees), resolution along the scan line (in kilometers), and resolution parallel to the satellite line of motion (in kilometers). For example, at 50° nadir angle, the ground resolution element of the THIR approximates a rectangle 31.8 kilometers long (east and west) by 14.0 kilometers wide (north and south). For the 6.7 μm

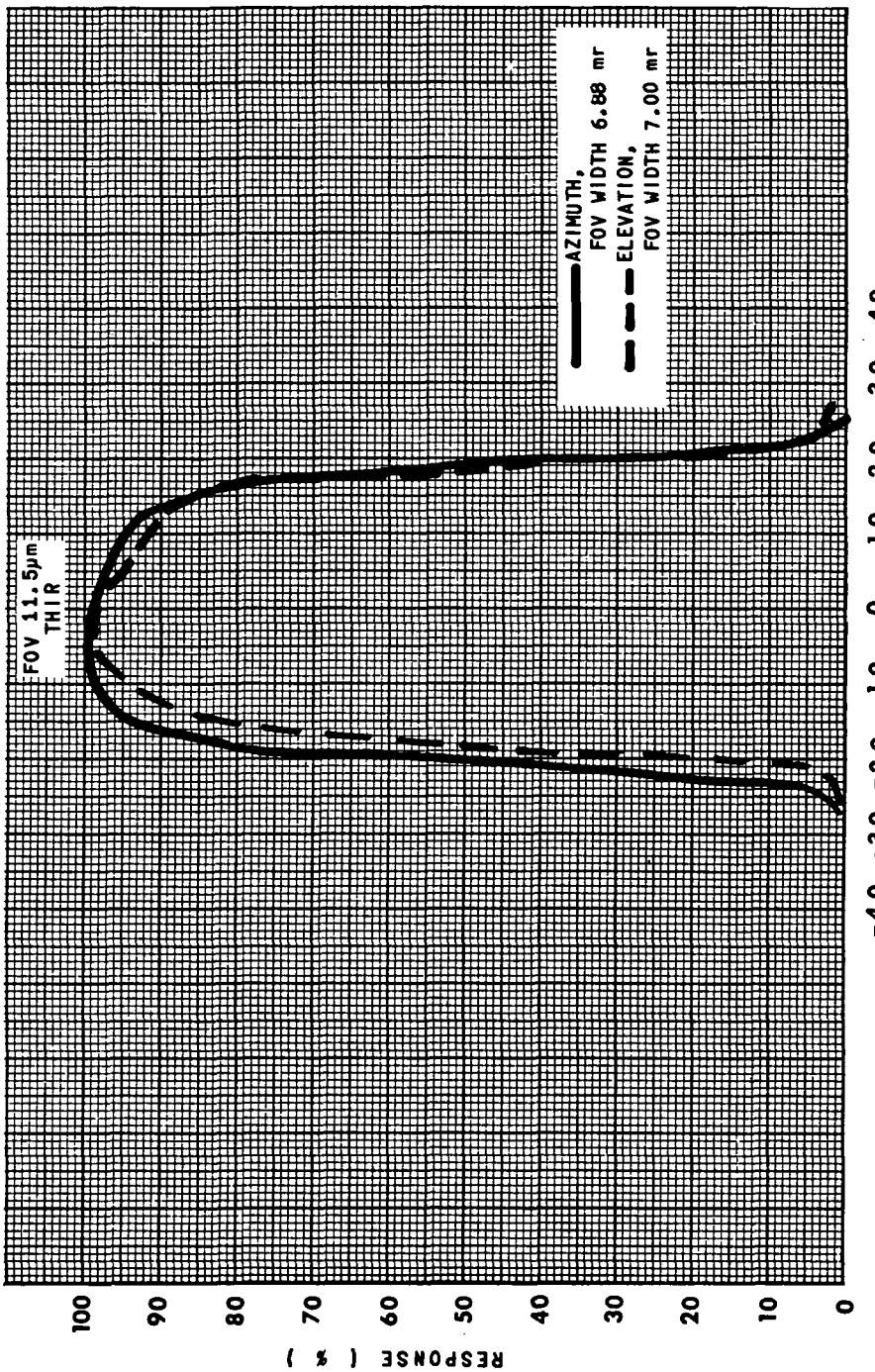

Figure 2-3. Field of View of the THIR 11.5μm Channel

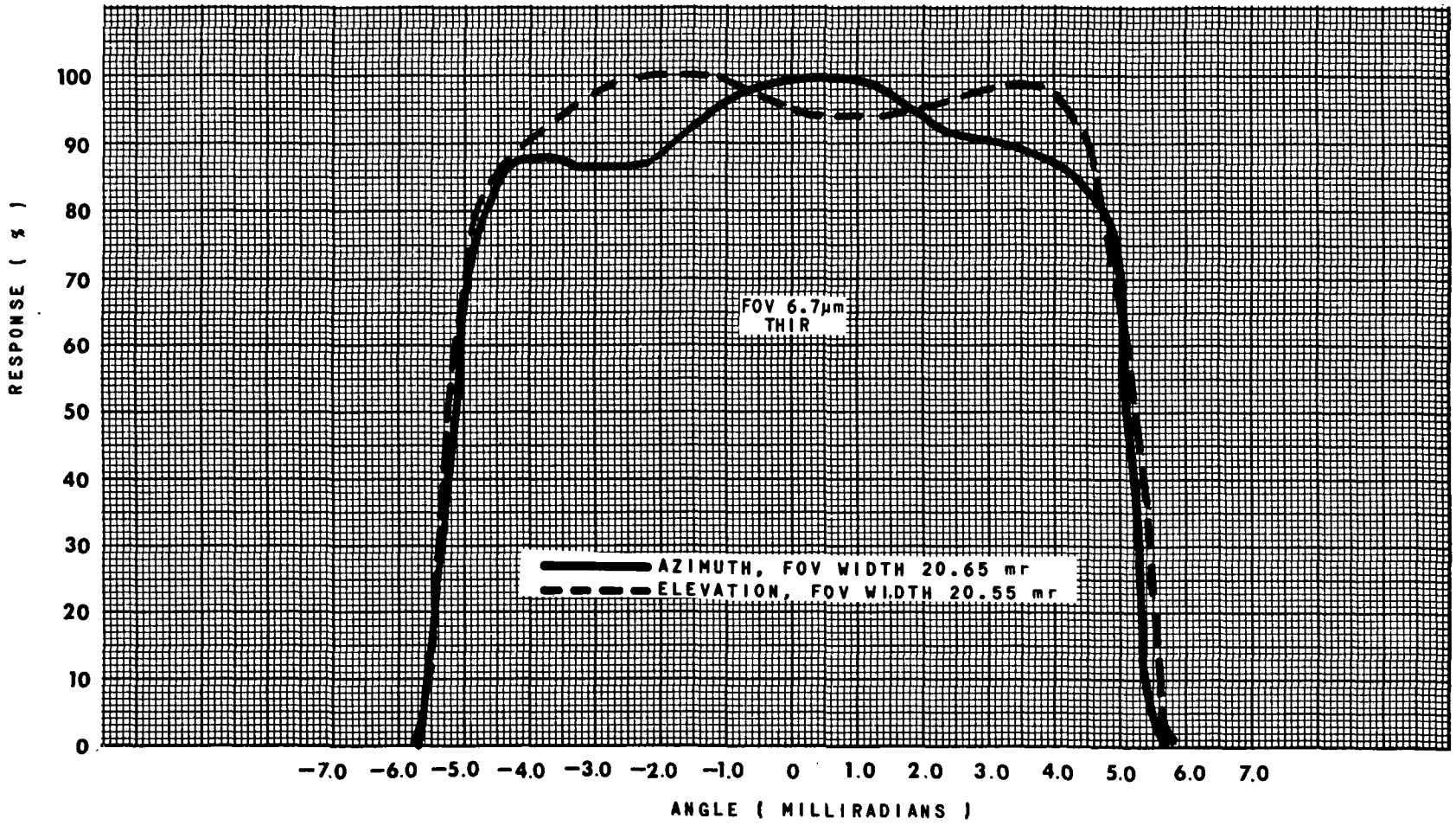

Figure 2-4. Field of View of the 6.7μm Channel

Table 2-1
Relative Spectral Response, ϕ_λ

6.7 μm Channel		11.5 μm Channel			
λ (μm)	Relative Response	λ (μm)	Relative Response	λ (μm)	Relative Response
6.20	.0000	9.9	.0000	12.7	.4623
6.25	.0061	10.0	.0105	12.8	.2513
6.30	.0122	10.1	.0282	12.9	.1134
6.35	.0761	10.2	.1306	13.0	.0437
6.40	.1399	10.3	.3019	13.1	.0093
6.45	.5088	10.4	.4327	13.2	.0000
6.50	.8777	10.5	.4638		
6.55	.9015	10.6	.6618		
6.60	.9253	10.7	.8025		
6.65	.8687	10.8	.8436		
6.70	.8120	10.9	.8089		
6.75	.8709	11.0	.8511		
6.80	.9298	11.1	.9447		
6.85	.9645	11.2	.9714		
6.90	.9991	11.3	1.0000		
6.95	.9995	11.4	.9985		
7.00	1.0000	11.5	.9925		
7.05	.9471	11.6	.9923		
7.10	.8943	11.7	.9660		
7.15	.6972	11.8	.8761		
7.20	.5001	11.9	.9012		
7.25	.2859	12.0	.9662		
7.30	.0717	12.1	.9649		
7.35	.0422	12.2	.9682		
7.40	.0127	12.3	.9118		
7.45	.0097	12.4	.8148		
7.50	.0067	12.5	.8572		
7.55	.0033	12.6	.5987		
7.60	.0000				

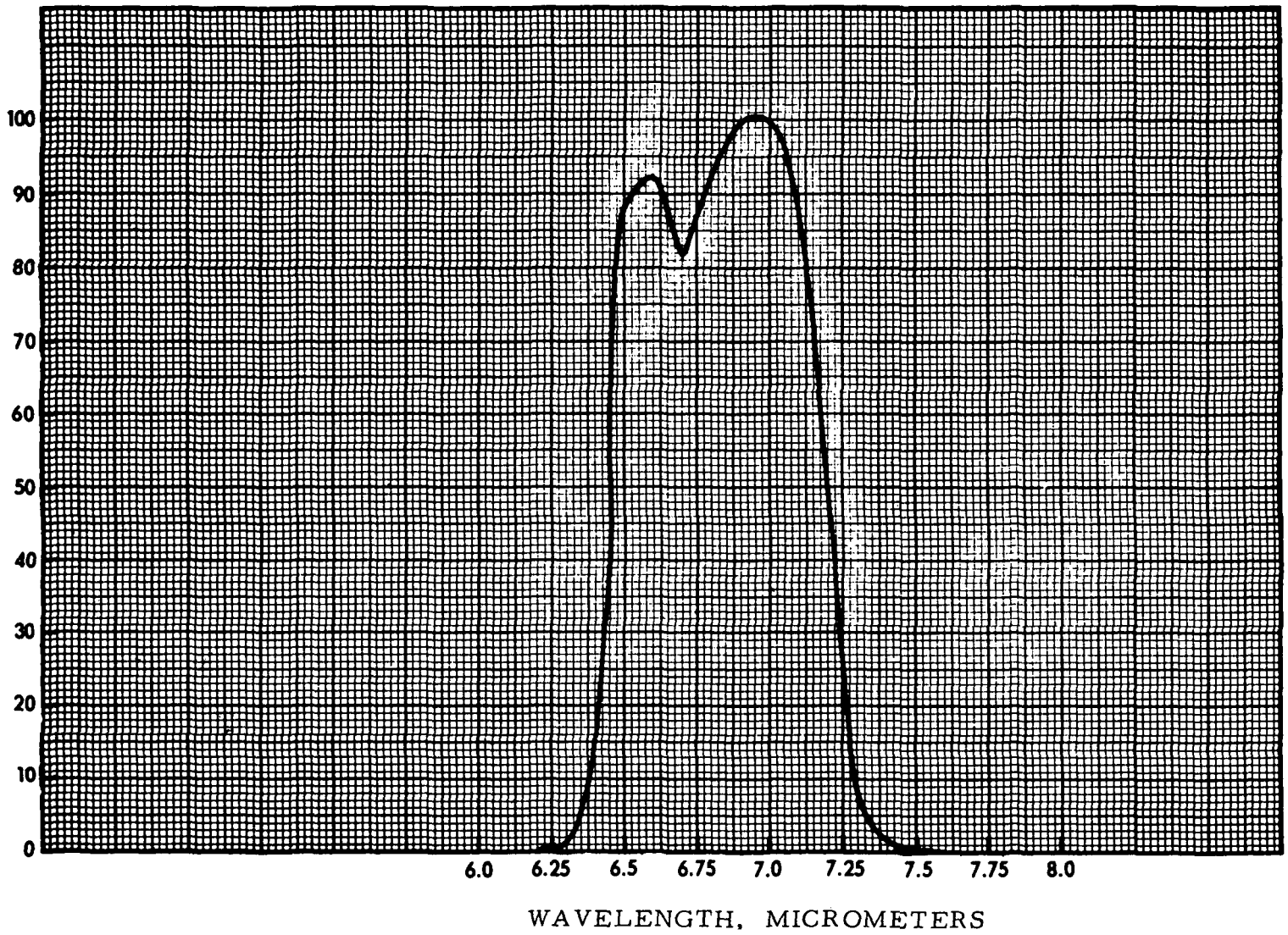

Figure 2-5. Relative Spectral Response of the 6.7 μm Channel

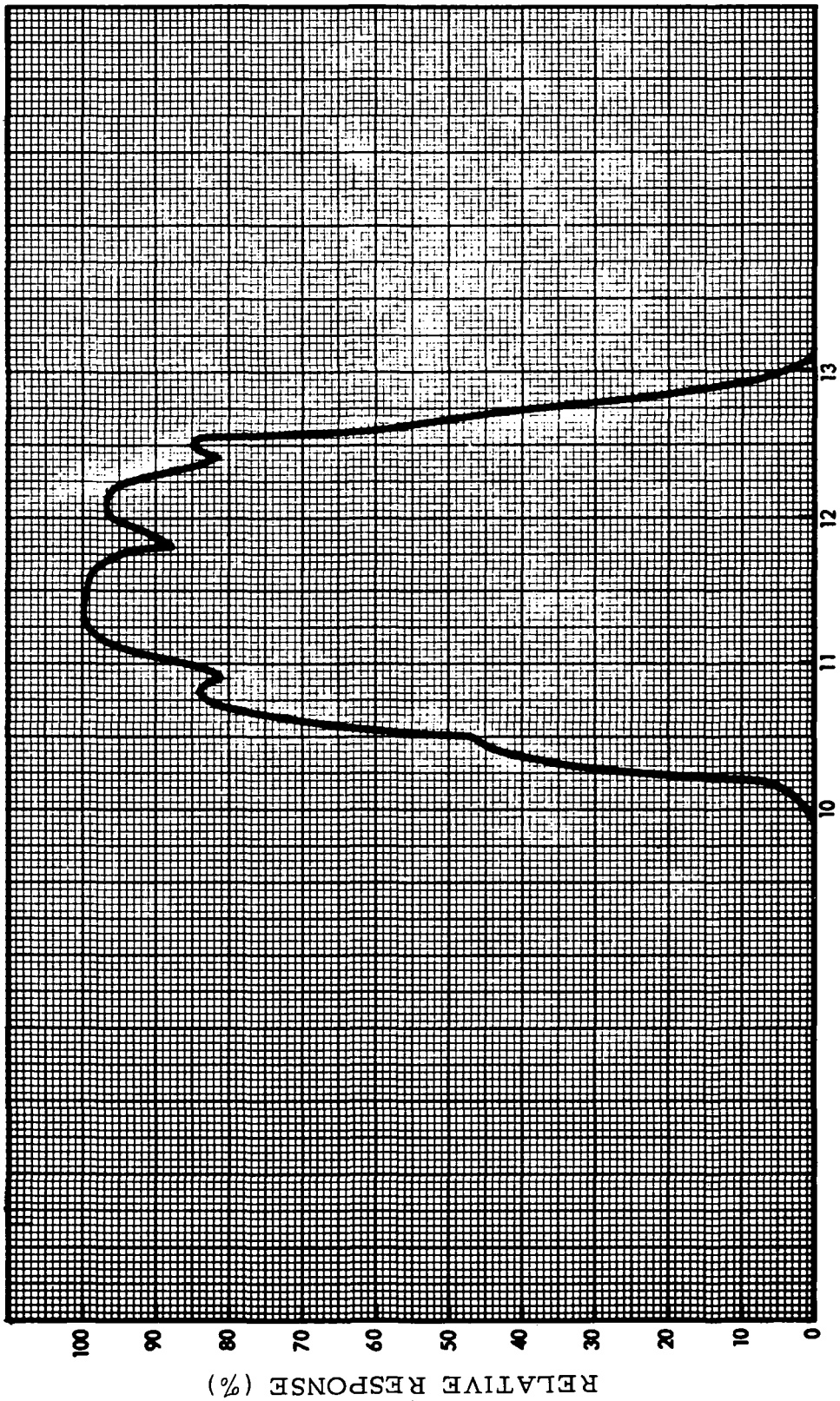

Figure 2-6. Relative Spectral Response of the 11.5 μm Channel

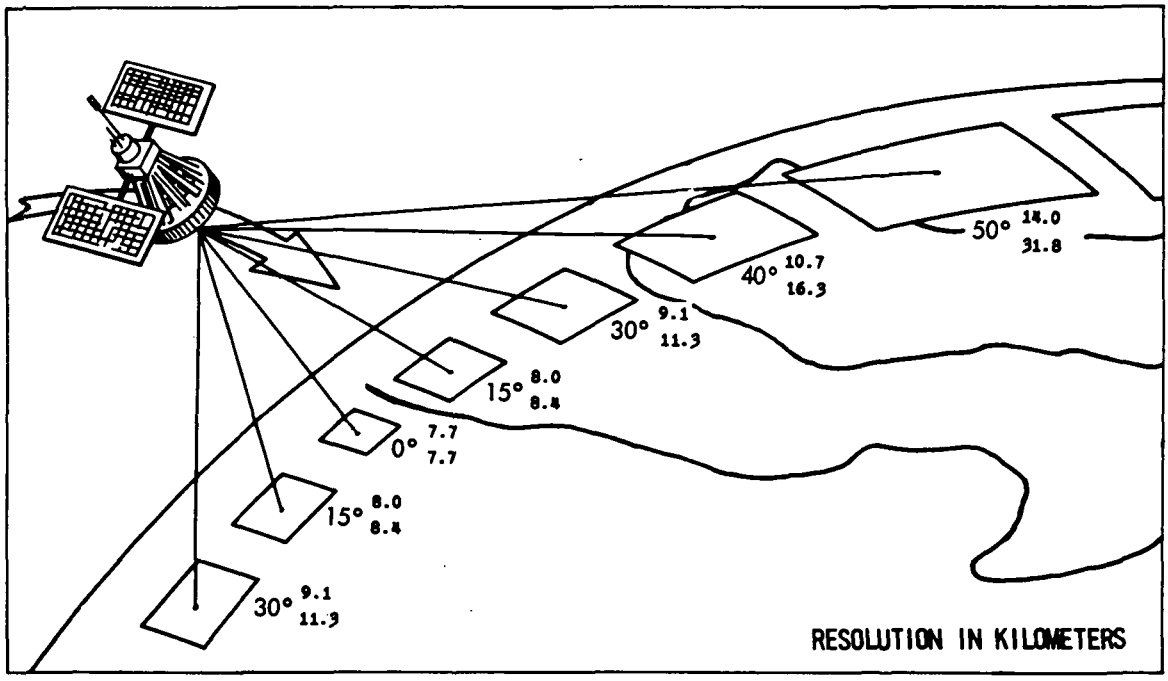

(a)

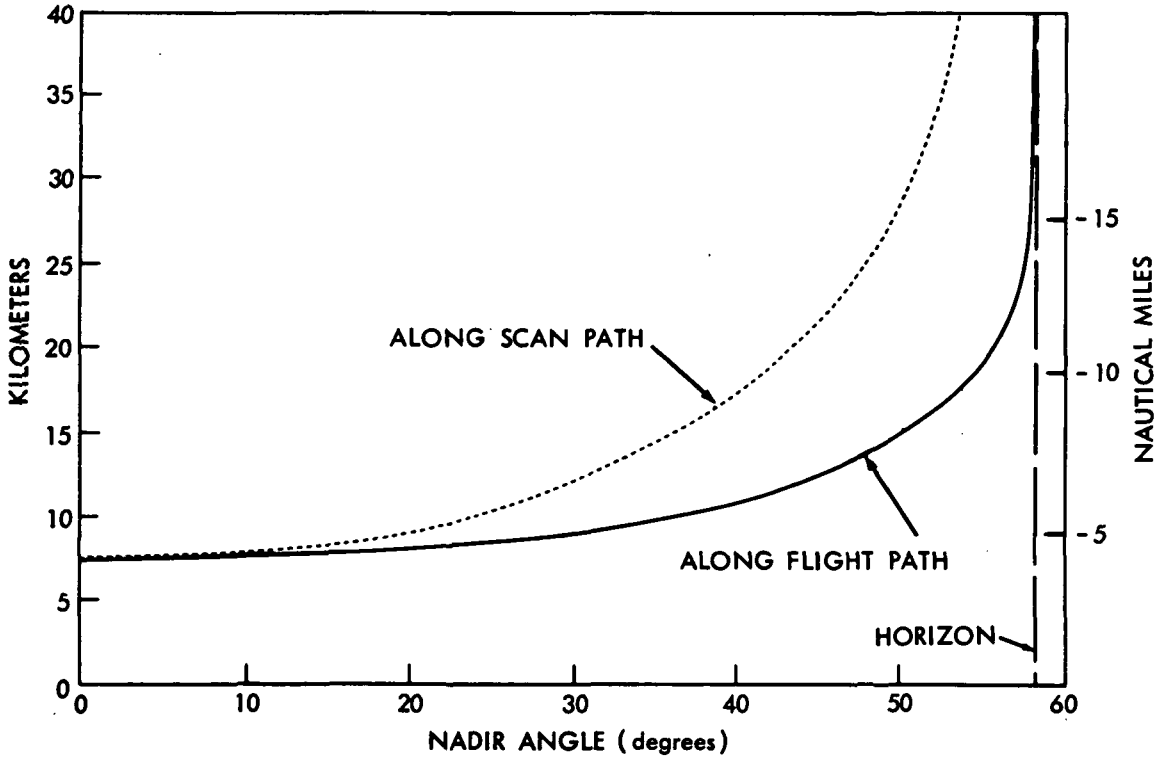

(b)

Figure 2-7. Relationship between Nadir Angle and Ground Resolution for the THIR 11.5 μm Channel at 1100 km (a) Pictorial (b) Graphical

channel a similar situation exists. The ground resolution at the subsatellite point is 22.6 km while at 50° nadir angle, the ground resolution element is 93.5 km long by 41.1 km wide.

In contrast to television, no image is formed within the radiometer; the THIR sensor merely transforms the received radiation into an electrical (voltage) output with an information bandwidth of 0.5 to 360 Hz for the 11.5 μm channel and 0.5 to 120 Hz for the 6.7 μm channel. The radiometer scan mirror continuously rotates the field of view of the detector through 360 degrees in a plane normal to the spacecraft velocity vector. The detector views in sequence the in-flight blackbody calibration target (which is a part of the radiometer housing), outer space, earth, outer space, and returns again to intercept the calibration target. The space and housing-viewed parts of the scan, which can be identified without difficulty, serve as part of the in-flight check of calibration. Information on housing temperature, which is monitored by thermistors, is telemetered to the ground stations and, for calibration purposes, is constantly compared with the temperature obtained from the radiometer housing scan. Even though the first stages of amplification are capacitor-coupled, the low frequency cutoff is so low that a dc restore circuit is necessary to provide a zero signal reference. This occurs during that portion of the scan when the optics are receiving zero radiation (space). The dc restore circuitry also provides additional gain to raise the signal to the desired output level and filtering to establish proper frequency characteristics.

An additional function of the dc restorer is to reduce the 6.7 μm channel gain to 1/3 of its former value when the bolometer views the housing. This is necessary to prevent saturation of the output signal when the housing temperature is beyond the dynamic range of the channel.

2.2.1.1 Scan Sequence

The scan mirror rotates at 48 rpm or 1.25 seconds per revolution. The scanner's total angular scan from the time the IFOV leaves the housing until it intercepts the housing again after scanning the earth is 150°. The earth subtends an arc of 128° at 740 kilometers and 117° at 1112 kilometers. This provides a minimum of 11° coverage above the horizon when scanning the earth. To assure an adequate scan period in space during dc restoration, the radiometer requires a mounting position rotated 5° about the spacecraft roll axis. This provides a minimum of 16° for operation of the dc restorer (for a 740 kilometer orbit).

Figures 2-8 and 2-9 illustrate the radiometer timing sequence relative to the angular position of the scan mirror for each scan cycle.

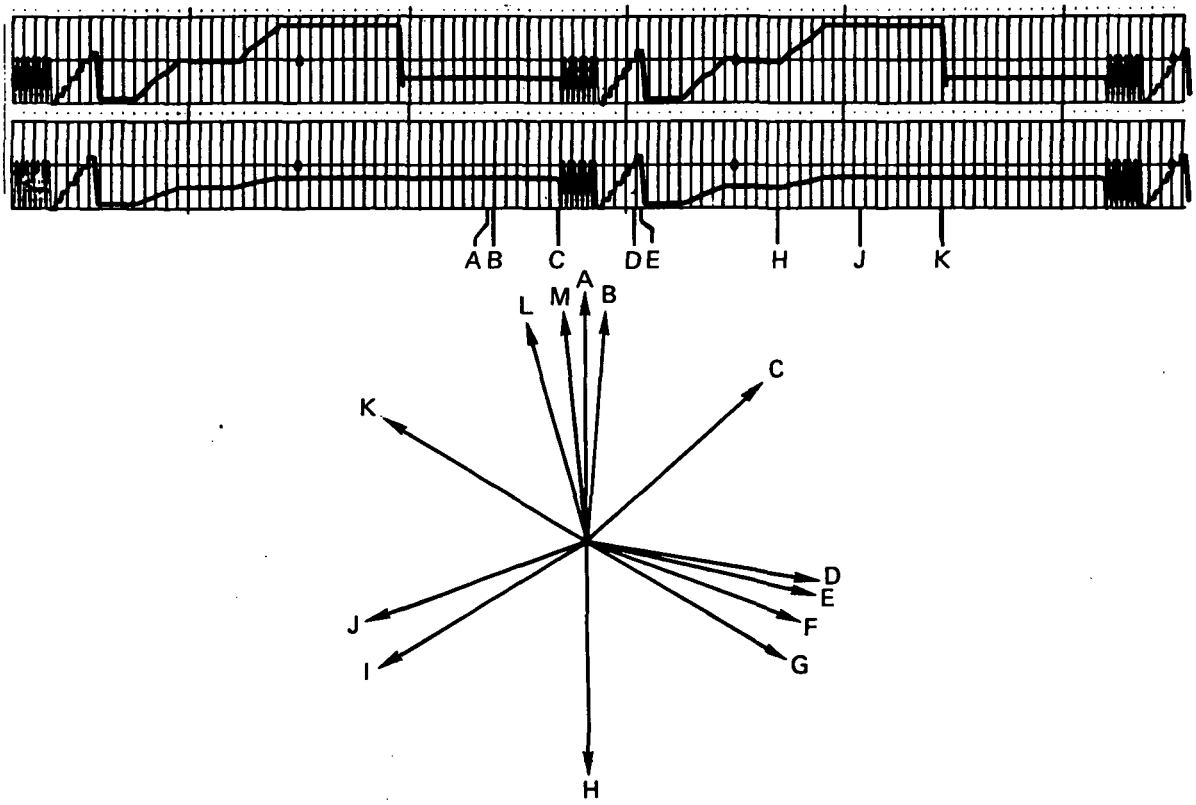

LEGEND

Reference Letter	Angle (degrees)	Time (ms)	Event
A :	0	0	Spacecraft zenith
B :	5	17.4	Radiometer IFOV just starting to leave housing
C :	48	166.7	Scan mirror position pip No. 1 occurs and radiometer sync word and calibration signal sequence is started. 6.7 μm channel gain returned to normal
D :	100	347.5	Radiometer IFOV just starting to see all of space
E :	103.5	359.4	Calibrate signal sequence ends and restore period starts
F :	110.7	384.4	Restore period ends
G :	121.5	422.2	Earth scan period begins (1100 km orbit)
H :	180	625.0	Spacecraft nadir
I :	238.5	828.8	Earth scan period ends (1100 km orbit)
J :	250	868.9	Radiometer IFOV just starting to see housing
K :	302	1048.5	Scan mirror position pip No. 2 occurs and 6.7 μm channel gain is attenuated by a factor of 3
L :	345	1197.9	Radiometer IFOV completely filled by housing
M :	355	1232.6	Radiometer Z-axis

Figure 2-8. THIR Scan Angle Information

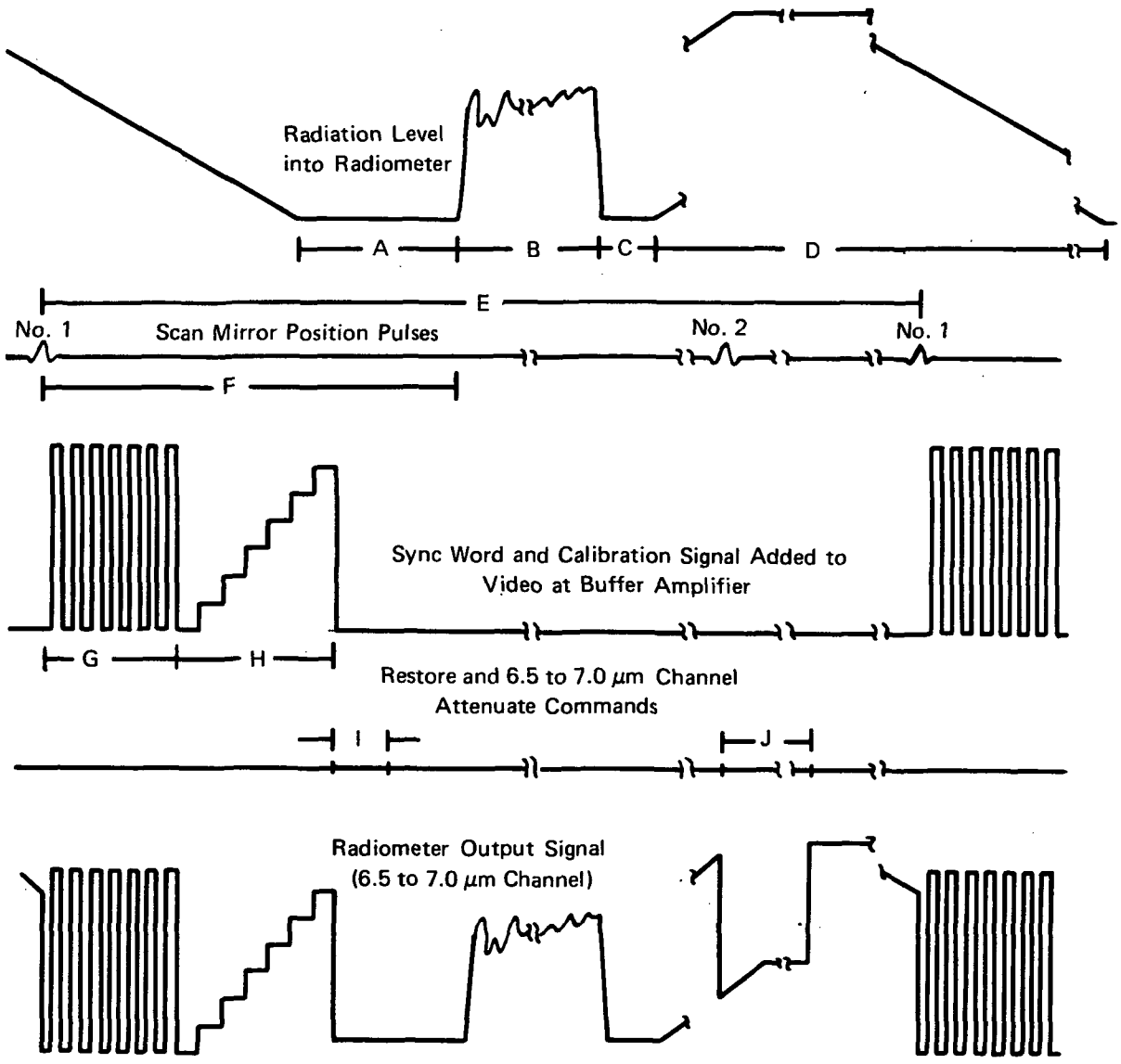

A - Space Scan (Prior to Earth Scan), 75 ms
B - Earth Scan, 407 ms
C - Space Scan (After Earth Scan), 40 ms
D - Housing Scan, 730 ms
E - Scan Period, 1250 ms
F - Sync Pulse to Earth Scan Period, 255.5 ms
G - Sync Word, 84 ms
H - Calibrate Signal, 105 ms
I - Restore Period, 25 ms
J - 6.5 to 7.0 μm Channel Attenuate Period, 181 ms

Figure 2-9. THIR Voltage Waveforms During Scan Period

The sync word and calibration sequence is started by scan mirror position pulse (PIP) No. 1. This PIP is generated in the magnetic pick-off head when the magnet located on the scan mirror passes the pick-off. The logic circuit timing sequence is also triggered by PIP No. 1, generating the sync word for 84 millisecond (ms) and the calibrate voltage staircase for 105 ms. At the end of the calibrate staircase, the radiometer IFOV is clear of the radiometer housing, and the restore period of 25 ms is started. After the restoration period, the radiometer IFOV for some time is in space before and after the scan of the earth. The IFOV then starts to cover the radiometer housing and PIP No. 2 occurs. PIP No. 2 is used to attenuate the gain of the 6.7 μm channel by a factor of 3 to extend the dynamic range of that channel to include the housing radiation level. The gain is returned to normal by PIP No. 1.

2.2.2 Subsystem

A simplified block diagram of the THIR subsystem is given in Figure 2-10. Each channel will produce two buffered outputs of 0 to -6.0 VDC to be recorded on two tracks of the HDRSS A or B. Information from the 11.5 μm channel and the 6.7 μm channel is also available through the VIP.

2.2.2.1 *Stored Data*

The THIR records on two tracks of the 5 track HDRSS along with the other experiments and the time code. There are two HDRSS in the spacecraft for increased reliability and data coverage.

The varying dc voltage from the THIR modulates a voltage controlled oscillator (VCO), and is recorded on the HDRSS tape recorder. Upon command, the recorder plays back (in reverse) 32 times faster than real-time into two channels of the multiplexer (MUX). The signal is doubled and beat against an 805 kHz local oscillator, producing a 657.8 kHz to 602.8 kHz FM signal. This is directed into the S-band transmitter and broadcast to the data acquisition station along with frequencies of the time code and other experiments.

2.3 Calibration

2.3.1 Laboratory Calibration

The main parameters for calibration of all electromagnetic radiation detection devices are essentially the same. Three fundamental quantities must be defined: the effective spectral response, ϕ_λ; the effective radiance, $\bar{N}$; and the equivalent blackbody temperature, T_B. Here ϕ_λ is a composite function involving all of the factors which contribute to the spectral response of the instrument,

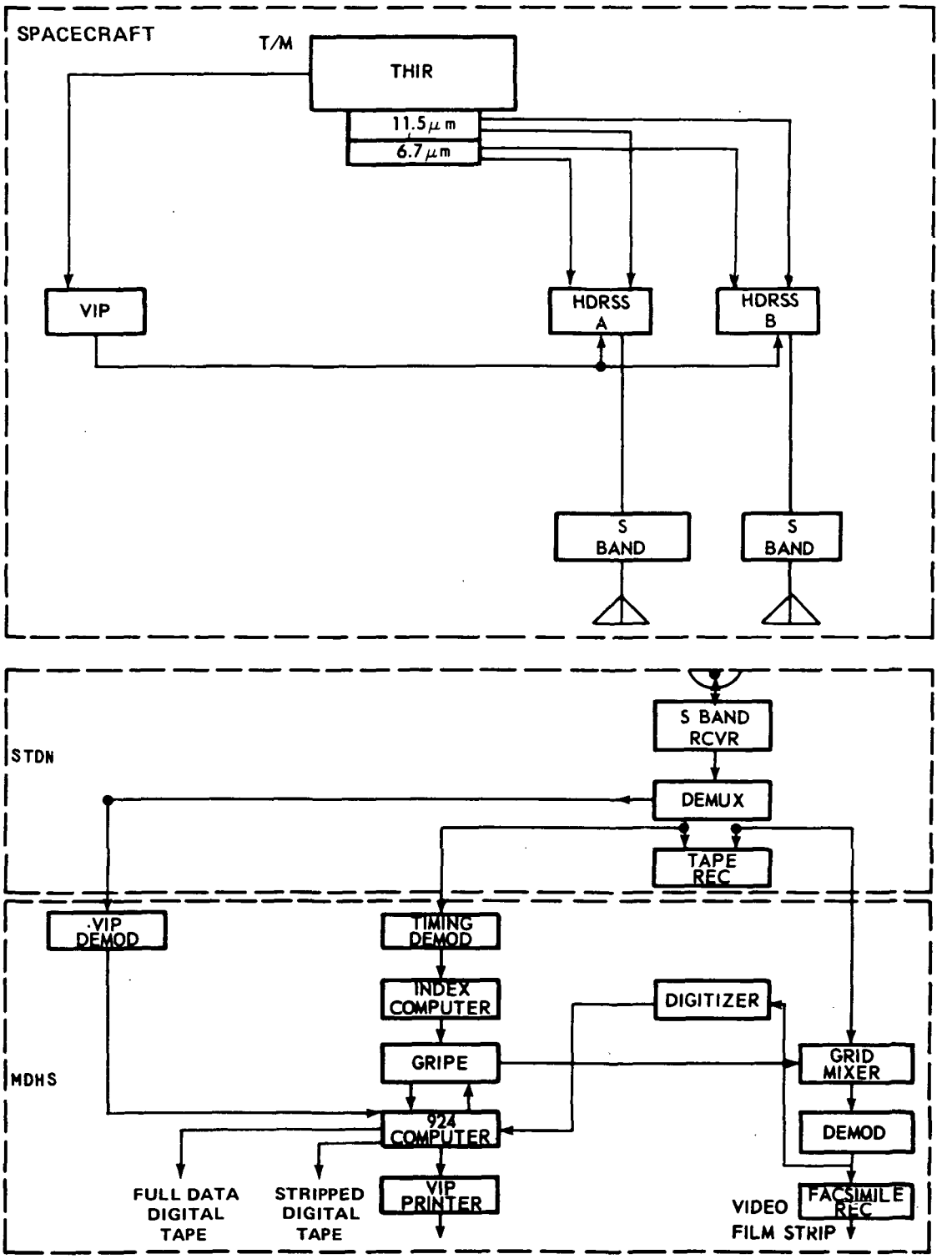

Figure 2-10. Simplified Block Diagram of the THIR Subsystem

such as filter transmission, mirror reflectances, and the spectral responsivity of the detector.

The effective radiance, $\bar{N}$, is defined as

$$\bar{N} = \int_0^\infty N_\lambda \, \phi_\lambda \, d\lambda \,, \tag{1}$$

where N_λ represents the generally non-Planckian radiation from the earth and its atmosphere.

Because of its narrow field of view, the THIR essentially measures beam radiation or radiance toward the satellite along the optical axis. In the preflight laboratory calibration, the FOV of the radiometer was filled by a blackbody target whose temperature could be varied and accurately measured over a range of 190°K to 340°K. From the temperature of the blackbody target, T_B, the spectral radiance of the target is determined by the Planck function B_λ. The integration of this function over the effective spectral response, ϕ_λ, yields that portion of the radiance of the target to which the radiometer responds, the "effective radiance," $\bar{N}$, given by

$$\bar{N} = \int_0^\infty B_\lambda \, (T_B) \, \phi_\lambda \, d\lambda \,. \tag{2}$$

The preflight laboratory calibration set-up is shown in Figure 2-11.

2.3.2 Equivalent Blackbody Temperature

The effective radiance to which the orbiting radiometer responds may be expressed by

$$\bar{N} = \int_0^\infty N_\lambda \, \phi_\lambda \, d\lambda \,, \tag{3}$$

where N_λ is the spectral radiance in the direction of the satellite from the earth and its atmosphere. It is convenient to express the measurement from orbit in terms of an equivalent temperature of a blackbody filling the field of view which would cause the same response from the radiometer. From Equations 2 and 3 it is seen that this "equivalent blackbody temperature" corresponds to the target temperature, T_B, of the blackbody used in the laboratory calibration. Therefore, the radiometer measurements can be expressed either as values of effective radiance, $\bar{N}$, or as equivalent blackbody temperatures, T_B. The $\bar{N}$ versus T_B function from Equation 2 is given in Figures 2-12, 2-13, and Table 2-2 for both channels.

THIR output voltages versus equivalent blackbody temperatures for both channels are given in Tables 2-3 and 2-4.

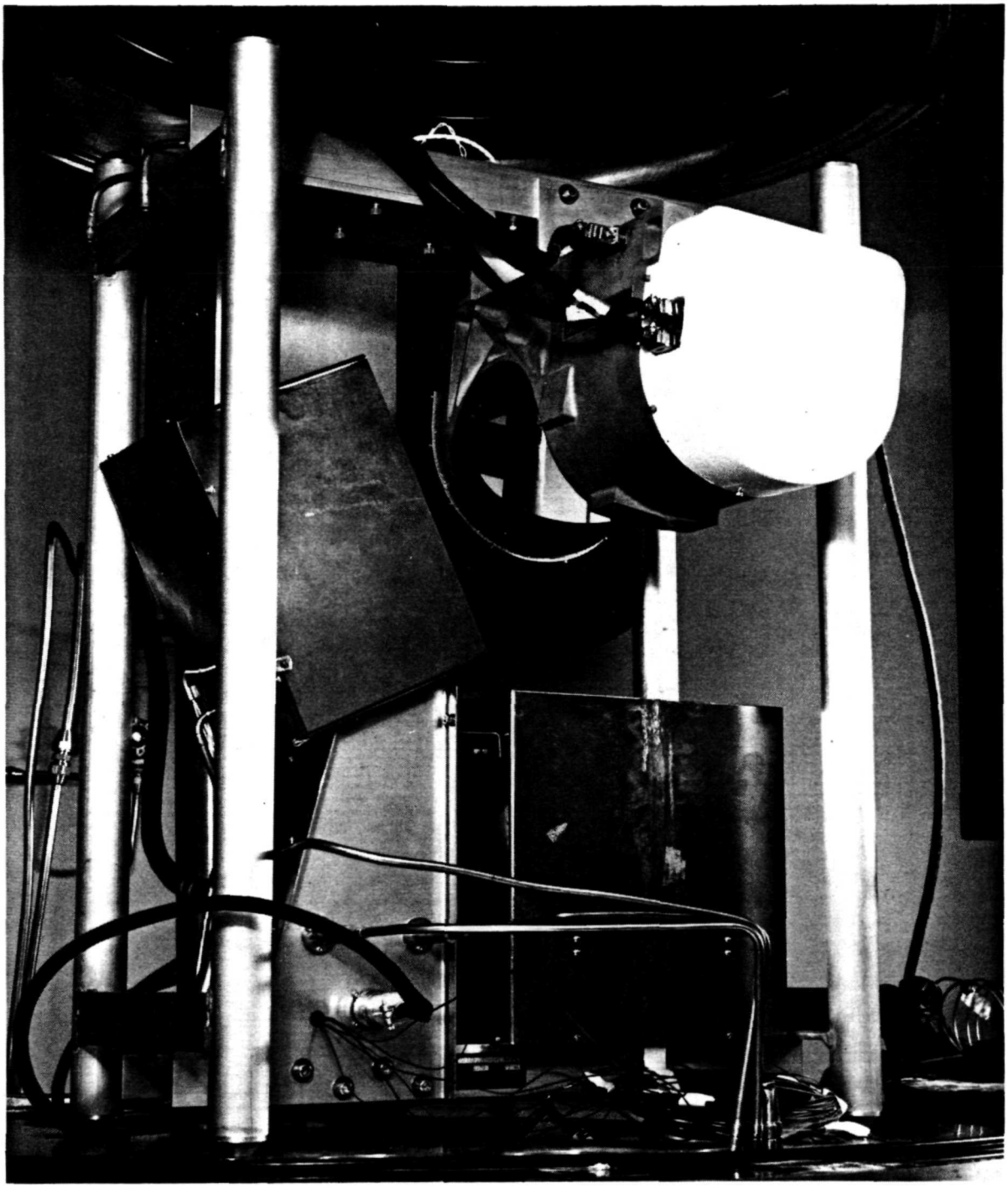

Figure 2-11. Preflight Laboratory Calibration Set-up for THIR

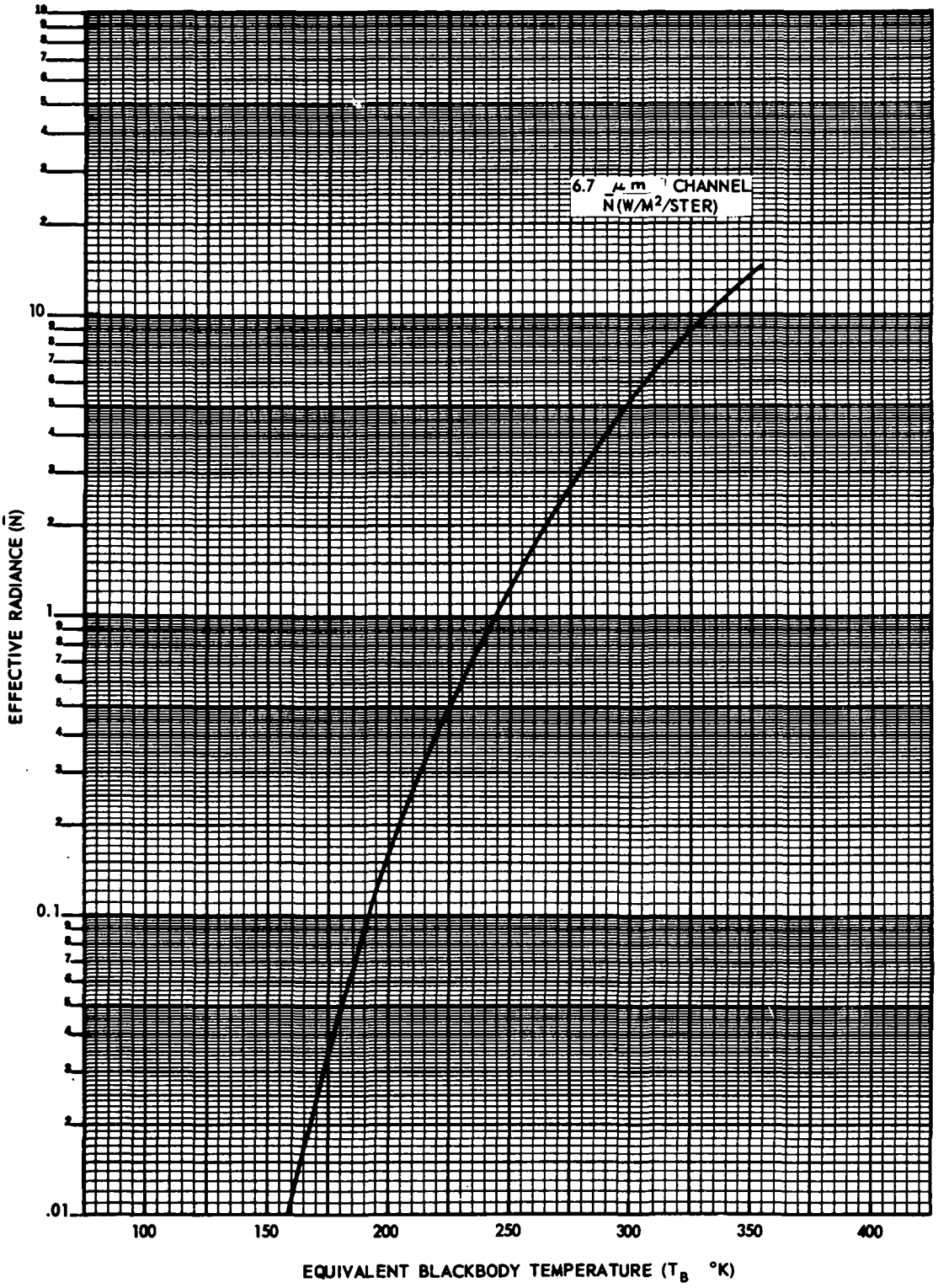

Figure 2-12. Effective Radiance versus Equivalent Blackbody Temperature for the 6.7 μm Channel

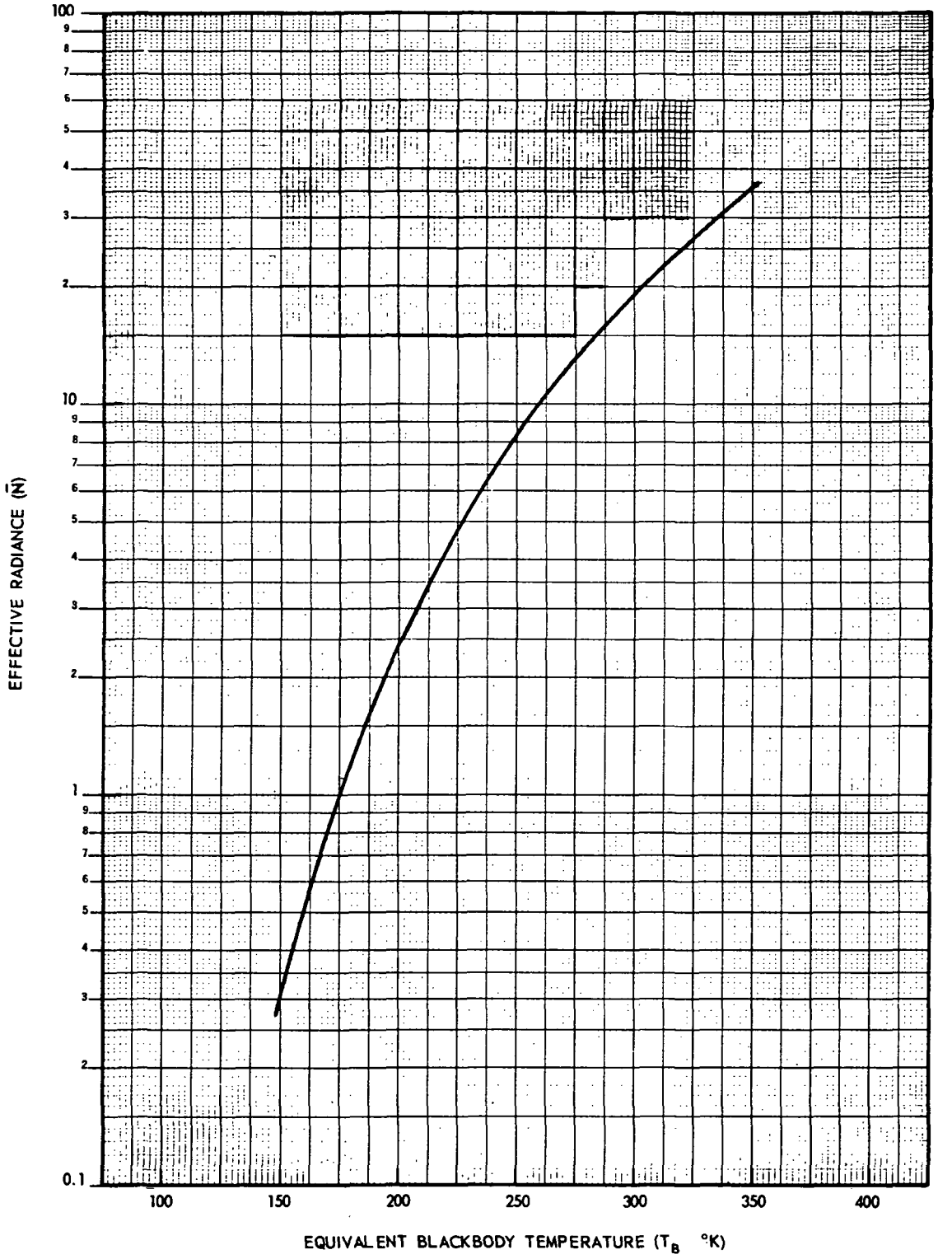

Figure 2-13. Effective Radiance versus Equivalent Blackbody Temperature for the 11.5 μm Channel

Table 2-2
Effective Radiance ($\bar{N}$) versus Equivalent
Blackbody Temperatures (T_B)

T_B °K	6.7μm Channel $\bar{N}$ (W/M^2/Ster)	11.5μm Channel $\bar{N}$ (W/M^2/Ster)
150	.0047	.3019
160	.0113	.5050
170	.0244	.7960
180	.0484	1.193
190	.0892	1.716
200	.1548	2.380
210	.2550	3.202
220	.4016	4.195
230	.6079	5.371
240	.8891	6.738
250	1.262	8.306
260	1.743	10.08
270	2.352	12.06
280	3.106	14.25
290	4.025	16.66
300	5.126	19.27
310	6.429	22.10
320	7.951	25.13
330	9.708	28.37
340	11.72	31.80
350	13.99	35.44

2.4 Data Processing, Archiving and Availability

Nimbus 5 THIR data are available from the NSSDC in three general forms: photofacsimile film strips, computer processed digital data and raw analog records. The film strips are separated into day and night files and by channels. The user has the choice of ordering positive or negative transparencies or paper print.

The form of data most readily available to the user is the film strip. Computer processing of the complex and voluminous data will be accomplished whenever requested by a user, as indicated in Section 2.4.2.

Table 2-3
THIR Output Voltages versus Equivalent Blackbody Temperature at Different Bolometer Temperatures for the 11.5 μm Channel

	11.5 μm Channel					
	HDRSS			VIP		
Bolometer Temperature	4°	17.5°	24°	4°	17.5°	24°
T_B (°K) ↓						
<190	-.520	-.520	-.520	-.520	-.520	-.520
190	-.857	-.848	-.843	-.808	-.820	-.809
200	-.952	-.975	-.940	-.904	-.946	-.909
210	-1.08	-1.10	-1.07	-1.04	-1.08	-1.04
220	-1.25	-1.24	-1.24	-1.20	-1.24	-1.21
230	-1.44	-1.43	-1.44	-1.40	-1.43	-1.42
240	-1.68	-1.66	-1.67	-1.64	-1.66	-1.65
250	-1.95	-1.94	-1.94	-1.91	-1.93	-1.92
260	-2.25	-2.25	-2.25	-2.22	-2.23	-2.23
270	-2.59	-2.59	-2.59	-2.56	-2.58	-2.57
280	-2.96	-2.95	-2.96	-2.94	-2.96	-2.95
290	-3.37	-3.36	-3.37	-3.36	-3.37	-3.36
300	-3.82	-3.81	-3.81	-3.81	-3.81	-3.80
310	-4.29	-4.29	-4.29	-4.29	-4.29	-4.28
320	-4.80	-4.78	-4.80	-4.81	-4.81	-4.79
330	-5.35	-5.33	-5.34	-5.37	-5.39	-5.34

2.4.1 Photofacsimile Film Strips

At the data acquisition site, the THIR information is demultiplexed and recorded on magnetic tape. It is then transmitted to the Goddard Space Flight Center where the FM signal is demodulated, synchronized, integrated with geographic grid marks and displayed by a photofacsimile processor. The facsimile processor converts the radiometer output signals and the grid marks into a continuous strip picture, line by line, on 70 mm film. Blanking circuits in the recorder reject unwanted sections of each scan line. Only the Earth scan and, for calibration purposes, very small portions of the space scan are recorded on the film strip. The 6.7 μm and 11.5 μm data are split and separate tape and film files compiled for user convenience. All of the THIR data are available on photofacsimile film strips.

Table 2-4
THIR Output Voltages versus Equivalent Blackbody Temperature at Different Bolometer Temperatures for the 6.7 μm Channel

	6.7 μm Channel					
	HDRSS			VIP		
Bolometer Temperature	4°C	17.5°C	24°C	4°C	17.5°C	24°C
T_B(°K) ↓						
< 190	-.540	-.540	-.540	-.540	-.540	-.540
190	-.788	-.765	-.801	-.685	-.70	-.748
200	-.916	-.828	-.944	-.821	-.84	-.886
210	-1.09	-1.02	-1.13	-1.03	-1.05	-1.08
220	-1.35	-1.35	-1.41	-1.33	-1.34	-1.37
230	-1.72	-1.79	-1.81	-1.76	-1.75	-1.79
240	-2.26	-2.35	-2.38	-2.34	-2.33	-2.37
250	-2.98	-3.08	-3.14	-3.12	-3.10	-3.14
260	-3.94	-4.07	-4.15	-4.11	-4.09	-4.13
270	-5.15	-5.36	-5.44	-5.38	-5.37	-5.39
280						
290						
300						
310						
320						
330						

Figure 2-14 is an example of portions of nighttime photofacsimile film strips from the Nimbus 4 THIR 6.7 μm and 11.5 μm channels. The data were acquired simultaneously and show a tropical storm developing over the Bay of Bengal.

2.4.1.1 Photographic Processing of Film Strips

The original photofacsimile film strips are processed by the NADUC photographic laboratory and archived at the NSSDC for safe and permanent storage. A copy created from the original film with uniform density exposure is then used as a master for producing all film strips requested by the user. Uniform or variable density exposure positive or negative film strips and paper prints are available to the THIR data user. (Uniform density film strips are produced at one, set exposure [to maintain original film temperature contrasts] while

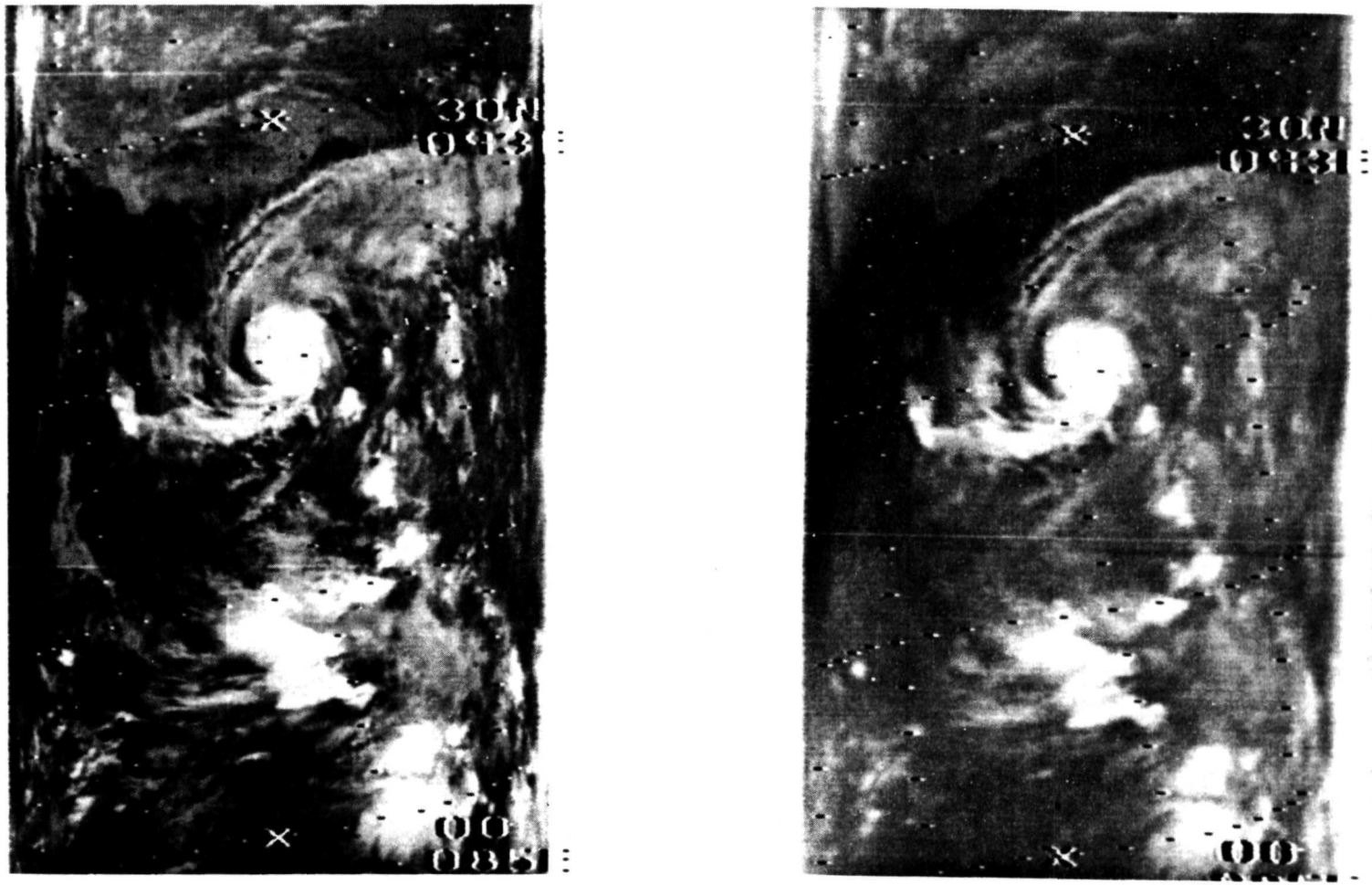

11.5 μm CHANNEL

6.7 μm CHANNEL

Figure 2-14. Simultaneously Recorded Photofacsimile Film Strips of Nimbus 4 THIR Showing a Storm in Bay of Bengal

variable density exposure processing enhances contrast between features at different temperatures and tends to produce a better "picture.") In the positive copy, lower temperatures are indicated by lighter areas, hence, the colder clouds appear white as in television pictures.

2.4.1.2 Gray Scale Calibration

The photofacsimile recorder is provided with the means for automatically producing on the film data a ten-step calibration gray scale wedge (Figure 2-15). A frequency generator provides ten distinct frequencies to the demodulator just prior to the receipt of THIR data. These frequencies which cover the dynamic range of the radiometer cause the demodulator to produce ten voltage levels which are recorded on the film. The ten levels correspond to ten equivalent blackbody temperatures on the film strips allowing a good estimate of the temperatures to be made.

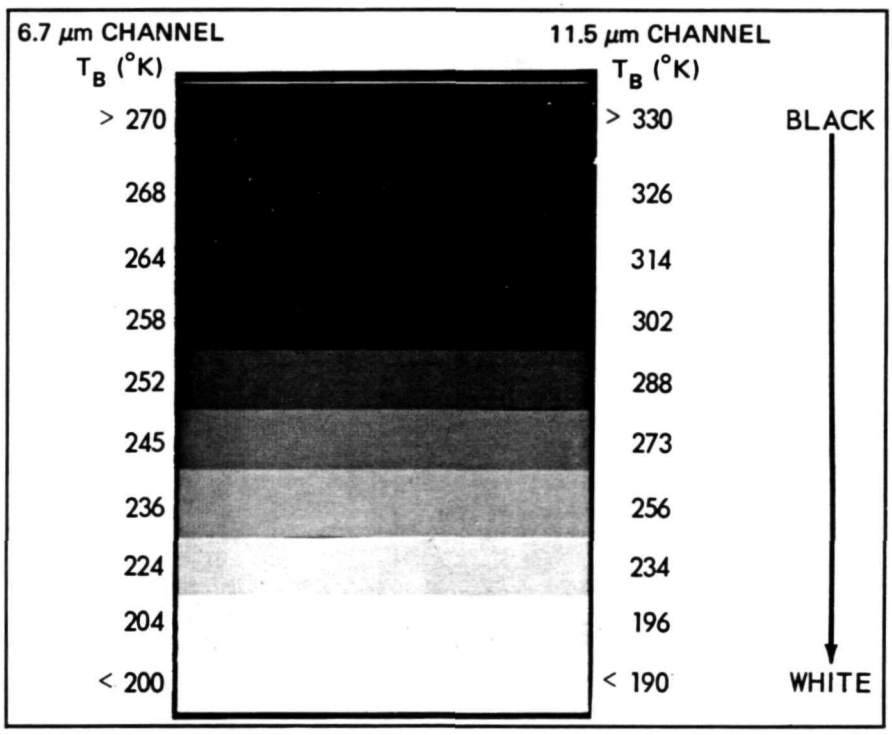

Figure 2-15. THIR Calibration Gray Scale Wedge for Positive Film. The Equivalent Blackbody Temperatures (T_B) are for an Expected Bolometer Temperature of 17.5°C

Because film processing is such that variations in density can and do occur, these values are only approximate, and accurate quantitative measurements cannot be obtained from the film.

2.4.1.3 Film Strip Identification

THIR data are archived in separate 6.7 μm and 11.5 μm daytime and nighttime swaths. Thus, the approximate coverage of a full swath is from pole to pole. Each swath is identified by a label with the data orbit number, the channel (6.7 μm or 11.5 μm) and whether it is daytime or nighttime. The nighttime swath is labeled with the orbit number followed by N. The daytime swath is identified by the ascending node orbit number (within the swath) followed by a D. Each data block is also provided with a label showing the day of the year and the correct universal time of the data scan nearest the label.

Figure 2-16 shows a film strip containing a Nimbus 4 label format, and computer produced grids with sensory data. The film strip has been gridded for daytime data. The label indicates a day (113), hour (08), minute (35), second (00), data orbit (202), daytime data (D), and that the imagery is from the 11.5 μm channel of Nimbus 4.

A series of time marks in increments of two minutes are found on the left side of the film (Figure 2-16). The first time mark for daytime data represents the first even minute after the start time given in the affixed label (for nighttime data it would represent the first even minute before the end time given in the affixed label). In Figure 2-16 the first time mark is 08:36:00 UT, the second is 08:38:00 UT, etc. The data are properly oriented when the film is held (shiny side toward the viewer) with the label at the bottom as shown in Figure 2-16.

2.4.1.4 Film Strip Gridding

The geographical location of each picture element scanned by the radiometer depends on the stability of the spacecraft. The Nimbus 5 control system has a pointing accuracy of about ±1 degree in pitch, roll and yaw. A pointing error of 1 degree corresponds to a subsatellite error of 20 km (11 n.m.) in the location of a picture element from an altitude of 1100 km (600 n.m.). On a global basis, this is an acceptable error for most meteorological analyses.

Automatic gridding of the data is accomplished by utilizing a CDC 924 computer to compute geographic coordinates, and a grid mixer which generates the grid points and adds them to the THIR data in analog form. These grid points are electronically superimposed on the film and manually checked to maintain an accuracy of better than ±1 degree of great circle arc at the subsatellite point. Referring to Figure 2-16 the grid point array makes lines for every 10° latitude and longitude, with points spaced at 2° intervals along each 10° line between 60°N and 60°S latitude. Outside of 60°N and 60°S latitude, there are latitude lines each 10°, longitude lines each 20°, latitude points each 2° and longitude points each 5°.

Figure 2-16. Nimbus 4 THIR Film Strip Grid and Label Format

A small cross is placed at the intersections of the 60°N, 30°N, 0°, 30°S, and 60°S latitude lines and the subsatellite track. The first cross from the bottom of Figure 2-16 marks the intersection of the subsatellite track and 0° at 49°E. The longitude and latitude of each cross (rounded to the nearest degree) is displayed at the extreme right (nighttime) or left (daytime) edge of the picture opposite that cross (latitude above longitude). The latitude format is XXY where $00 \leq XX \leq 90°$, and Y is N or S. The longitude format is XXXY where $000 \leq XXX \leq 180°$, and Y is E or W.

2.4.1.5 Ordering THIR Film Strips

When ordering THIR photographic data from NSSDC the following information should be given (in addition to that in Section 1.7):

- Satellite (e. g., Nimbus 5)
- Date of data
- Data orbit number, channel (11.5 μm or 6.7 μm) and whether day or night data
- Data format, i.e., positive or negative transparencies, or prints
- Exposure, i.e., uniform or variable density

2.4.2 Digital Data

Quantitative data are obtained when the original analog signals are digitized with full fidelity and the digital data are processed by an IBM 360 computer where calibration and geographic referencing are applied automatically.

A simplified block diagram of the analog-to-digital (A/D) processing system is shown in Figure 2-17. The analog magnetic tape is fed to an A/D converter which utilizes a CDC 924 computer to prepare a digital tape. This tape is then operated upon by the IBM 360 which prepares a reduced radiation data tape called the Nimbus Meteorological Radiation Tape-THIR (NMRT-THIR). The NMRT can be used to generate grid print maps or to accomplish special scientific analyses. The format of this tape, the same as for Nimbus 4 THIR, is given in Section 2.5.

An example of a grid print map presentation is shown in Figure 2-18, where the central portion of a low pressure system over Texas and Oklahoma is displayed. This map was made from Nimbus 4 THIR data. The presentation from

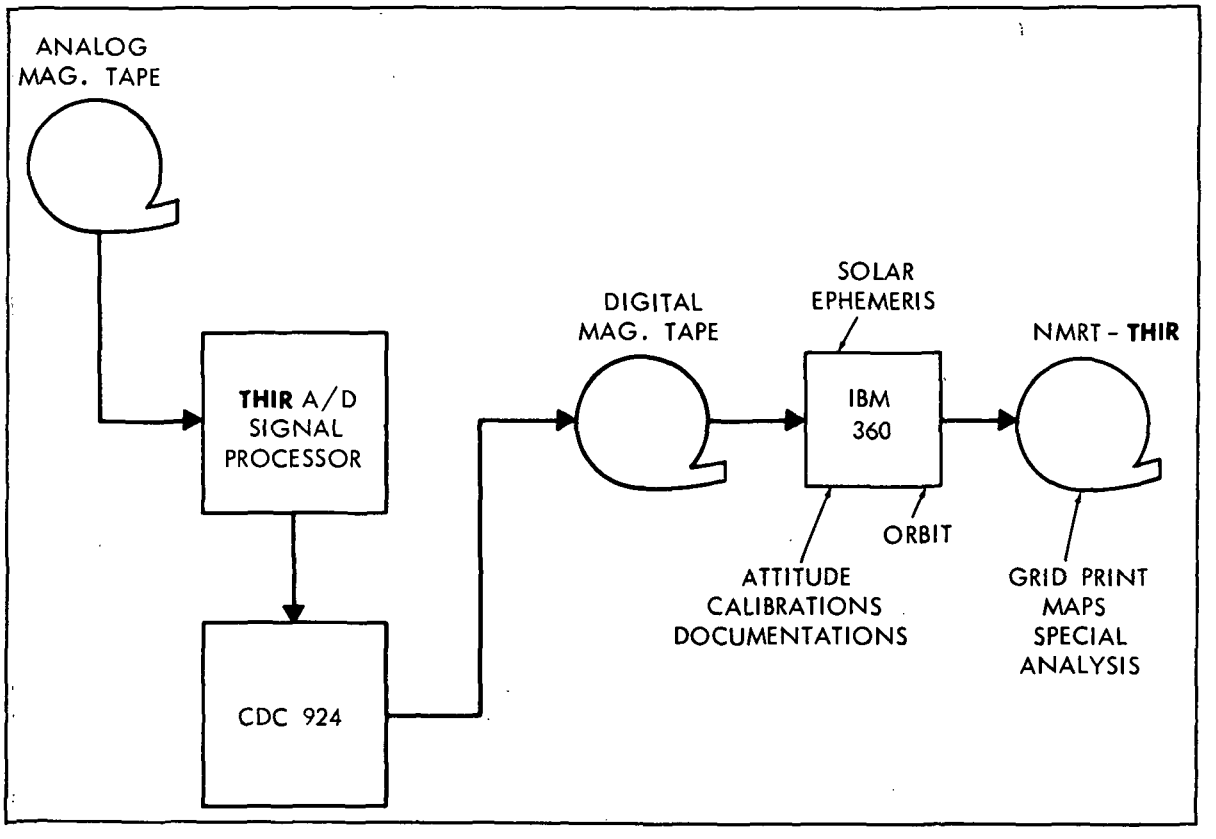

Figure 2-17. Simplified Block Diagram of the A/D Processing System

Nimbus 5 THIR is expected to be identical. The advantages of this form of presentation are the display of absolute values of temperatures in their approximate location, geographical rectification of the data, and the possibility of automatically composing measurements from consecutive orbits into quasi-synoptic maps. However, due to the scanning geometry, either a loss of detail will result from smoothing in the center portions of each swath or data gaps (being larger than the grid interval) will occur at some distance from the subsatellite point.

2.4.2.1 Availability of Processed Digital THIR Data

Due to the large volume and the long computer running time required for processing it into NMRTs, Nimbus 5 THIR digital data are not routinely reduced to final NMRT format. Only those data which are specifically requested by the user will be processed. Requests should be made through NSSDC. It is anticipated that requested NMRT-THIR will begin to be available through NSSDC six months after launch. The user is urged to make full use of the film strips which are abundantly available in nearly real-time from the NSSDC.

Figure 2-18. Computer Produced Grid Print Map of a Low Pressure System over Texas and Oklahoma Utilizing Nimbus 4 THIR 6.7 μm Data. Nimbus 5 THIR Data will have the Same Format.

A series of programs produce printed and contoured data referenced to a square mesh grid on Polar Stereographic or Mercator map bases. Grid print maps may be produced for either a single orbit or a composite of several orbits. The following standard options are available and should be specified when requesting grid print maps from NSSDC:

- Map and Approximate Scale

  1. Polar Stereographic 1/30 million

  2. Polar Stereographic 1/10 million

3. Multi-resolution Mercator maps are available down to 1/1 million scale

- Maximum Sensor Nadir Angle (50° is practical limit)

- Field Values and Contouring. Unless otherwise specified, all maps will include field values and contouring except Mercator maps of scales larger than 1/20 million. A data population map, indicating the number of individual measurements contained in each grid point average, as well as a latitude-longitude description for geographically locating the data, will be provided along with each grid print map.

When ordering grid print map data, the following identifying information should be given (in addition to that listed in Section 1.7):

- Satellite (e. g., Nimbus 5)

- Sensor (THIR)

- Channel (6.7 μm or 11.5 μm)

- Data Orbit Number

- Calendar Date of Equator Crossing

- Beginning and Ending Times of Data in GMT

- Format Desired (see 2.4.2.1, items 1, 2, 3)

When ordering NMRTs, the "Calendar Date of Equator Crossing" and "Format Desired" can be omitted.

2.4.3 Analog Data

Analog records (not shown) can be made from the original spacecraft interrogation records. These Visicorder oscillograph records permit accurate measurement of temperature as a function of time and sensor scan angle as long as the user has adequate knowledge of the workings of the instrument and all parameters involved.

However, the requirements for a comprehensive knowledge of the total THIR subsystem and the sheer volume of the data prohibits the use of this method, except for extremely special case studies.

2.5 Format of the NMRT-THIR

The Nimbus Meteorological Radiation Tape-THIR will be a basic repository for requested radiation data from the Nimbus Temperature-Humidity Infrared Radiometer. This tape will contain data in binary mode at a density of 800 bits per inch.

The first file on this tape contains a BCD label. The label consists of fourteen words of BCD information followed by an end-of-file. The remaining files on this tape contain formatted THIR data in the format described on the following pages. The first record in this data file is a documentation record which describes the data to be found in the succeeding records. This first record contains seventeen words (see Table 2-5). The remaining records in the file will be of variable length, but this length will be consistent within the file (see Table 2-6). The length (L) of the data record can be computed as follows:

L = (SWATHS PER RECORD) X (WORDS PER SWATH)
+ (NUMBER OF NADIR ANGLES) + 7

Ninety degrees are added to all latitudes and attitude data to eliminate negative signs.

Table 2-7 defines the flags which appear in the data records.

Table 2-5
NMRT-THIR Documentation Record Format

Word No.	Quantity	Units	Scaling	Remarks
1	Channel ID	Integer	B=35	Equals 115 for 11.5 μm channel and 67 for 6.7 μm channel
2	Date	MMDDYY	B=35	Date of interrogation for this orbit, i.e., 2/5/64 would be $(020504)_8$. Only the last digit of year is used.
3	Nimbus Day	–	B=35	Start time for this file of data
4	Hour	Z hour	B=35	
5	Minute	Z minute	B=35	
6	Seconds	Z seconds	B=35	
7	Nimbus Day	–	B=35	End time for this file of data
8	Hour	Z hour	B=35	
9	Minute	Z minute	B=35	
10	Seconds	Z seconds	B=35	
11	Mirror Rotation Rate	Deg/Sec	B=26	Rotation rate of radiometer mirror
12	Sampling Frequency	Samples/Sec	B=35	Digital sampling of frequency per second of vehicle time
13	Orbit Number	–	B=35	Orbit Number
14	Station Code	–	B=35	Data acquisition site identification code
15	Swath Block Size (325)	–	B=35	Number of 35-bit words per swath
16	Swaths/Record	–	B=35	Number of swaths per record
17	Number of Locator Points	–	B=35	Number of anchor points per swath for which latitudes and longitudes are computed.

Table 2-6
NMRT-THIR Data Record Format

Word No.	Quantity	Units	Scaling	Remarks
1D	Nimbus Day	–	B= 17	Start time for this record of data
1A	Hour	Z hour	B= 35	
2D	Minutes	Z minute	B= 17	
2A	Seconds	Z seconds	B=35	
3D	Roll Error	Degrees	B= 14	Roll error at time specified in words one and two.
3A	Pitch Error	Degrees	B= 32	Pitch error at time specified in words one and two.
4D	Yaw Error	Degrees	B= 14	Yaw error at time specified in words one and two.
4A	Height	Kilometers	B= 35	Height of spacecraft at time specified in words one and two.
5D	Detector Temperature	Degrees K	B= 17	Measured temperature of detector cell at time specified in words one and two.
5A	Electronics Temperature	Degrees K	B= 35	Measured temperature of electronics at time specified in words one and two.
6D	Reference Temperature A	Degrees K	B= 17	Measured temperature of housing at time specified in words one and two.
6A	Reference Temperature B	Degrees K	B= 35	
7D	Reference Temperature C	Degrees K	B= 17	
7A	Reference Temperature D	Degrees K	B= 35	

Table 2-6 (Continued)

Word No.	Quantity	Units	Scaling	Remarks
8 . . . N	Nadir Angle Nadir Angle	Degrees Degrees	B=29 B=29	Nadir angles corresponding to each locator point, and measured in the plane of the radiometer
(N+1)D	Seconds	Z Seconds	B=8	Seconds past time in words 1A & 2D for beginning of this swath.
(N+1)A	Data Population	–	B=35	Number of data points in this swath.
(N+2)D	Latitude	Degrees	B=11	Latitudes of subsatellite point for this swath
(N+2)A	Longitude	Degrees	B=29	Longitude of subsatellite point for this swath, positive westward 0 to 360°.
N+3	Flags	–	–	Reserved for flags describing this swath
(N+4)D	Latitude	Degrees	B=11	Latitude of viewed point for the first anchor spot
(N+4)A : : MD MA	Longitude Latitude Longitude	Degrees Degrees Degrees	B=29 B=11 B=29	Longitude of viewed point for first anchor spot, positive westward 0 to 360°. Latitude and longitude for Mth anchor spot
(M+1)D (M+1)A . . . K(A or D)	THIR Data THIR Data THIR Data	– – –	B=14 B=32 B=32 B=14	THIR measurements. Tag and prefix reserved for flags. Last THIR data measurement

The above data constitute what is essentially the documentation portion of a data record. These data will be followed by several blocks of data with each block representing a swath. The number of these blocks in a record as well as the size of each block is specified in the documentation record represented on the previous page.

All remaining or unused portions of a swath data block are set to zero, giving a swath block size as specified in the documentation record. The above data on this page are repeated for the number of swaths in each record.

Table 2-7
Definition of Flags Describing Each THIR Swath

Flag	Bit	Definition	Yes	No
1	35	Summary flag (all checks defined by flags 2 thru 12 are satisfactory, i.e., each flag is zero)	0	1
2	34	Consistency check between sampling rate and vehicle time is satisfactory	0	1
3	33	Vehicle time is satisfactory	0	1
4	32	Vehicle time has been inserted by flywheel	1	0
5	31	Vehicle time carrier is present	0	1
6	30	Vehicle time has skipped	1	0
7	29	Water vapor data	1	0
8	28	Sync pulse recognition was satisfactory	0	1
9	27	Dropout of data signal was detected	1	0
10	26	Window data	1	0
11	25	Unassigned		
12	24	Swath size is satisfactory when compared with the theoretical swath size	0	1
13	23	Unassigned		

Flags For Individual Measurements

Prefix	Tag	Definition	Yes	No
S	18	The particular measurement is below the earth-space threshold	1	0
1	19	Unassigned		
2	20	Unassigned		

BIBLIOGRAPHY

1. Aeronomy and Meteorology Division, 1965: Nimbus I High Resolution Radiation Data Catalog and User's Manual, NASA, Goddard Space Flight Center, Greenbelt, Maryland.

2. Allison, L. J., J. Steranka, G. T. Cherrix and E. Hilsenrath, 1972: "Meteorological Applications of the Nimbus 4 Temperature-Humidity Infrared Radiometer, 6.7 micron Channel Data", Bulletin of the Ameri. Met. Society, Vol. 53, No. 6, June 1972, pp. 526-535.

3. King, Jean I. F., "Meteorological Inferences from Satellite Radiometer." J. of Atmos. Sciences, 20, 245-250, July 1963.

4. NASA Special Publication SP-89, Observations from the Nimbus I Meteorological Satellite, 1966.

5. Nimbus Project, 1966: Nimbus II User's Guide, NASA, Goddard Space Flight Center, Greenbelt, Maryland.

6. Nimbus Project, 1966: Nimbus II HRIR Montage Catalog, NASA, Goddard Space Flight Center, Greenbelt, Maryland.

7. Nimbus Project, 1969, The Nimbus III User's Guide, NASA, Goddard Space Flight Center, Greenbelt, Maryland.

8. Nimbus Project, 1969, The Nimbus III Data Catalog, Volumes 1-5, NASA, Goddard Space Flight Center, Greenbelt, Maryland.

9. Nimbus Project, 1970, The Nimbus IV User's Guide, NASA, Goddard Space Flight Center, Greenbelt, Maryland.

10. Nimbus Project, 1970-1972, The Nimbus 4 Catalog, Volumes 1-8, NASA, Goddard Space Flight Center, Greenbelt, Maryland.

11. Nordberg, W., McCulloch, A. W., Foshee, L. L., and Bandeen, W. R., "Preliminary Results from Nimbus II," Bulletin of the American Meteorological Society, Vol. 47, No. 11, Nov. 1966.

12. Pederson, Finn, and Tetsuya Fujita: "Synoptic Interpretation of TIROS III Measurements of Infrared Radiation." Research Paper No. 19, Mesometeorology Project, Department of Geophysical Sciences, The University of Chicago, October 1963.

13. Rasool, S. I., "Cloud Heights and Nighttime Cloud Cover from TIROS Radiation Data." J. of the Atmos. Sciences, 21, 152-156, March 1964.

14. Steranka, J., L. J. Allison V. V. Salomonson, 1972: "Improvement of Synoptic Scale Moisture and Wind Field Analyses Using the Nimbus 4 THIR 6.7 μm Observations." Proceedings of the Conference on Atmospheric Radiation, AMS, Ft. Collins, Colo., Aug. 7-9, 1972, pp. 138-144.

15. Wark, D. Q., G. Yamamoto, and J. H. Lienesch. "Methods of Estimating Infrared Flux and Surface Temperatures from Meteorological Satellites." J. of the Atmos. Sciences, 19, 369-384, September 1962. (Also "Infrared Flux and Surface Temperature Determinations from ITOS Radiometer Measurements." Meteorological Satellite Laboratory Report No. 10 (1962) and Supplement thereto (1963), U. S. Weather Bureau, Washington, D.C.)

16. Warnecke, G., Allison, L., Kreins, E. and McMillin, L., A Typical Cyclone Development as Revealed by Nimbus II High Resolution Infrared and ESSA-3 Television Data, NASA X-622-68-39, January 1968.

17. Wexler, R., "Interpreation of Satellite Observations of Infrared Radiation." Scientific Report No. 1, Contract No. AF 19(604)-5968, Allied Research Associates, Inc., Boston, Mass., April 20, 1961.

18. Wexler, R. and L. J. Allison, 1972: "Radar and Nimbus 4 Infrared Measurements of the Oklahoma City Tornados, 30 April 1970", Proceedings of the 15th Conference on Radar Meteorology, Urbana, Ill., Oct. 10-12, 1972.

SECTION 3

THE SURFACE COMPOSITION MAPPING RADIOMETER (SCMR) EXPERIMENT

by
W. A. Hovis, Jr.
National Aeronautics and Space Administration
Goddard Space Flight Center

3.1 Introduction

The Surface Composition Mapping Radiometer (SCMR) for Nimbus 5 is a three channel instrument with two channels sensing terrestrially emitted radiation in the 8.3 to 9.3 (8.8) and 10.2 to 11.2 (10.7) micrometer (μm) range and one channel sensing reflected solar energy in the 0.8 to 1.1 (0.95) μm interval. Because of telemetry limitations, only two channels can be utilized at one time—either the 8.8 and the 10.7 μm channels or the 0.95 and the 10.7 μm channels. The selection of channels is by real-time or stored command and will be determined on a case by case basis by the experimenter. For nighttime operation, only the 8.8 and 10.7 μm channels will be used.

The instrument scans across the direction of the spacecraft track with a rotating mirror. The instantaneous field of view of each channel is 0.6 x 0.6 milliradians resulting in a field of view of 660 x 660 meters, in the nadir, from the projected 1100 km orbital altitude. The scan mirror rotates at 10 rps to provide contiguous scan lines with a useful scan width limited to about 800 km because of distortion and atmospheric interference.

The detectors for the two long wavelength channels are cooled by a radiative cooler to approximately 100°K. The cooler will be allowed to outgas for approximately two weeks after launch before cooling and collection of long wavelength data is begun. The 0.95 μm channel will begin operation soon after launch.

3.2 Optical Configuration

The optical configuration of the instrument is shown schematically in Figure 3-1. The large rotating scan mirror fills the 20 cm diameter primary lens of a Cassegrain telescope. The secondary lens collimates the energy to a dichroic splitter that transmits the short wavelength range. The transmitted energy is focused onto a silicon diode detector and filtered to produce the desired bandpass. The short wavelength detector and filter are matched to those used in the ERTS 1 Multi-Spectral Scanner, Band 4 (Figure 3-2).

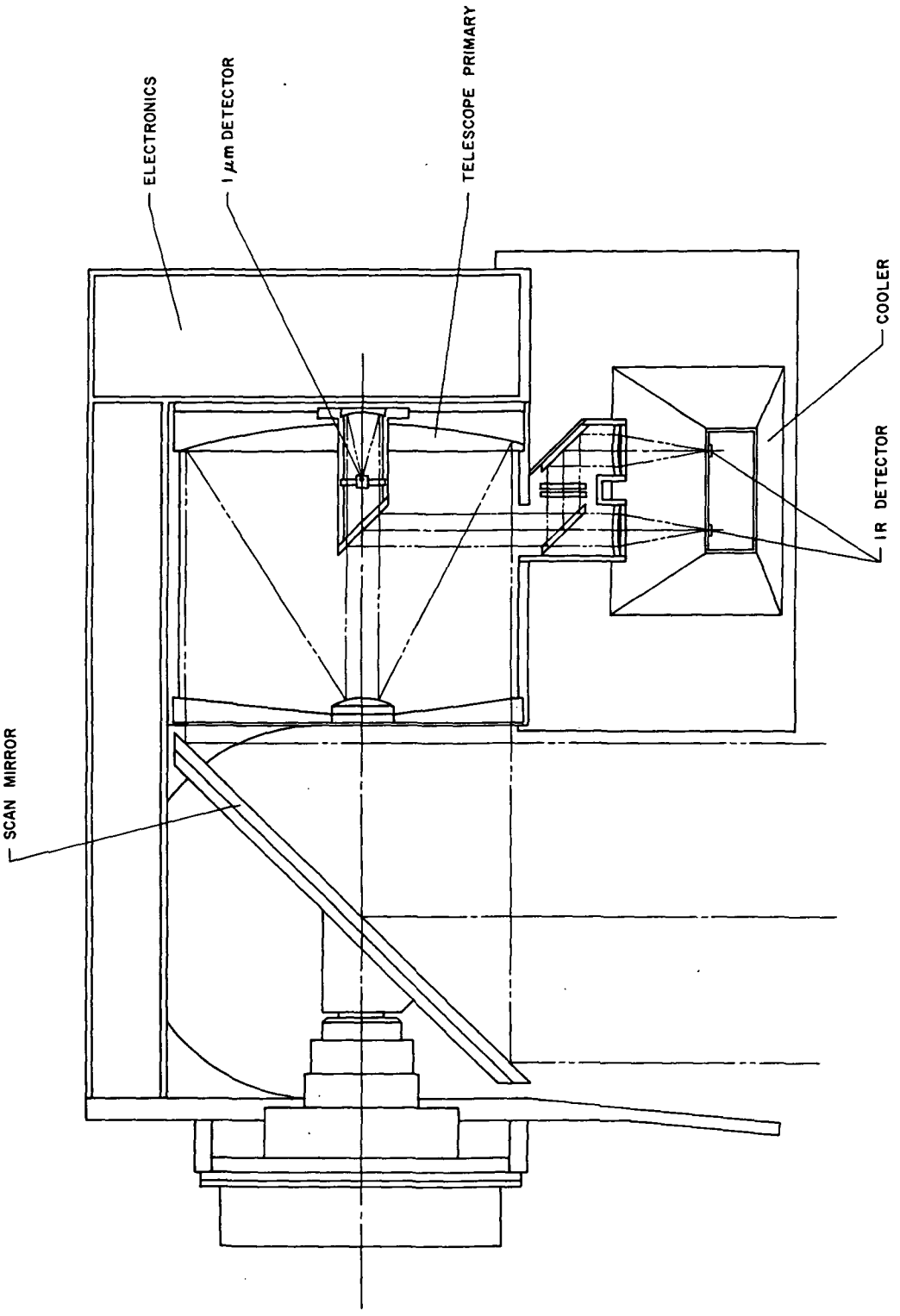

Figure 3-1. SCMR Optical Configuration

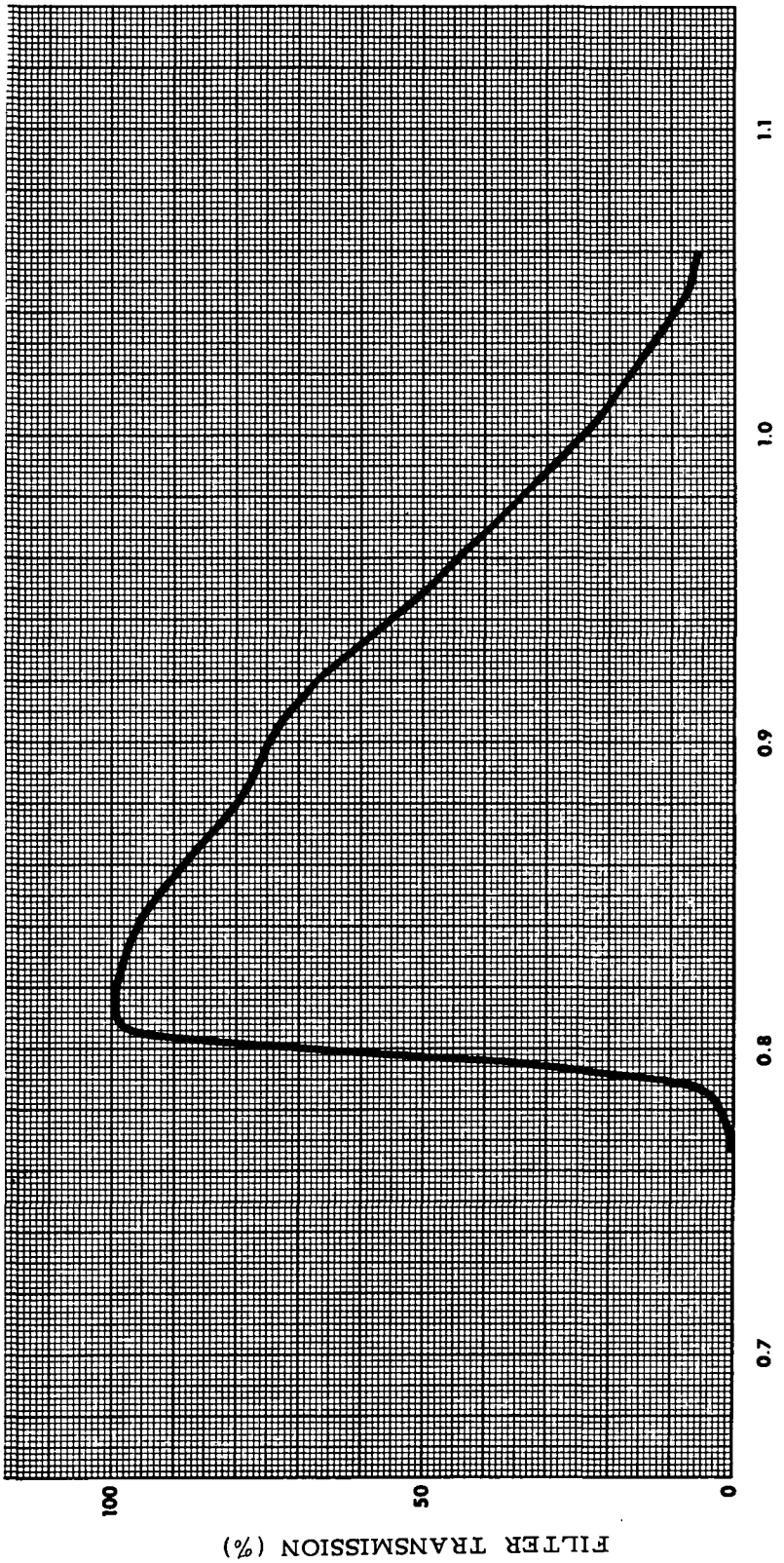

Figure 3-2. Spectral Response of 0.8-1.1 μm Channel

The reflected long wavelength energy is split again by a dichroic splitter that transmits the longer wavelength interval (10.7 μm) and reflects the shorter (8.8 μm). The longer wavelength radiation is then focused, through a filter that defines the 10.2 to 11.2 micrometer interval, onto a mercury-cadmium-telluride detector. The shorter wavelength radiation is reflected off a plane mirror and then focused, through a 9.3 to 10.3 μm filter, onto another mercury-cadmium-telluride detector. Both detectors are mounted on the patch of the radiative cooler.

3.3 Channel Selection

The 8.8 and 10.7 μm channels were selected to coincide with the reststrahlen features of acidic (high silica content) and basic (low silica content) rocks, soils, and consolidated sediments. The object is to sense the radiation in both channels, convert them to equivalent blackbody temperatures and determine if a temperature difference occurs. Since reststrahlen manifests itself as a decrease in emissivity, variable in wavelength with silica content, the polarity of the temperature difference should indicate if the surface material is acidic or basic. Figure 3-3 illustrates the effects of reststrahlen on radiated energy from a granite, representing the acidic case, and from a dunite, representing the basic case, where both are at a true temperature of 290°K. It can be seen that the minimum for granite occurs near 8.8 μm and for dunite near 10.7 μm. The 9.6 μm ozone band is shown to illustrate why the reststrahlen for intermediate materials cannot be observed.

A breadboard instrument, with the same long wavelength channels as the SCMR, was built and flown on an aircraft. Figure 3-4 shows the location of the two long wavelength channels and the laboratory measured emissivity of a sample of serpentine from Rockville, Maryland. Figure 3-5 shows the equivalent blackbody temperature, measured in the nadir, when flying over the serpentine quarry. Over trees and fields on either side of the quarry the two temperatures agree very well, while over the quarry the shorter wavelength channel produces a warmer equivalent blackbody temperature than the long wavelength channel. Since both measurements were made simultaneously, the difference is due only to the emissivity variation with wavelength.

The reststrahlen band of intermediate materials is obscured by ozone absorption, but much of the intermediate surface material is basaltic and a poor reflector of incident solar energy. The 0.95 μm channel offers the opportunity to observe surface material reflectance and detect basaltic areas.

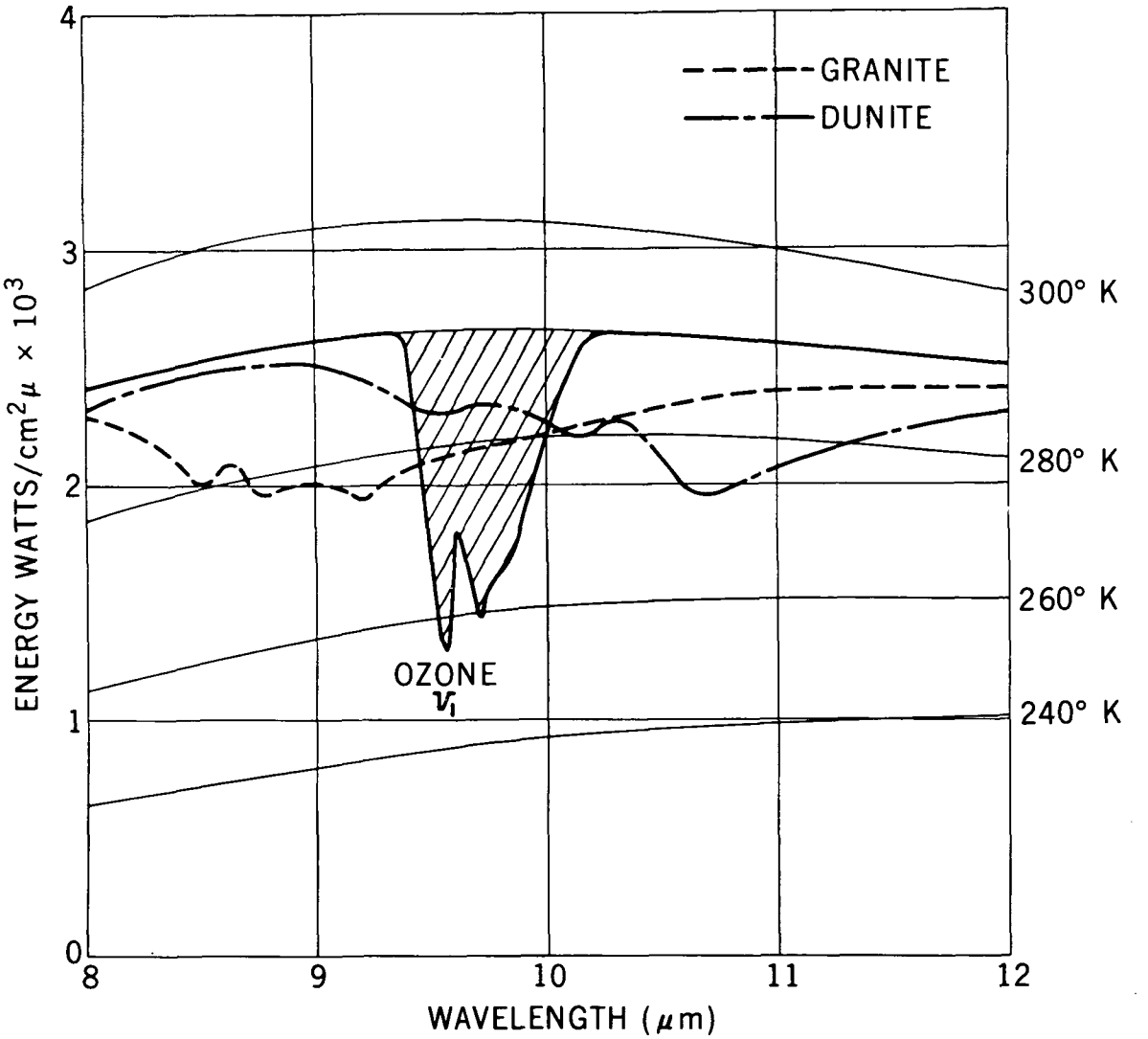

Figure 3-3. Reststrahlen Effects on Radiated Energy From a Granite and a Dunite

3.4 Operation Constraints

The SCMR data is transmitted in an analog format by an S-band transmitter on Nimbus 5. At present only five stations are equipped to receive such data. They are at Rosman, North Carolina; Goldstone, California; Fairbanks, Alaska; Honeysuckle Creek, Australia and Madrid, Spain. The acquisition circles for real time data acquired by these stations are shown in Figure 3-6.

The SCMR tape recorder will provide a maximum of 8 minutes of recording time between readouts, programmable in 1 minute intervals by stored command.

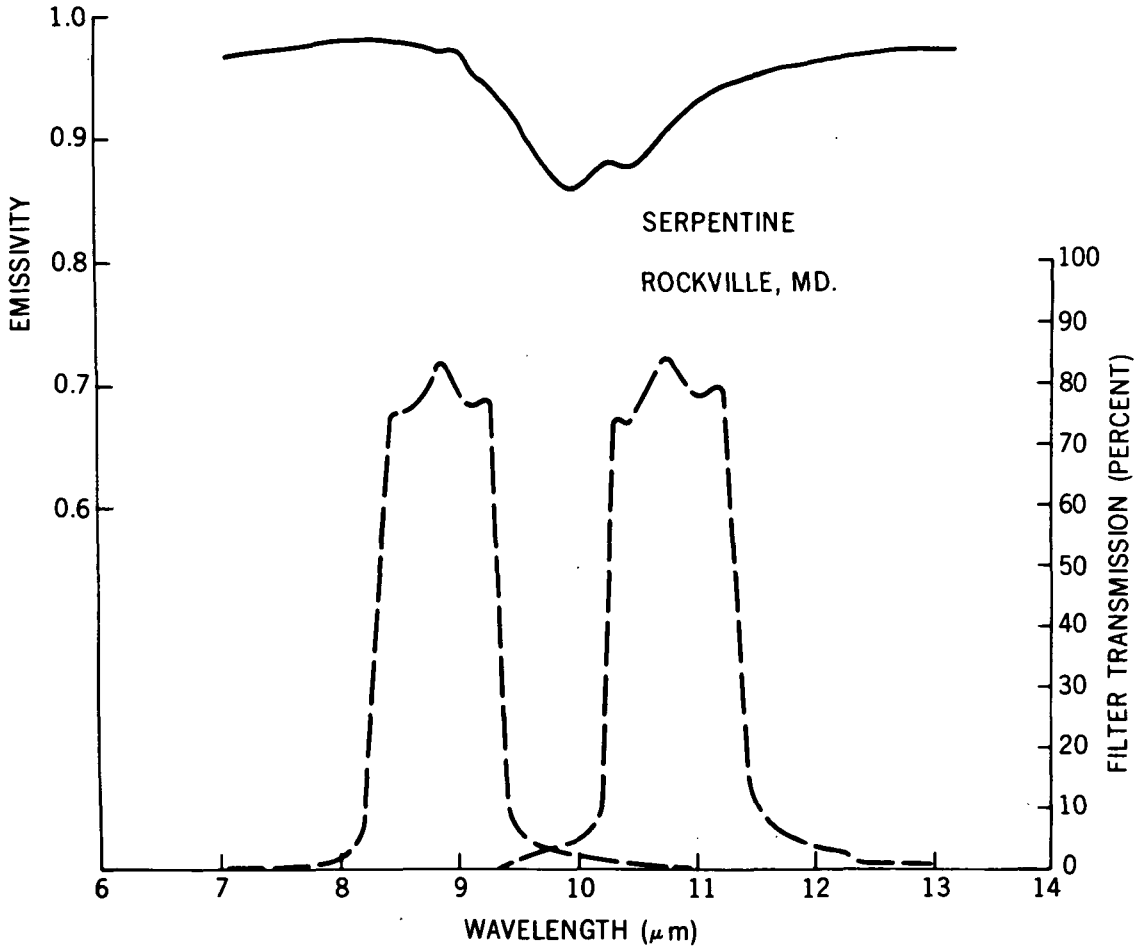

Figure 3-4. Laboratory Measured Emissivity of Serpentine Sample

Since there is only one transmitter, any time spent acquiring data stored on the tape recorder is lost for real-time data acquisition. Only data collected at Rosman can be transmitted by a wideband data link to GSFC for immediate processing. Because of data link noise, this data will not be of archival quality. Therefore, all data will be taped and sent to GSFC for archival processing.

Every attempt will be made to acquire data concerning phenomena with diurnal variations.

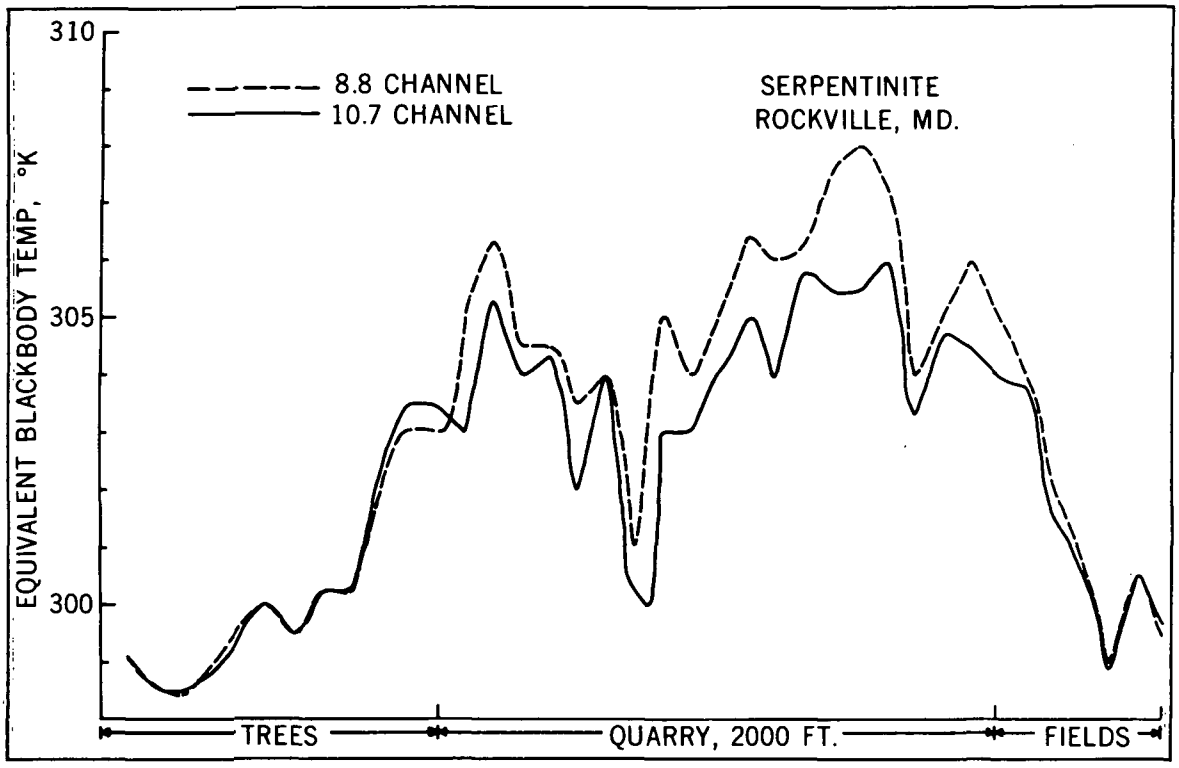

Figure 3-5. SCMR 8.8 μm and 10.7 μm Equivalent Blackbody Temperatures Over a Serpentine Quarry

3.5 Data Processing

3.5.1 Analog Data

The first product from the SCMR data will be a quick look black and white picture with 13 gray levels. This will be produced as a 4 x 5 inch picture in the MDHS. With nominal spacecraft attitude, gridding at this stage of processing will be accurate to ±0.1° in latitude and longitude near the subsatellite track. This picture can cover either horizon-to-horizon or ±37° from nadir. The gray scale is such that equal incremental excitation temperatures correspond to equal density increments from 0.3 to 1.3, representing a temperature range of from 265°K to 325°K.

For the long wavelength channels, either a simple voltage to density display or an analog voltage to temperature display will be utilized. Since in the 0.95 μm channel the output voltage is linear with respect to incident energy, only a voltage to density display will be utilized.

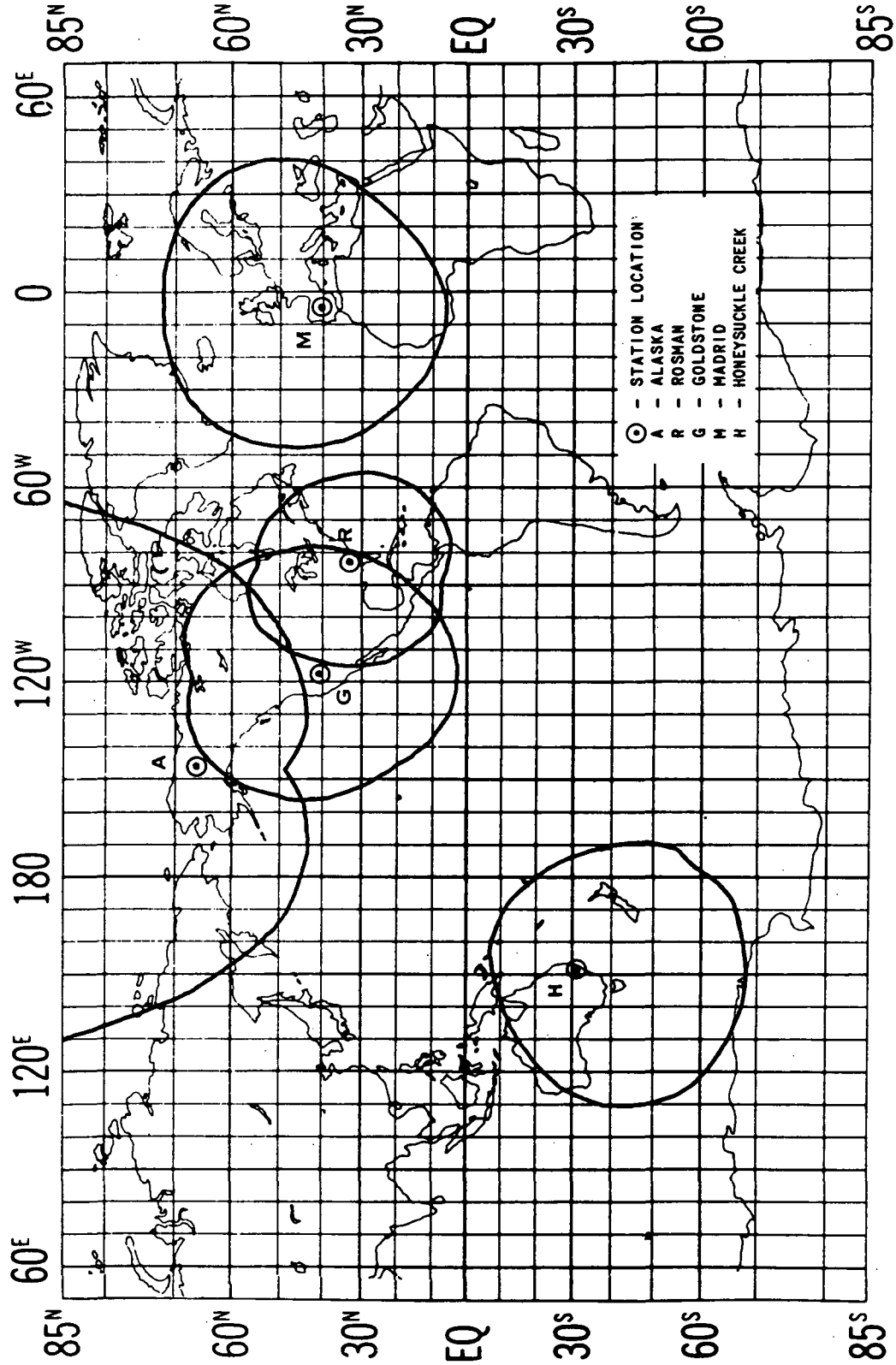

Figure 3-6. Station Data Acquisition Areas

A pictorial product showing the temperature difference between the two long wavelength channels can also be produced. In this mode, channel-to-channel temperature differences up to ±6°K are represented in the 13 step gray scale in 1° increments. More accurate differences are possible in digital processing when the inflight calibration is included.

All data received will be processed to 4" x 5" black and white pictures, and an optically reduced 70 mm roll format copy.

3.5.2 Digital Processing

The SCMR pictures will be examined and a decision made as to whether to digitize the data. The primary basis for this decision will be amount of cloud cover.

Analog data will be digitized to 8 bits and output on a 9 track 1600 BPI tape. Each record will consist of the following:

- 60 bytes of Header
- 31 bytes of Synch
- 62 bytes of Deep Space
- 93 bytes of Voltage Calibration (with instrument in the calibration loop)
- 3475 bytes of Earth Data
- 187 bytes of Voltage Calibration (with instrument out of the calibration loop)
- 137 bytes of reference blackbody
- 31 bytes of reference blackbody temperature thermistor

for each data channel exclusive of the header for a total of 8100 bytes/scan/record.

These data will then be processed by the Laboratory for Meteorology and Earth Sciences (LMES)/GSFC and a final tape consisting of temperature (for the longwave channels) or energy (for the 0.95 μm channel) and orbital information, etc. will be produced. Data will be in units of degrees Kelvin or milliwatts/cm^2 μm depending on the data channels used. The tape will be FORTRAN compatible and will contain all pertinent information. The format of this archival tape will be defined in a future Nimbus catalog.

3.5.3 Digital Display Products

A variety of computer programs are under development at the LMES which will yield the following products:

- Contoured maps
- Black and White pictures
- Color pictures

With accurate satellite ephemeris and nominal attitude data as input, the SCMR data points near the subsatellite track will be correctly gridded to within one half a resolution element. However, the data-to-grid location differences may be as much as ±11 km (6 n. m.).

3.5.4 Availability of SCMR Data

All SCMR data, photographic or digital, will be archived, initially, by the experimenter. Any requests for SCMR data and all queries on availability of SCMR data should be directed to:

Dr. Warren Hovis, Code 652
Goddard Space Flight Center
Greenbelt, Maryland 20771
Telephone: 301-982-6465

SECTION 4

THE ELECTRICALLY SCANNING MICROWAVE RADIOMETER (ESMR) EXPERIMENT

by
T. Wilheit
National Aeronautics and Space Administration
Goddard Space Flight Center

4.1 Introduction

The Electrically Scanning Microwave Radiometer (ESMR) consists of four major components:

- A phased array microwave antenna consisting of 103 waveguide elements each having its associated electrical phase shifter. The aperture area is 83.3 cm x 85.5 cm. The polarization is linear, parallel to the spacecraft velocity vector.
- A beam steering computer which determines the coil current for each of the phase shifters for each beam position.
- A microwave receiver with a center frequency of 19.35 GHz and an IF bandpass of from 5 to 125 MHz; thus it is sensitive to radiation from 19.225 to 19.475 GHz, except for a 10 MHz gap in the center of the band.
- Timing, control, and power circuits.

The unit is arranged to scan perpendicular to the spacecraft velocity vector beginning 50° to the left of nadir and scan, in 78 steps, to 50° to the right of nadir every four seconds. The beam width is 1.4° x 1.4° near nadir and degrades to 2.2° crosstrack x 1.4° downtrack at the 50° extremes. For a nominal orbit of 1100 km altitude, the resolution will be 25 km × 25 km near nadir degrading to 160 km crosstrack × 45 km downtrack at the ends of the scan, as shown in Figure 4-1.

The area viewed by the instrument for two successive orbits is shown in Figure 4-2. Here the extent of the overlap between orbits can be seen. Since the orbit to orbit coverage overlaps at the equator, complete global coverage can be obtained in 12 hours counting both day and night portions of the orbit.

Brightness temperatures are measured at each scan position which, when properly displayed, will produce a microwave image of the portion of the earth

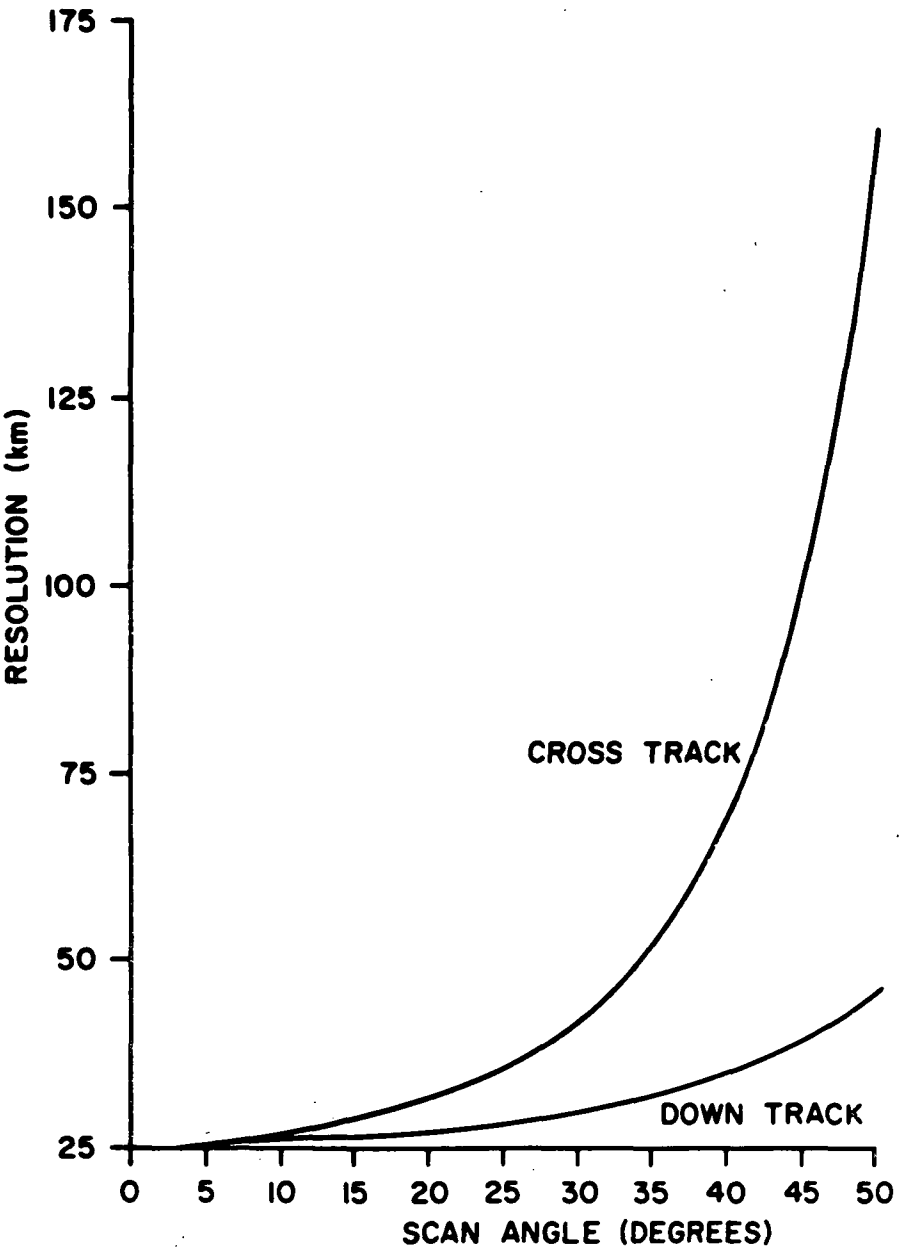

Figure 4-1. ESMR Resolution

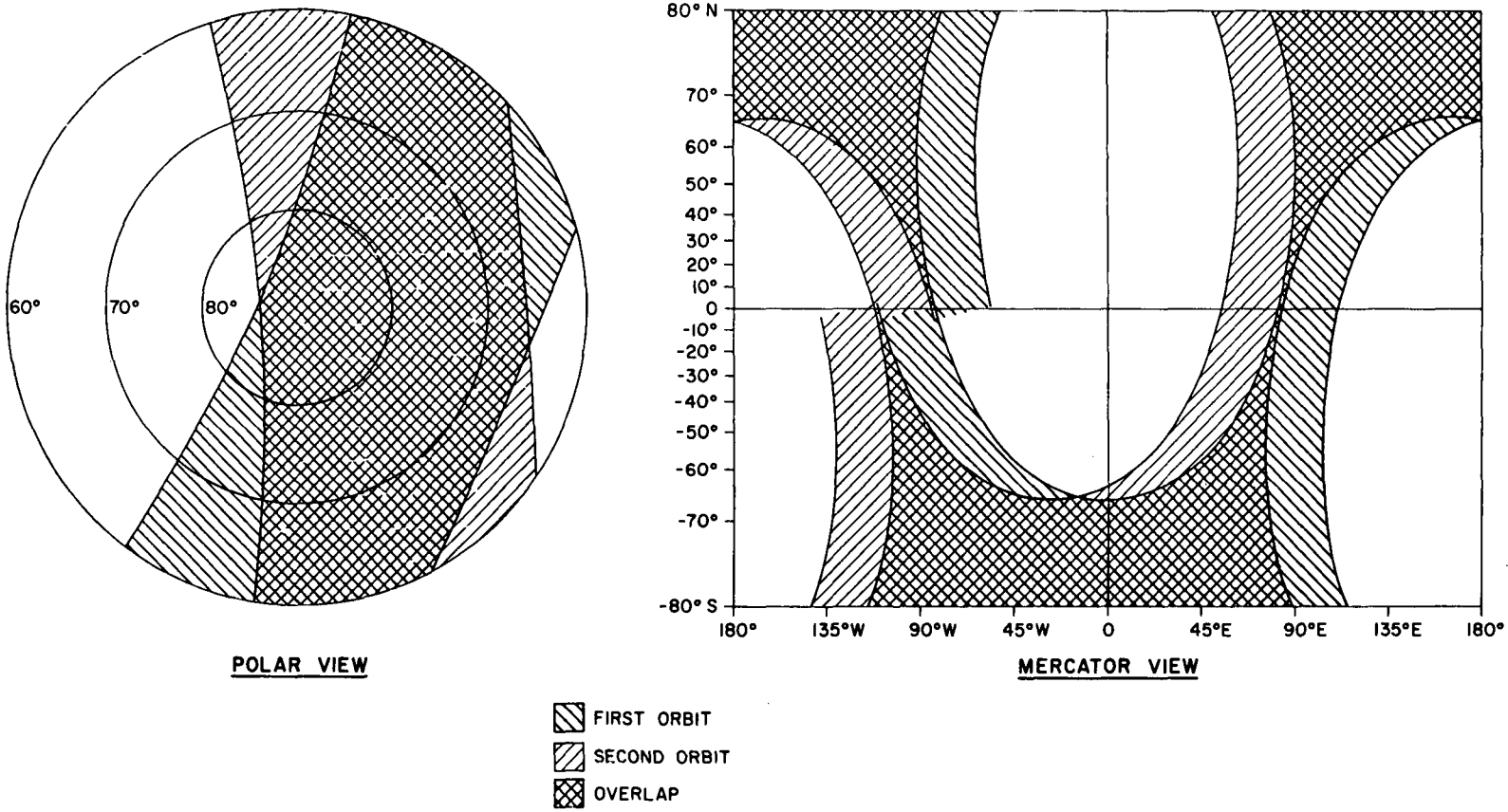

Figure 4-2. Expected ESMR Coverage

near the satellite track. The most obvious feature of these images will be the outline of the continents. However, with some understanding of the physics involved, information concerning ice cover, hydrologic features, cloud liquid water content and areas of rain can be gleaned from these data.

4.2 Physics of Microwave Radiative Transfer

At microwave frequencies (1-500 GHz) and at temperatures typical of the Earth and its atmosphere (200-300°K), the Rayleigh Jeans approximation for the intensity of thermal radiation from a blackbody works quite well; thus the equation of radiative transfer for an isotropic, non-scattering medium may be written

$$\frac{d\,T_B\,(\theta,\phi)}{dX} = \gamma\,[\,T\,(X) - T_B\,(\theta,\phi)\,]\ , \qquad (1)$$

where $T_B\ (\theta,\phi)$ is the radiance in the particular direction (θ, ϕ) expressed as equivalent blackbody temperature, T (X) is the thermodynamic temperature of the absorbing medium and γ is the absorption coefficient in units of X^{-1}. The derivitive on the left side is along a ray path. The physical meaning of this equation is made clear if we examine the effect on microwave radiation incident at an angle θ, on an absorbing slab of uniform temperature, T_o, absorptivity γ_o, and of thickness δ as shown in Figure 4-3. The radiation coming out the other side consists of the incident radiation as attenuated by the slab $T_B\ e^{-\gamma_o \delta \sec\theta}$ + a reradiation component $(1-T_B\ e^{-\gamma_o \delta \sec\theta})\ T_o$. If the expression $\gamma_o \delta \sec\theta$ is quite small or if $T_o - T_B$ is small, the slab has no effect on the intensity of the radiation; whereas, if the slab is opaque ($\gamma_o \delta \sec\theta = \infty$) the radiation emerging is characterized by the thermodynamic temperature of the slab independent of the intensity of the incident radiation.

In the atmospheric case there are three major contributors to γ: water vapor, liquid water, and molecular oxygen. In Figures 4-4, 4-5, and 4-6 we show the approximate magnitude of each of these contributions. Detailed discussions of each of these can be found in References 3, 8 and 12. In Figure 4-7, we show schematically the typical microwave Earth-viewing geometry. The observed brightness temperature is

$$T_B = \int_0^H T\,(h)\ \frac{dt\,(h)}{dh}\ dh\ +\ t\,(H)\ [\,\epsilon T_0 + (1-\epsilon)\,T_s\,]\ , \qquad (2)$$

where $t(h) = e^{-\int_0^h \gamma(x)\sec\theta\,dx}$, T(h) is the atmospheric temperature profile, H is the altitude of the observation, ϵ the emissivity of the surface and T_o the thermodynamic temperature of the surface. The reflected sky temperature contribution,

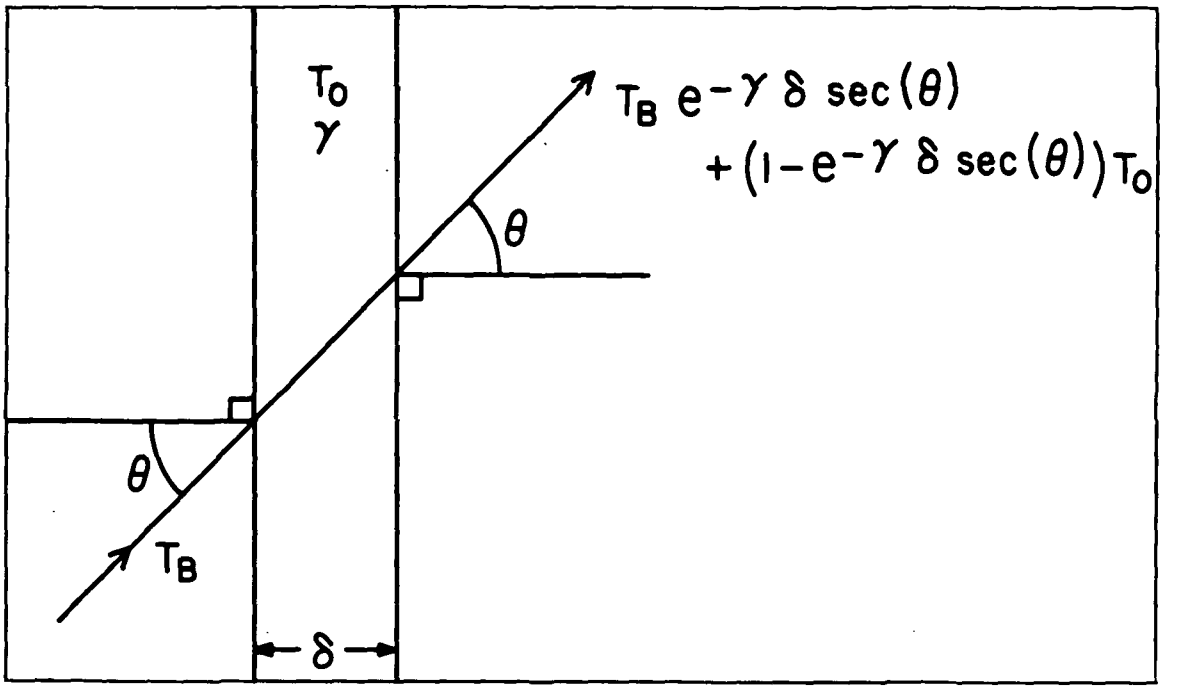

Figure 4-3. The Effect on Microwave Radiation at an Angle, θ, on an Absorbing Slab of Uniform Temperature, Absorptivity, and Thickness

T_s, must be averaged over the appropriate distribution of angles since few natural surfaces are specular reflectors of microwaves.

$$T_s = \frac{\int T_z(\theta, \phi)\, P(\theta, \phi)\, d\Omega}{\int P(\theta, \phi)\, d\Omega} \tag{3}$$

where $T_z(\theta, \phi)$ is the downwelling radiation intensity from the direction (θ, ϕ) and $P(\theta, \phi)$ is the probability of radiation from the direction (θ, ϕ) being reflected from the surface in the direction of the radiometer. The integral in the denominator makes the normalization of P arbitrary.

Unfortunately, there is little data or theory available to help in determining this distribution so we must resort to approximation. The simplest approximation is to assume a specular surface, i.e., ignore the roughness of the surface. On the other hand, we can assume that the surface is infinitely rough and apply the Lambertian approximation (Reference 10)

$$P(\theta, \phi) = \cos\theta. \tag{4}$$

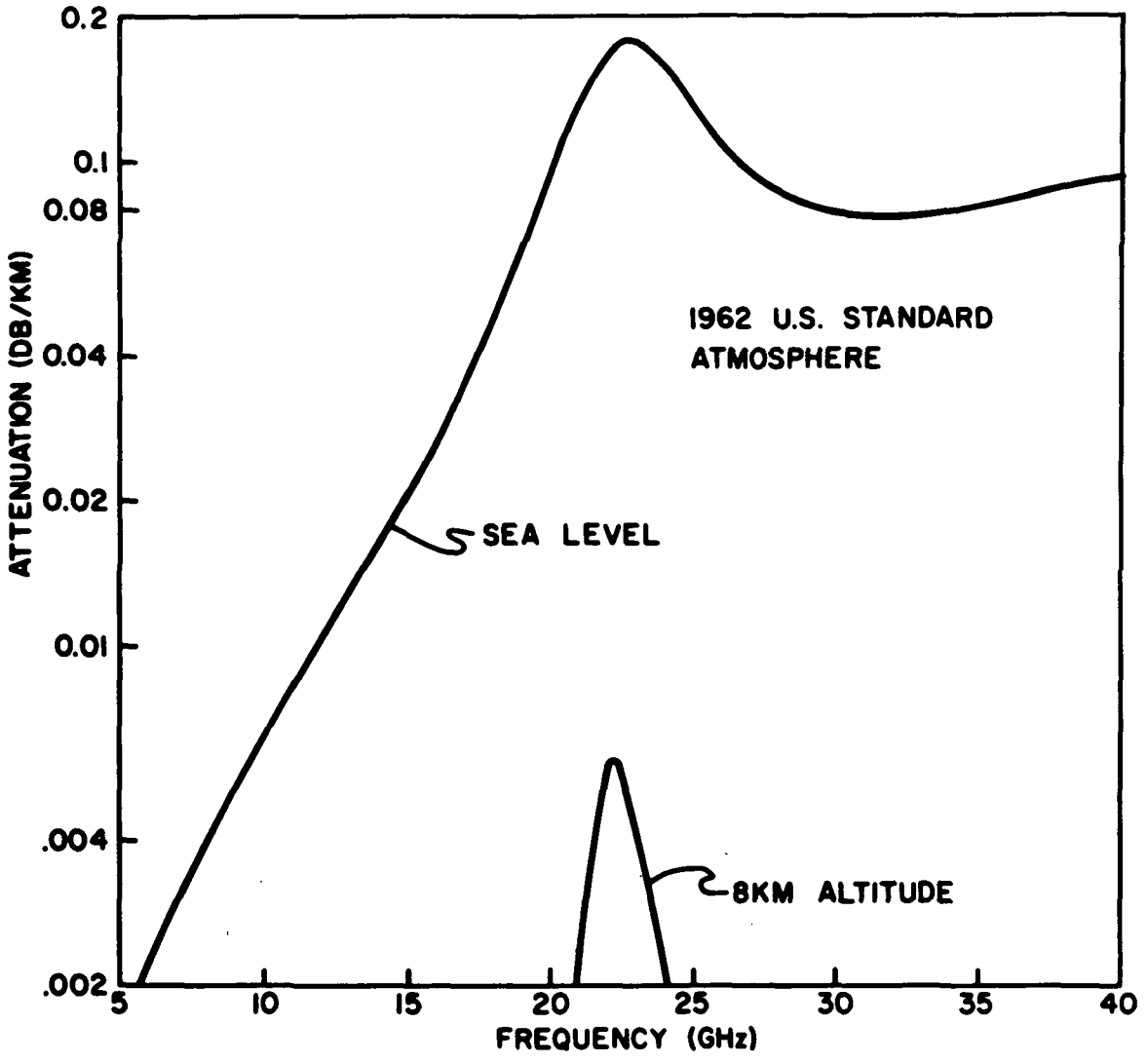

Figure 4-4. Microwave Attenuation Due to Atmospheric Water Vapor

Most real situations would lie somewhere between the specular and the Lambertian approximations. However, due to the multiplicity of effects altering the microwave signature of the Earth and its atmosphere, the consequence of choosing either approximation is lost in the overall uncertainties.

At the operating frequency of the ESMR (19.35 GHz) and of the two low frequency channels of NEMS (22.235 GHz and 31.4 GHz) the variations in ϵ dominate the variations in T_B over the earth's surface. The major contribution to variations in ϵ is liquid water with its extremely large dielectric constant at microwave frequencies. Figure 4-8 shows the real part k' and the imaginary part k'' of the dielectric constant of both fresh and sea water at 20°C as calculated

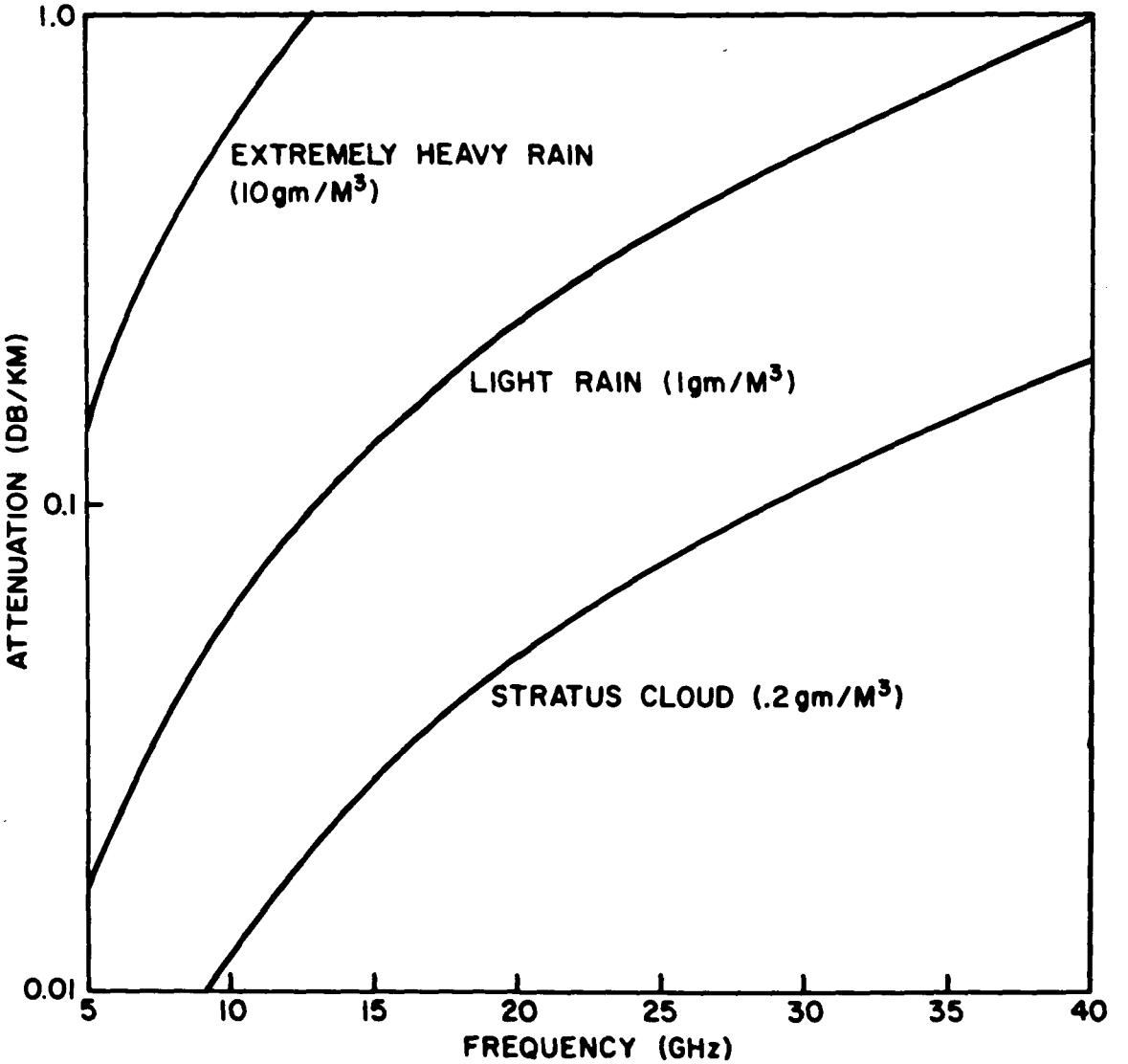

Figure 4-5. Microwave Attenuation Due to Liquid Water (Approximate)

from Reference 7. The conductivity data were obtained from Reference 5 and are included as a contribution to k'' in Figure 4-8.

If a smooth water surface is assumed, the emissivity can be calculated for any angle and polarization from simple electromagnetic theory (Reference 6). Figure 4-9 shows the emissivity as a function of frequency at 20°C for sea and fresh water for viewing directly at the nadir and for viewing at 45° in both vertical and horizontal polarization. Note, in particular, that at the ESMR frequency of 19.35 GHz, there is essentially no sensitivity to the salinity; fresh and sea water are indistinguishable. The dielectric constant of water is a function of temperature as well as frequency and salinity. In particular, at the ESMR frequency, the emissivity varies very nearly as 1/T so that the brightness

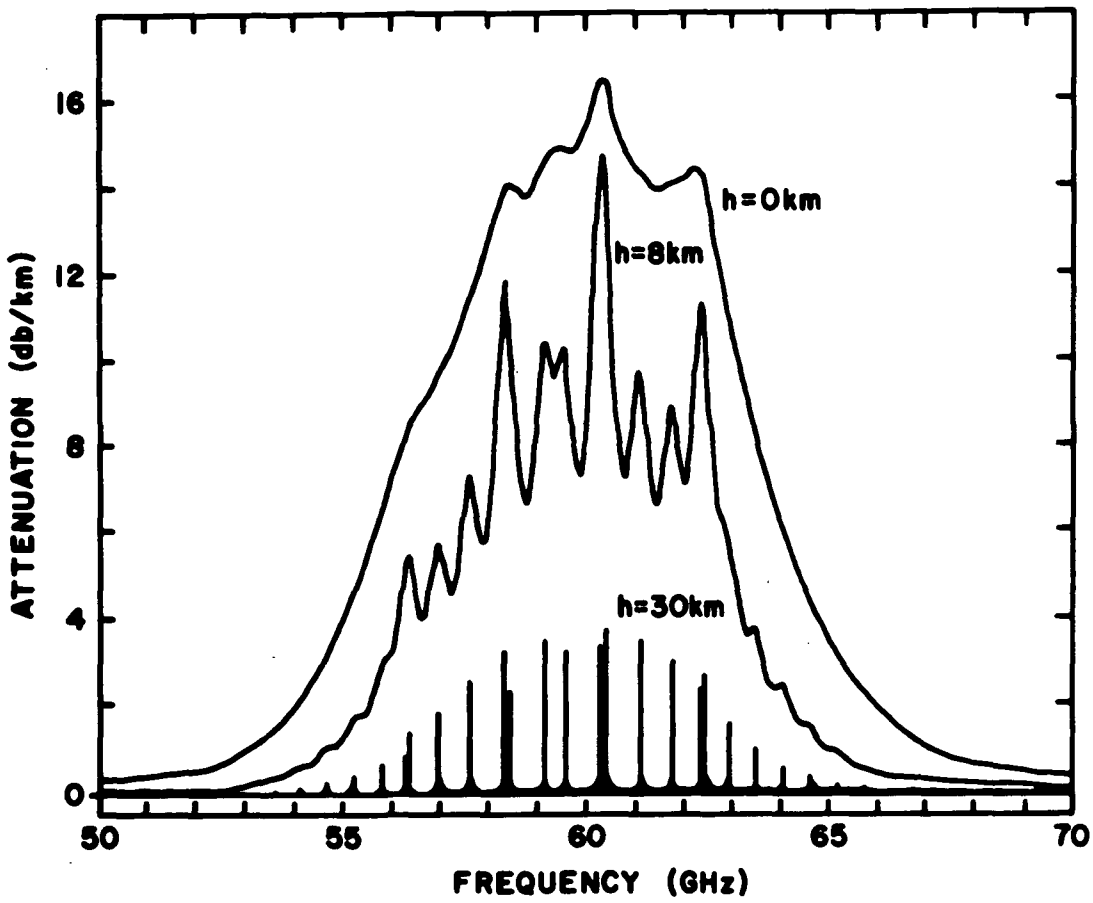

Figure 4-6. Microwave Absorption by Atmospheric Oxygen from Meeks and Lilley J. Geophys. Research, 68, 1683 (1963)

temperature of a smooth water surface is virtually independent of the thermodynamic temperature of water. The emissivity of the sea surface does, however, depend on the roughness and foam cover and thus on the wind at the surface. This has been studied theoretically (Reference 13) and experimentally (References 2, 4, 9, 14). Figure 4-10 shows the strength of the effect for nadir viewing at 19.35 GHz as given in Reference 9. In that paper, it is concluded that, at least at the nadir, the dominant effect is foam coverage. As will be seen later in this discussion, the microwave effect is not distinguishable from cloud and water vapor effects, at least with a single frequency measurement, so wind speeds are only obtainable where independent information on cloud cover and water vapor is available.

The emissivity of a land surface is typically greater than 0.9 so the brightness temperature contrast between land and water is greater than 100°K; therefore, the outlines of the continents will be quite visible in the ESMR images.

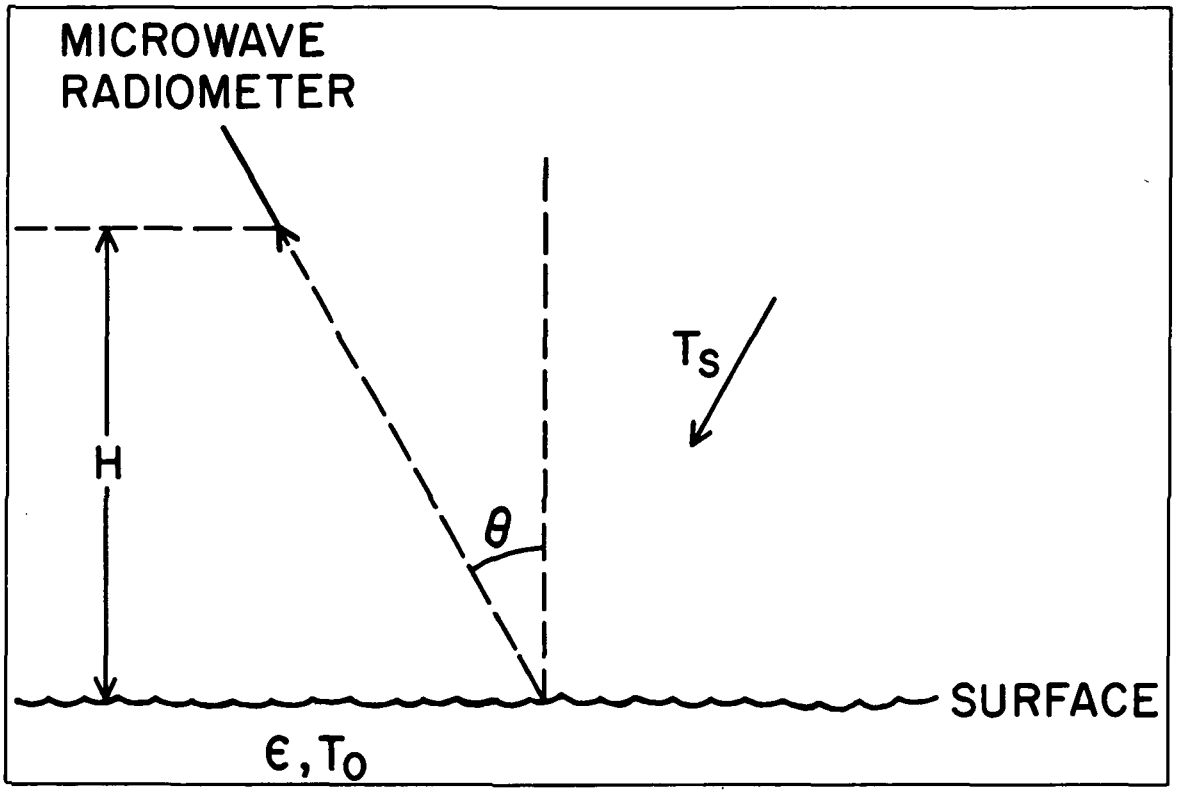

Figure 4-7. Typical Microwave Earth-Viewing Geometry

This will provide a convenient geographic reference but little scientific value. However, in areas with little vegetation, the moisture content of the soil affects the microwave signature markedly. Figure 4-11 (from Reference 11) shows data taken with the aircraft model of the ESMR on two flights over test fields near Phoenix, Arizona. Note that for this soil (a clay loam) the brightness temperature decreases rapidly for soil moisture values greater than about 20% by weight. There is a large scatter in the data but soil moisture estimates to the nearest 5% are possible in the 20-40% range. Such measurements may provide useful information in the arid regions where large areas with little vegetation are found.

In contrast with soils, the liquid water content of snow seems to increase the radiometric brightness (Reference 2). Very dry snow, less than 1% free water content by volume, showed anomalously low emissivities, less than 0.5 at 26 GHz, whereas moist snow, greater than about 5% free water content by volume, showed emissivities greater than 0.9. This effect has been qualitatively observed at 19.35 GHz (Reference 15). The effect is not understood theoretically nor adequately characterized experimentally, as yet. Nonetheless, it offers an interesting possibility of observing the onset of melting of the snow in the spring, and of mapping the snow cover in winter.

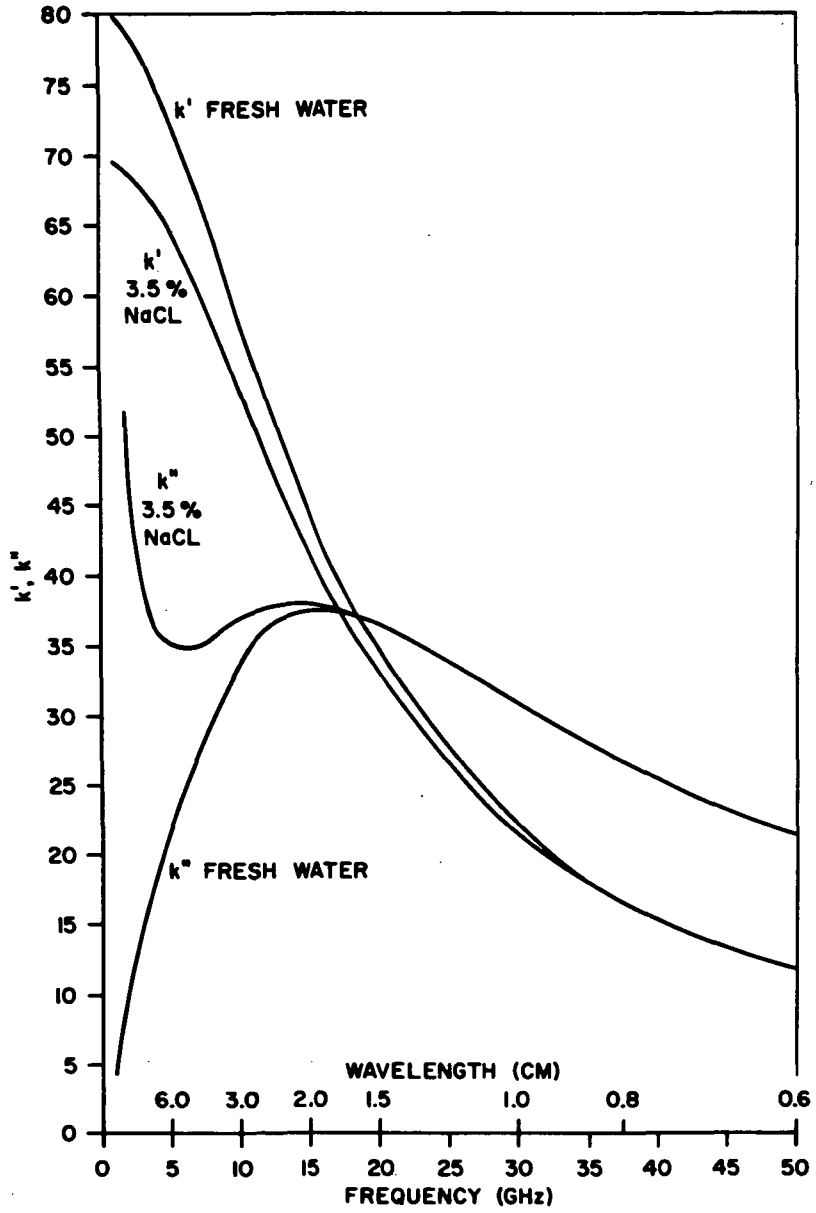

Figure 4-8. Dielectric Constant of Water k = (k'+ik") at 20°C

Like land/water boundaries, ice shows a significant emissivity contrast with water but unlike the case of land/water boundaries, ice/water boundaries are quite variable and their locations are definitely of interest to the meteorological and maritime communities. These features are frequently covered with clouds which makes visible or infrared remote sensing difficult; it is expected that these clouds will rarely, if ever, be dense enough to alter significantly the microwave images. The ice/water boundary has been observed through clouds

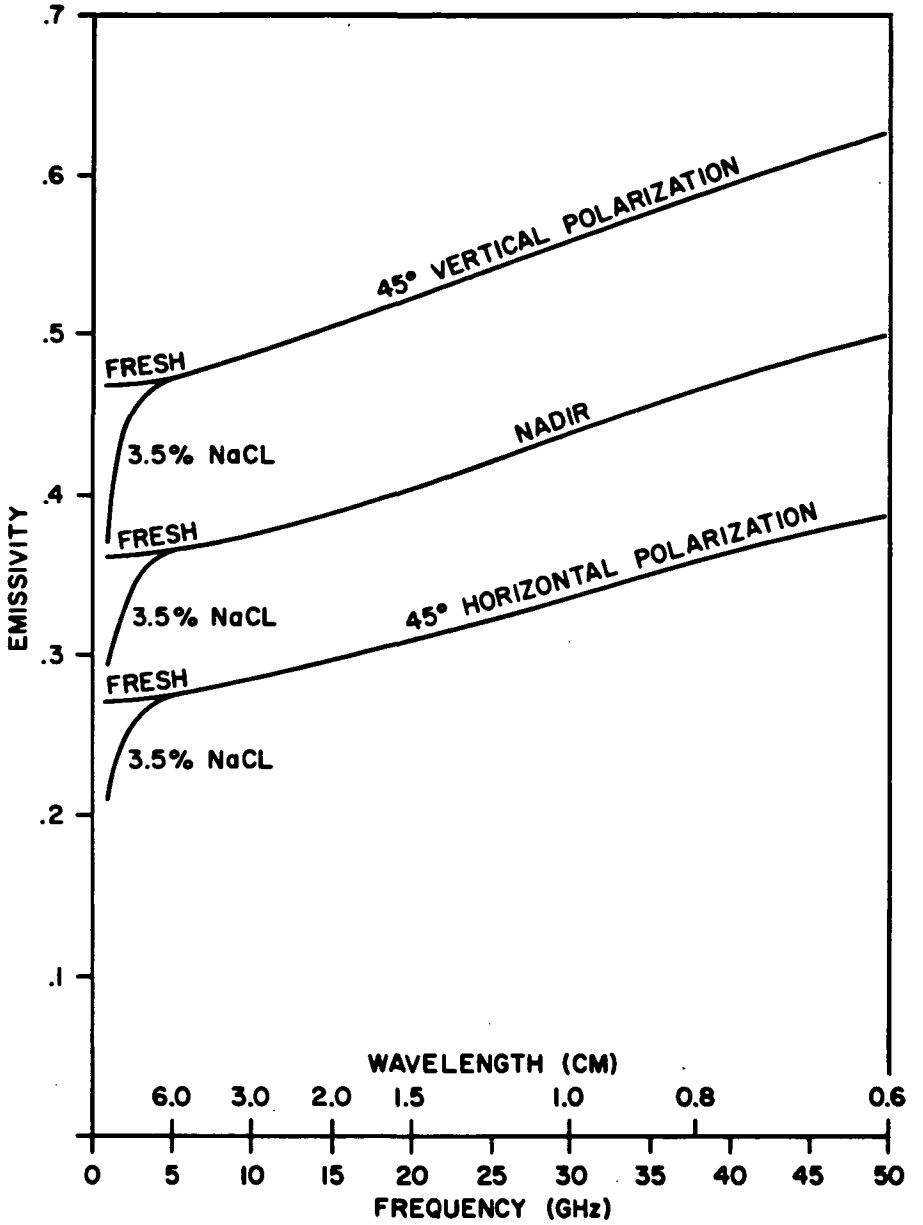

Figure 4-9. Emissivity of Water at 20°C

(Reference 15). The sea itself has been observed to have emissivity variations (Reference 15). These variations, at this point, are thought to be related to age, first year ice being more emissive than multi-year ice. Figure 4-12 shows the spectral nature of these two types of ice. Note that the contrast between the two ice types seems to increase linearly with frequency and amounts to about 12% at 19.35 GHz. This is about 20% of the contrast between new ice and open water; therefore, in the non-beam filling situation, this effect will contribute

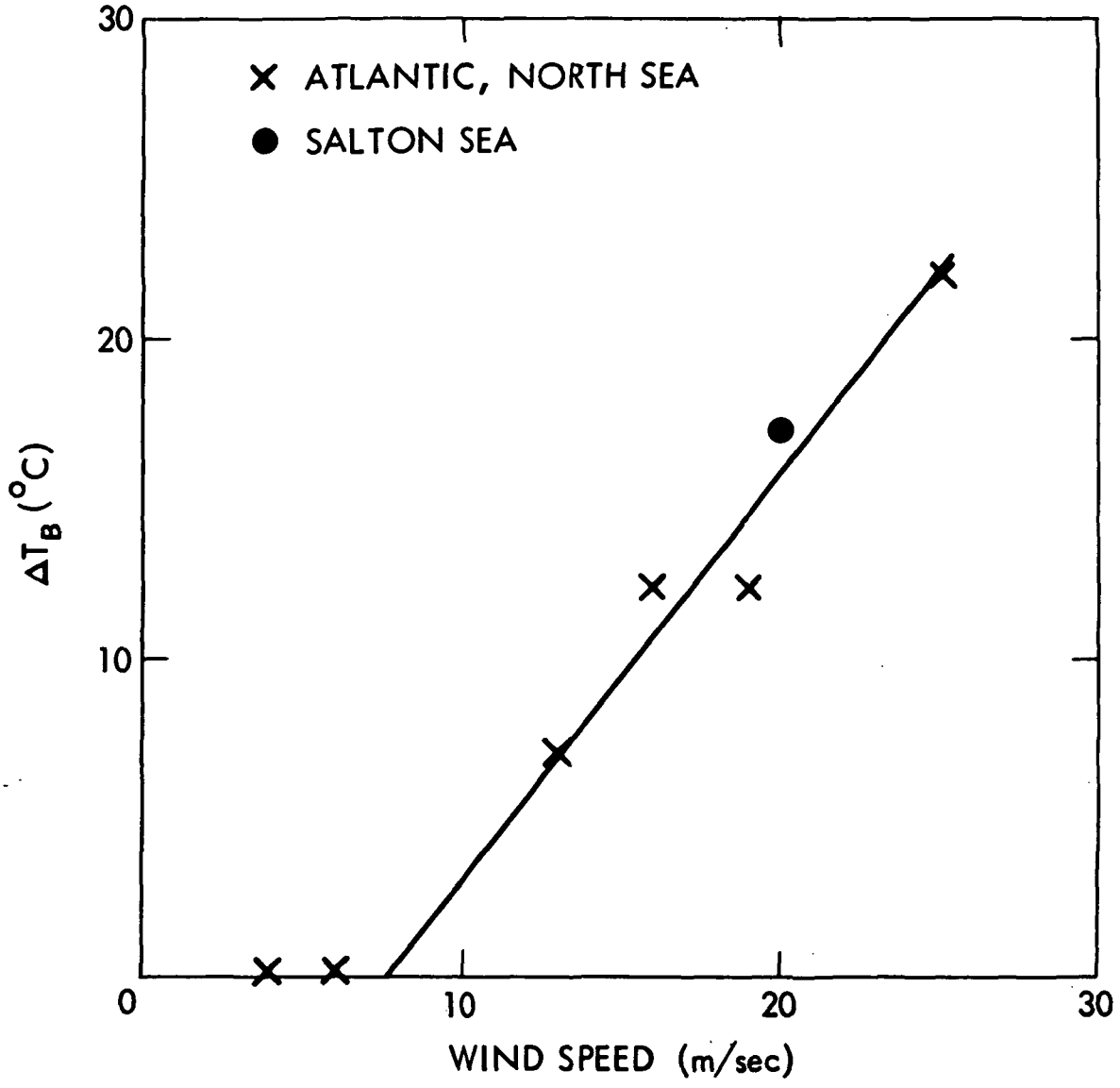

Figure 4-10. Wind Speed Versus Temperature of a Sea Surface

about 10% uncertainty to estimates of the percentage of ice within one resolution element.

Over the oceans, the variations in the atmospheric water content will cause significant variations in the microwave brightness. If we assume the ocean is a Lambertian reflector (Reference 10) we can calculate the dependence of the brightness temperature on the atmospheric water content. There is some variation due to the vertical distribution but the results are summarized by

$$T_B = 125^\circ K + AV + BL, \quad (5)$$

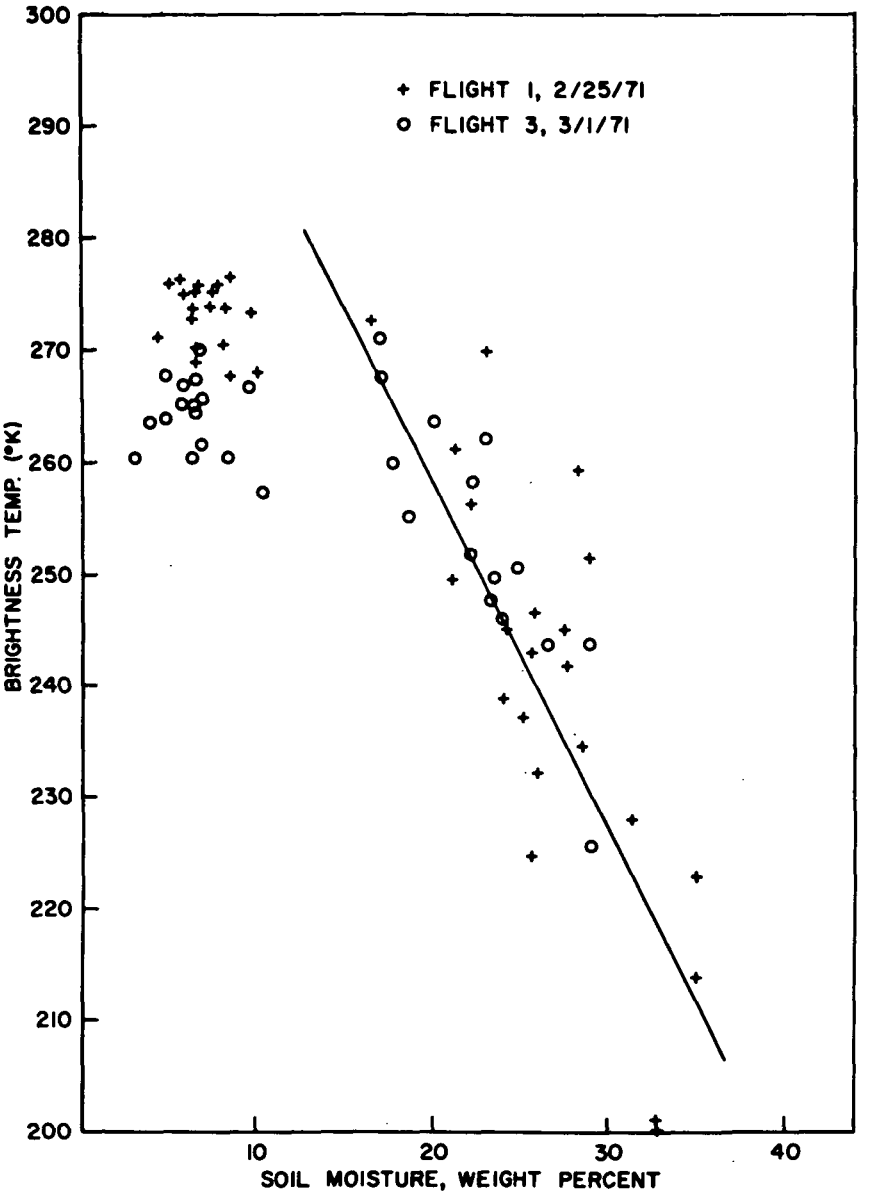

Figure 4-11. Brightness Temperature Results of Bare Fields with Clay Loam Soils, 1.55 cm Radiometer, Phoenix, Arizona

where V is the net amount of water vapor in a vertical column, L is the net liquid water in the form of non-raining clouds in a vertical column, and

$$A = 6.8^\circ \text{ K/gm/cm}^2$$

and

$$B = 300^\circ \text{ K/gm/cm}^2$$

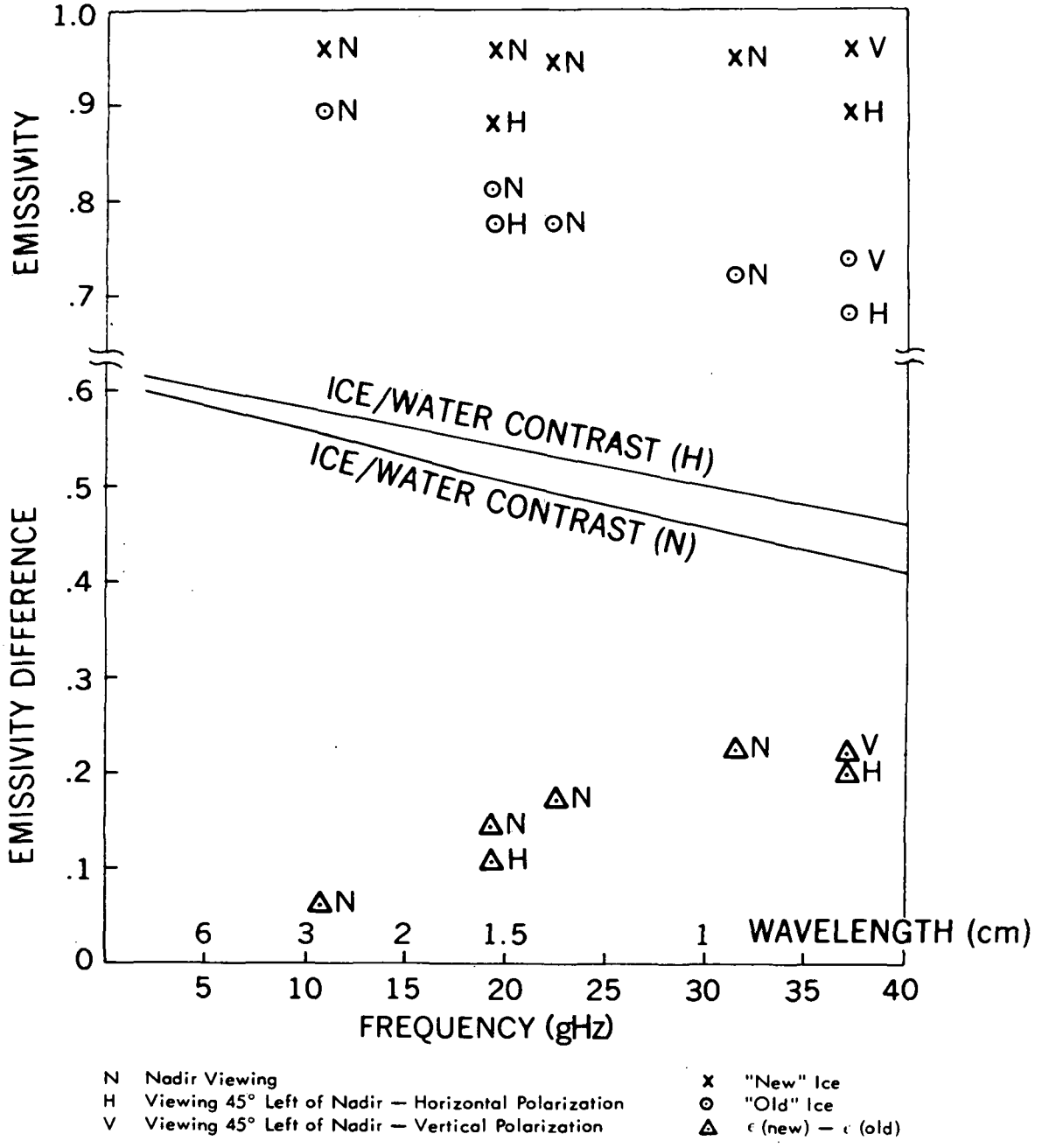

Figure 4-12. Microwave Emissivity Contrasts of Old and New Ice.

Since $V \cong 2 - 4\ gm/cm^2$

and $L \cong 0 - 0.02\ gm/cm^2$

the contributions are quite comparable. The surface wind also makes a contribution to the brightness of the oceans as shown in Figure 4-10. Thus, the 19.35 GHz brightness temperature cannot be unambiguously interpreted in terms of any one atmospheric variable but rather as a linear combination of surface wind, water vapor and liquid water content. It may be possible to resolve this ambiguity using the data from the two low frequency NEMS channels but these interpretations depend critically on the spectral nature of the surface wind effect, which is not well known at this point.

When there is rain, the cloud particles are larger and resonant effects greatly increase the absorptivity of the clouds (Reference 3). It has been observed that raining areas in clouds are effectively opaque at 19.35 GHz so that they appear as very bright areas in the microwave images. They have been observed to have brightness temperatures greater than 250°K (Reference 1). The data received by the ESMR will be affected by water vapor, clouds, rain, surface winds, soil moisture, snow and ice cover and thus information on all of these is available, but rarely without ambiguity. Additional data and interpretation skill will have to be used in resolving these ambiguities.

4.3 The Instrument

For purposes of understanding, the ESMR can be considered as two basic systems. The first is the electrically steered phased array antenna and the microwave radiometer receiver. The remainder of the system consists of straightforward power supply, control and formatting electronics and has little to do with understanding the data from the instrument.

The phased array (Figure 4-13) shows the spacing and orientation of the slots. The size of the waveguide determines the direction of the beam in the α_x dimension while the spacing of the waveguide and its relative phase determines the pointing of the beam in the α_y dimension. The relative phase is controlled by the electric phase shifters in series with each waveguide element. Each phase shifter consists of a rod of ferrite material located in the center of a waveguide section which is inside a coil. A current in the coil produces a magnetic field along the rod; the strength of the field determines the index of refraction of the ferrite material and thus the phase length of the waveguide section. Therefore, the beam may be steered in the α_y dimension by appropriate variation of the currents in the phase shifters.

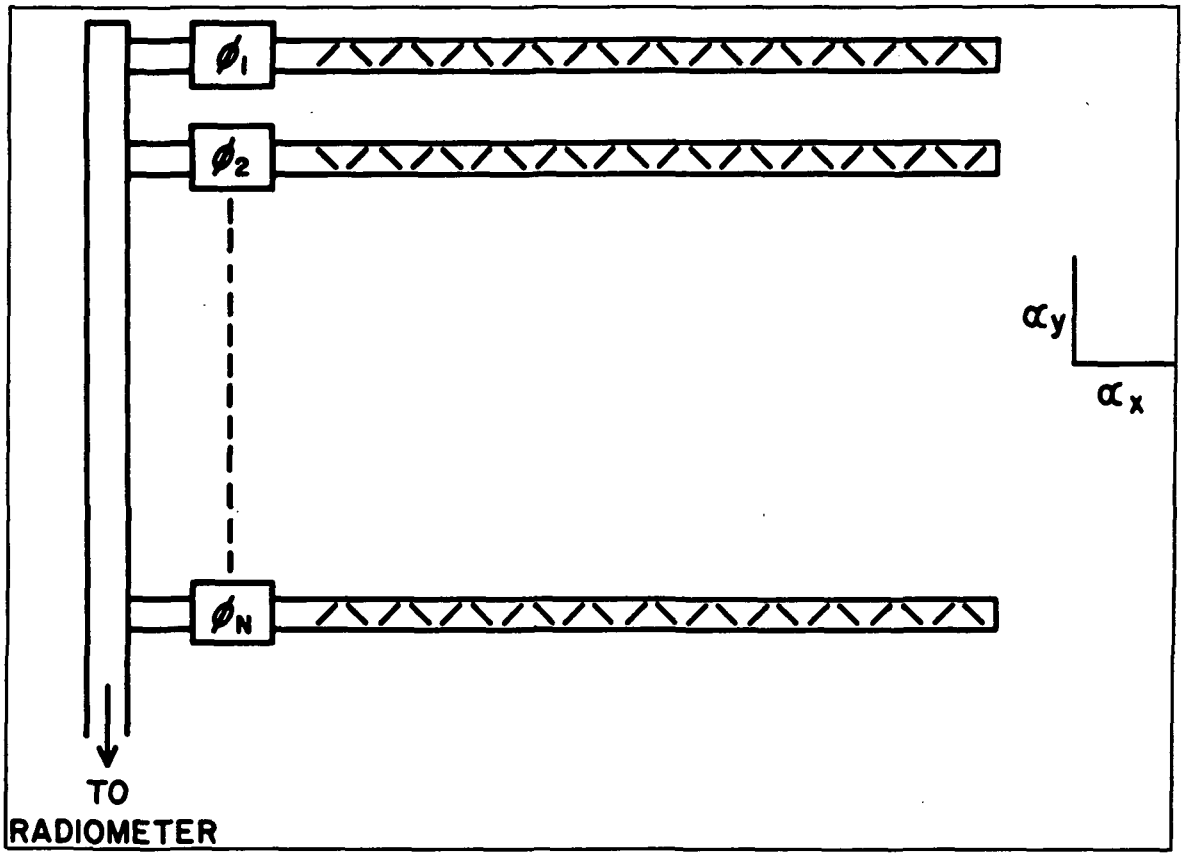

Figure 4-13. Phased Array Antenna

The gain function of such an antenna may be expressed as a product of two gain functions:

$$G(\alpha_x, \alpha_y) = g(\alpha_x)\, g'(\alpha_y)$$

These two functions, as measured on the flight model antenna, are shown for beam positions 1 and 40 in Figures 4-14 through 4-17. Note that the two g (α_x) measurements are similar and that the sidelobe level is quite low when compared to the sidelobe seen in the g' (α_y) plots. This is because the quality of g (α_x) is determined by purely geometric tolerances which may be held quite close. The electrical tolerances, which determine g' (α_y), are much more difficult to control. Use will be made of this difference in the computational details of data reduction.

The definitions of the beam width and beam center are illustrated in Figure 4-18. The beam width is proportional to 1/cos (α_y) and the scan control logic is arranged to increase the angular separation between adjacent beam positions accordingly. The nominal center of the Jth beam position is:

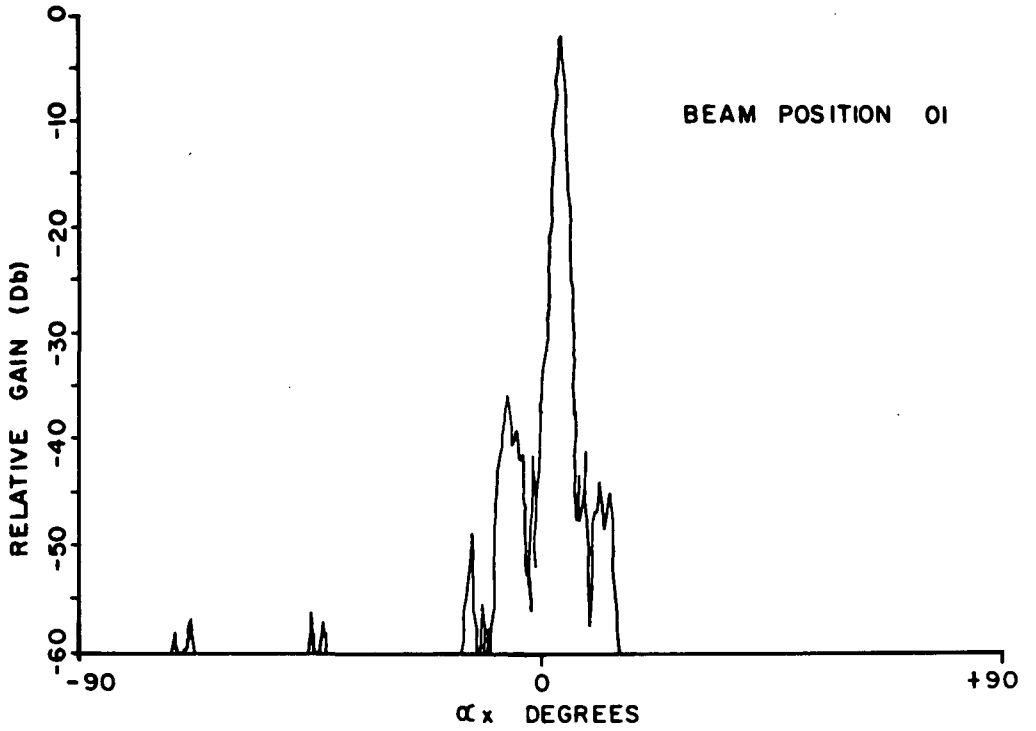

Figure 4-14. ESMR Antenna Gain for Beam Position 01 ($\alpha_x°$)

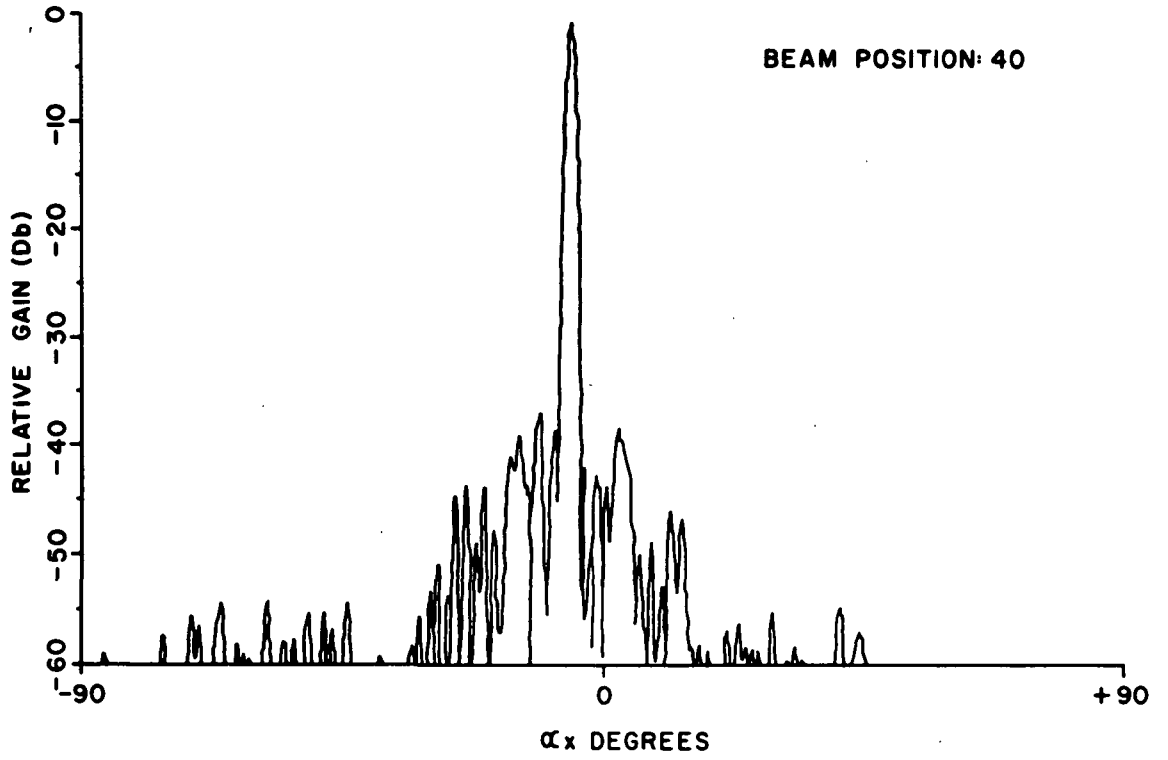

Figure 4-15. ESMR Antenna Gain for Beam Position 40 ($\alpha_x°$)

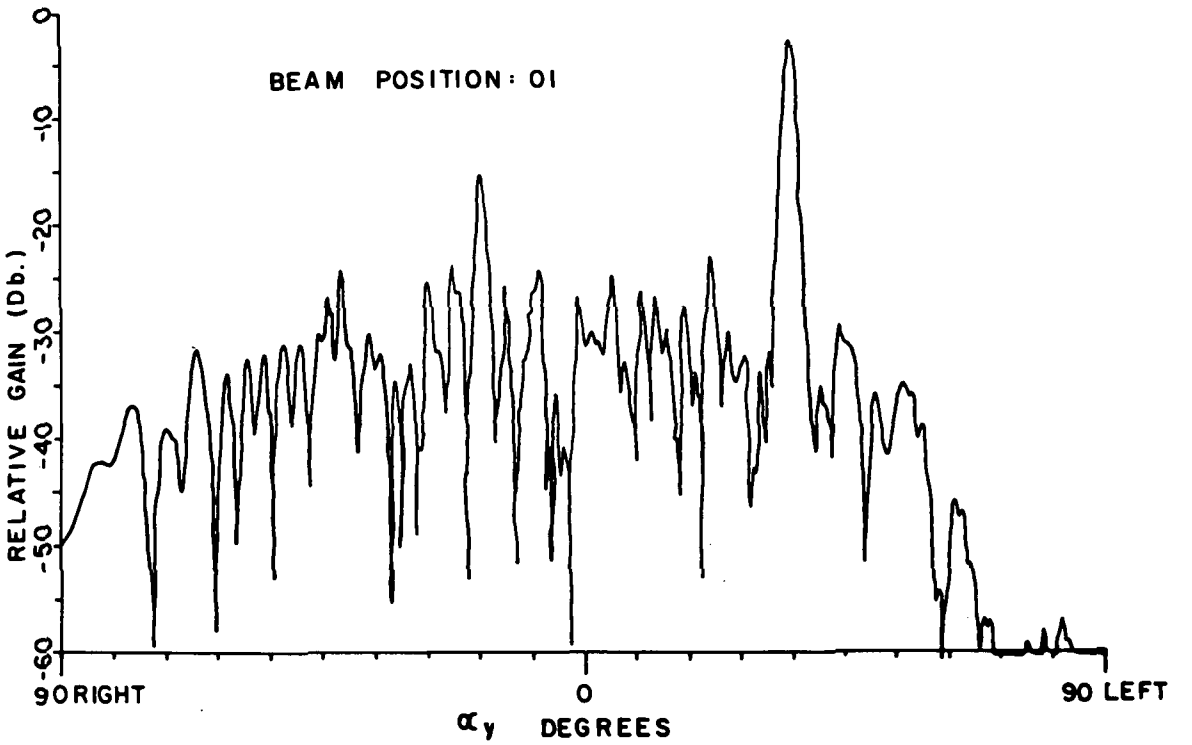

Figure 4-16. ESMR Antenna Gain for Beam Position 01 ($\alpha y°$)

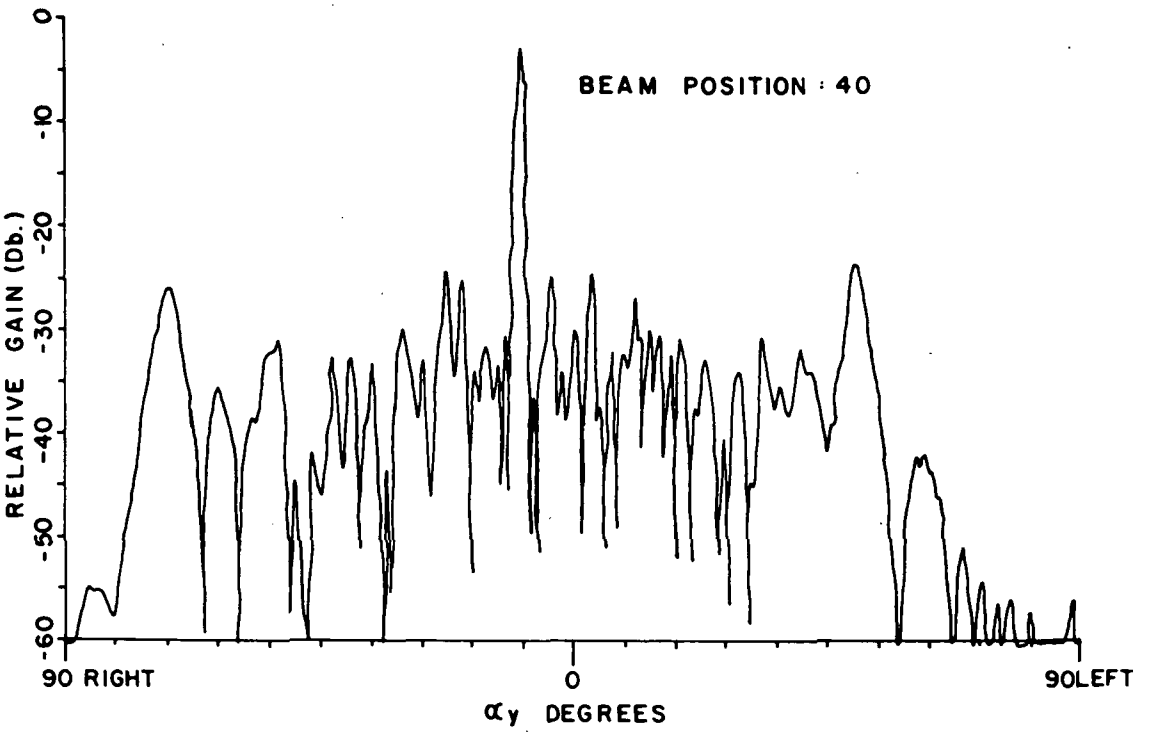

Figure 4-17. ESMR Antenna Gain for Beam Position 40 ($\alpha_y°$)

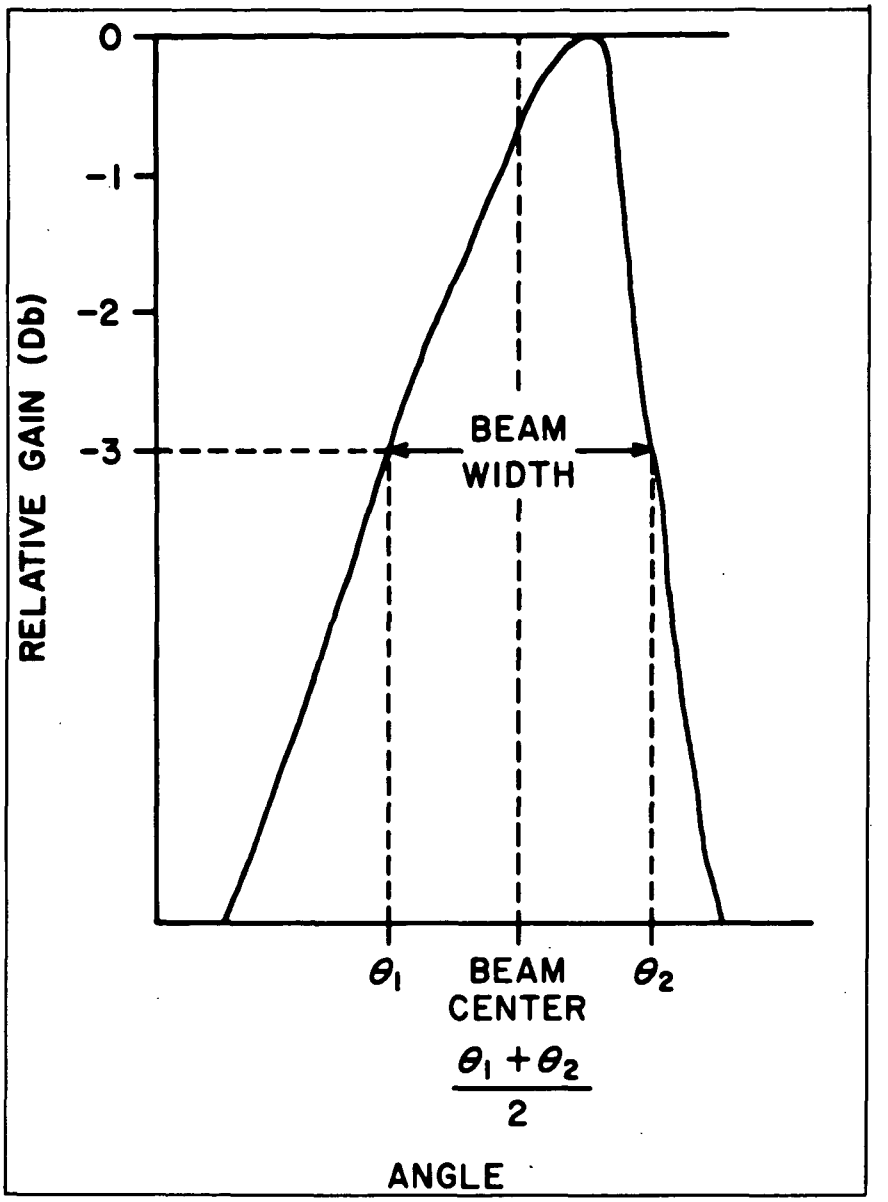

Figure 4-18. Definitions of Beam Width and Center

$(\alpha_y)_0$ = ARCSIN [SIN (50°) (2J - 79)/77],

thus $(\alpha_y)_1$ = - 50° (50° to the left of spacecraft)

and $(\alpha_y)_{78}$ = + 50° (50° to the right of spacecraft).

There is no beam position which is exactly nadir-viewing. Table 4-1 shows the nominal beam positions, the actual beam positions, and beam widths as measured on the flight model antenna.

Table 4-1
Beam Characteristics
Flight Model ESMR Antenna

Beam Position	Nominal Center	Measured Center	Measured Beam Width	Beam Position	Nominal Center	Measured Center	Measured Beam Width
1	50.0 L	49.8 L	2.0	40	.6 R	.5 R	1.4
2	48.3 L	48.0 L	2.0	41	1.7 R	1.7 R	1.4
3	46.6 L	46.3 L	1.8	42	2.9 R	-	-
4	44.9 L	44.7 L	1.8	43	4.0 R	4.0 R	1.4
5	43.4 L	43.2 L	1.8	44	5.1 R	5.1 R	1.4
6	41.8 L	41.7 L	1.8	45	6.3 R	6.3 R	1.4
7	40.3 L	40.1 L	1.7	46	7.4 R	7.4 R	1.4
8	38.8 L	38.7 L	1.7	47	8.6 R	8.6 R	1.4
9	37.4 L	37.3 L	1.6	48	9.7 R	9.7 R	1.4
10	35.9 L	35.8 L	1.6	49	10.9 R	10.9 R	1.4
11	34.5 L	34.4 L	1.6	50	12.1 R	12.1 R	1.4
12	33.2 L	33.1 L	1.6	51	13.2 R	13.2 R	1.4
13	31.8 L	31.8 L	1.6	52	14.4 R	14.4 R	1.4
14	30.5 L	30.4 L	1.6	53	15.6 R	15.6 R	1.4
15	29.2 L	29.1 L	1.6	54	16.8 R	16.8 R	1.4
16	27.9 L	27.9 L	1.5	55	18.0 R	18.0 R	1.4
17	26.6 L	26.5 L	1.5	56	19.2 R	19.2 R	1.4
18	25.3 L	25.3 L	1.5	57	20.4 R	20.4 R	1.4
19	24.1 L	24.0 L	1.5	58	21.6 R	21.6 R	1.4
20	22.8 L	22.8 L	1.4	59	22.8 R	22.8 R	1.4
21	21.6 L	21.6 L	1.4	60	24.1 R	24.1 R	1.4
22	20.4 L	20.4 L	1.4	61	25.3 R	25.3 R	1.4
23	19.2 L	19.1 L	1.4	62	26.6 R	26.6 R	1.4
24	18.0 L	17.9 L	1.4	63	27.9 R	27.9 R	1.5

Table 4-1 (Continued)

Beam Position	Nominal Center	Measured Center	Measured Beam Width	Beam Position	Nominal Center	Measured Center	Measured Beam Width
25	16.8 L	16.8 L	1.4	64	29.2 R	29.2 R	1.5
26	15.6 L	15.6 L	1.4	65	30.5 R	30.5 R	1.5
27	14.4 L	14.4 L	1.4	66	31.8 R	31.9 R	1.6
28	13.2 L	13.4 L	1.4	67	33.2 R	33.2 R	1.6
29	12.1 L	12.1 L	1.4	68	34.5 R	34.5 R	1.6
30	10.9 L	10.9 L	1.4	69	35.9 R	36.0 R	1.6
31	9.7 L	9.8 L	1.4	70	37.4 R	37.4 R	1.6
32	8.6 L	8.6 L	1.4	71	38.8 R	38.8 R	1.6
33	7.4 L	7.5 L	1.4	72	40.3 R	40.3 R	1.6
34	6.3 L	6.3 L	1.4	73	41.8 R	41.8 R	1.8
35	5.1 L	5.2 L	1.4	74	43.4 R	43.4 R	1.8
36	4.0 L	4.0 L	1.4	75	44.9 R	45.0 R	1.8
38	2.9 L	2.9 L	1.4	76	46.6 R	46.6 R	1.8
38	1.7 L	1.8 L	1.4	77	48.3 R	38.3 R	1.9
39	.6 L	.6 L	1.4	78	50.0 R	50.1 R	2.0

All angles in degrees

L = Left
R = Right

Figure 4-19 shows a block diagram of a typical microwave radiometer. The three ferrite switches are actually reversible circulators but may be considered as SPDT switches, as drawn, for present purposes. Switches 1 and 2 select among the input and the two calibration sources. The calibration sources are, typically, matched loads at known thermodynamic temperatures. The selected signal is then modulated by switching rapidly (10-10 GHz) between the input and a third reference source. The resulting signal is beat with the local oscillator signal in the mixer according to the familiar superhetrodyne principle and is then amplified in the IF amplifier which has a gain of 60-90 db. The received spectrum consists of two bands

$$\nu_{LO} - \nu_{IF} - \beta_{IF}/2 \leq \nu \leq \nu_{LO} - \nu_{IF} + \beta_{IF}/2$$

and

$$\nu_{LO} + \nu_{IF} - \beta_{IF}/2 \leq \nu \leq \nu_{LO} + \nu_{IF} + \beta_{IF}/2$$

where ν is the received frequency, ν_{LO} is the frequency of the local oscillator, ν_{IF} is the center frequency of the IF amplifier and β_{IF} is the bandwidth of the IF amplifier.

From the IF amplifier the signal is detected with a square law detector, further amplified, detected synchronously with the modulation in switch 3 and integrated for a time period t. The resulting voltage is, in principle, proportional to the difference between the input signal (in temperature) and the temperature of the calibration load. However, there is a possibility of an offset due to pickup of the modulation frequency or a bias in the synchronous detector or integrator, so it is necessary to use two calibration sources to relate the output voltage, V, to an input signal temperature, T_{in}. This relationship is

$$T_{in} = T_1 + (T_2 - T_1) \frac{V_1 - V}{V_1 - V_2}, \tag{6}$$

where T_1 and T_2 are the two calibration temperatures, and V_1 and V_2 the respective output voltages. The noise uncertainty in the measured temperature is given by the radiometer noise relation

$$\Delta T = \frac{k (T_S + T_N)}{\sqrt{\beta t}}, \tag{7}$$

where ΔT is the uncertainty due to noise, T_S is the signal temperature, and T_N is the noise temperature of the system which may be measured independently. β is the bandwidth and t is the integration time. The value of k is a matter of contention but if β is considered to be the RF bandwidth (twice the IF bandwidth) then a value of 2 for k gives good agreement with observed ΔT's in a rms sense.

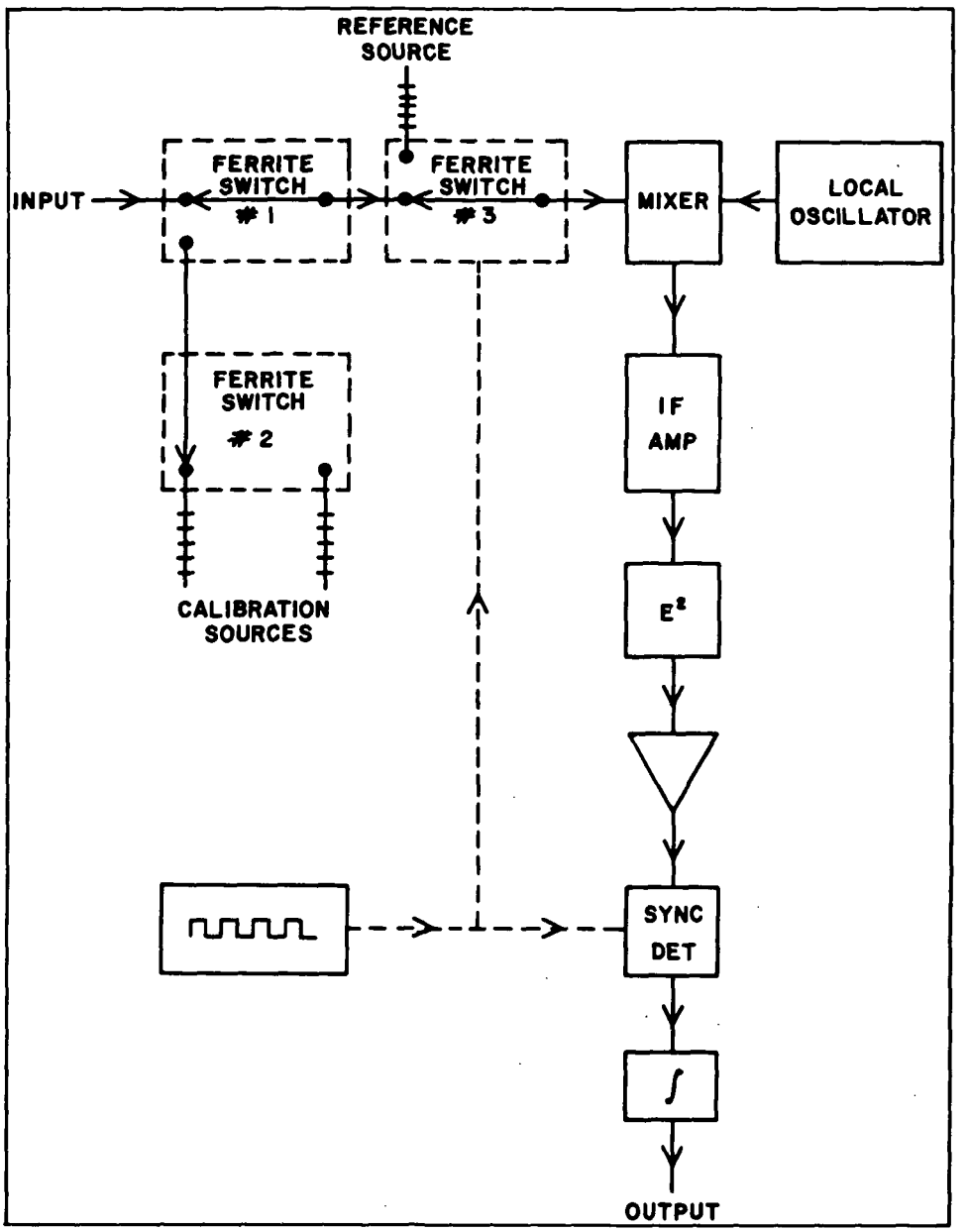

Figure 4-19. Typical Microwave Radiometer Block Diagram

This uncertainty does not include systematic errors due to calibration offset. The state of the art in calibration is on the order of 0.5°-1°K.

The typical radiometer block diagram shown in Figure 4-19 is clearly imbedded in the ESMR block diagram in Figure 4-20. The sky horn gives a view of the 3°K background for a cold reference and the floating ambient termination serves for the other calibration point. Figure 4-20 is mostly self explanatory but a few features need explanation. The stepped automatic gain control (AGC)

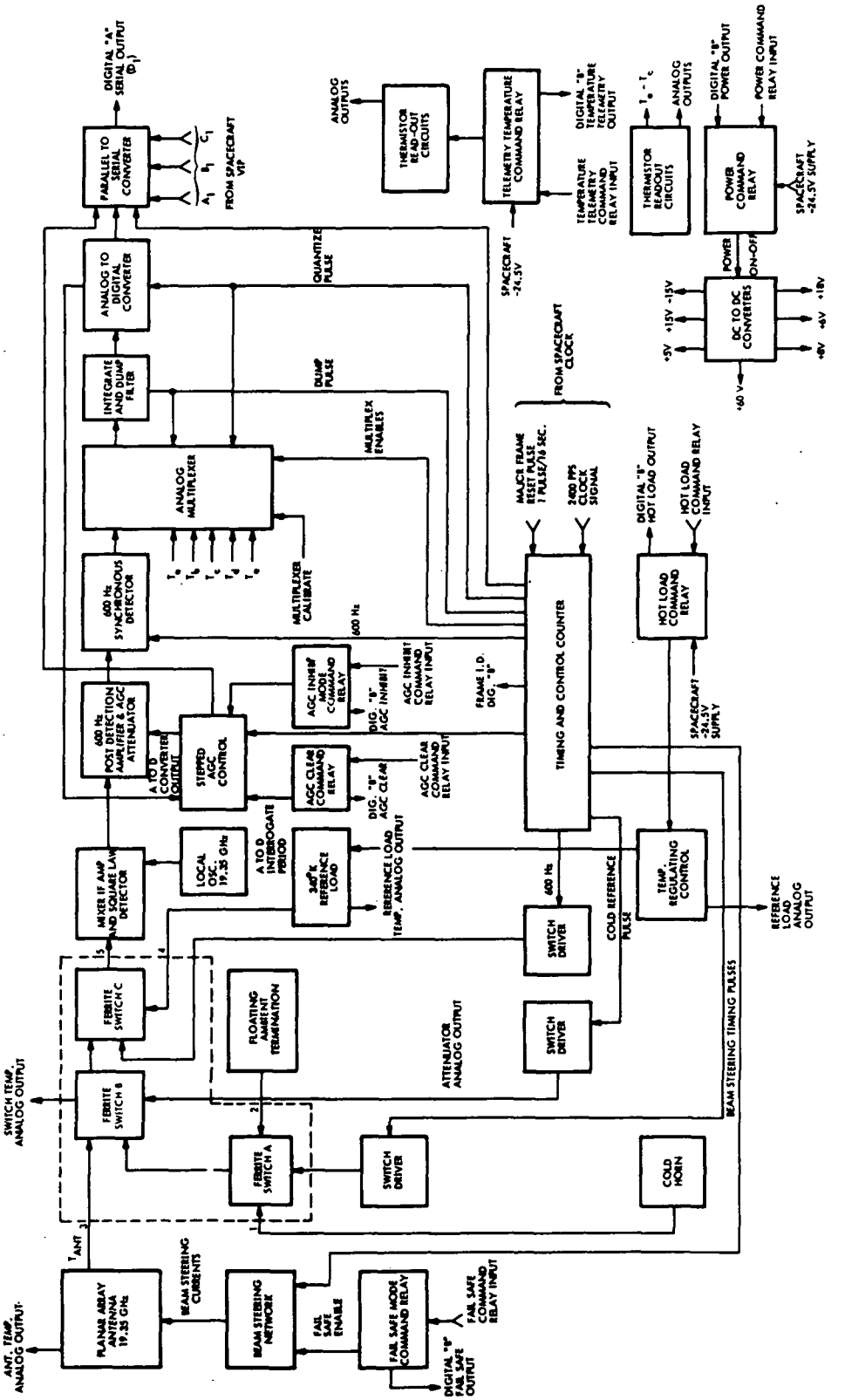

Figure 4-20. ESMR Block Diagram

controls the gain of the post detection amplifier in 1/4 db steps. Its function is to make optimum use of the dynamic range of the 10 bit analog to digital converter. Its logic is arranged to keep the calibration voltage corresponding to the sky horn (by far the coldest observable signal) between 896 and 991 counts so that the converter does not saturate or give excessive round-off error. Obviously, one should not average calibration counts across a step on the AGC setting. The AGC may be locked by use of the AGC inhibit command and may be set to a nominal operating value by the AGC clear command. Other commands permit turning on the 340°K reference load to preheat (Hot load command) and locking the scan at 13.7° to the left (Failsafe command) in case of a failure of the beam steering network. The unit has three types of outputs:

- "Digital A" is the main data stream. It is a serial bit stream which consists of the radiometer outputs multiplexed with the AGC step number and all the thermistor data necessary for data reduction. The data rate is 200 bits/second. The total data cycle takes 32 seconds (2 VIP major frames); the format is given in Table 4-2. Table 4-3 gives the calibration data (flight model) for the thermistors multiplexed in position 80 of this format.

- "Digital B" is a set of 1 bit status words to indicate the position of each of the command relays and one to identify the VIP major frame of the Digital A cycle. They are sampled once per 16 seconds.

- "Analog" is a set of 16 voltages of engineering interest, each sampled once per 16 seconds.

The losses in the ferrite switch and the various waveguides may be accounted for essentially like the atmospheric loss described in the previous section. That is, if the signal entering a lossy element is T_B, its transmissivity is t, and its thermodynamic temperature is T_O, then the emerging signal is $t\,T_B + (1-t)\,T_O$. The calculation of the calibration temperatures is obtained by repeated application of this relation. The values of the calibration temperatures depend on the scan number within a Nimbus major frame because on even scans ferrite switch A is open to the cold horn and on odd scans it is open to the ambient load. The isolation of ferrite switch B is less than 20 db for some switch temperatures which results in a variation of the signal leakage on the order of 3°K between even and odd scans. The size of this correction will be called δ, and the value of the cold and ambient calibration for odd scans will be T_{CC} and T_{AC}, respectively. In principle all three of these (δ, T_{CC} and T_{AC}) are functions of both the ferrite switch temperature, multiplex number 3 (MUX 3) (see Table 4-6) and of the ambient load temperature (MUX 4), but, since the ambient load and the ferrite switch are in close thermal contact, their actual temperatures will never differ by more than 5°K. It is thus accurate, to a few tenths of a degree, to consider

Table 4-2
ESMR Framing Format

Digital A

First VIP Frame			Second VIP Frame		
Code	Scan Number	Description	Code	Scan Number	Description
1	1	Beam Position 1	1	5	Beam Position 1
2	1	Beam Position 2	2	5	Beam Position 2
⋮	⋮	⋮	⋮	⋮	⋮
78	1	Beam Position 78	78	5	Beam Position 78
79	1	Hot Reference	79	5	Hot Reference
80	1	Average Antenna Temp.	80	5	Dicke Load Temp
1	2	Beam Position 1	1	6	Beam Position 1
2	2	Beam Position 2	2	6	Beam Position 2
⋮	⋮	⋮	⋮	⋮	⋮
78	2	Beam Position 78	78	6	Beam Position 78
79	2	Cold Reference	79	6	Cold Reference
80	2	Average Phase Shifter Temp.	80	6	AGC Count
1	3	Beam Position 1	1	7	Beam Position 1
2	3	Beam Position 2	2	7	Beam Position 2
⋮	⋮	⋮	⋮	⋮	⋮
78	3	Beam Position 78	78	7	Beam Position 78
79	3	Hot Reference	79	7	Hot Reference
80	3	Ferrite SW. Temp.	80	7	Multiplex Calibrate
1	4	Beam Position 1	1	8	Beam Position 1
2	4	Beam Position 2	2	8	Beam Position 2
⋮	⋮	⋮	⋮	⋮	⋮
78	4	Beam Position 78	78	8	Beam Position 78
79	4	Cold Reference	79	8	Cold Reference
80	4	Ambient Load Temp.	80	8	Frame Identification (0000)

Table 4-3
Thermistor Calibrations for Flight Model ESMR

T(°C)	Mux(1)	Mux(2)	Mux(3)	Mux(4)	Mux(5)
-10	909	905	918	902	-
- 5	879	876	888	872	-
0	844	840	853	838	-
5	804	801	814	799	-
10	760	757	770	756	-
15	711	709	722	709	-
20	660	657	671	659	-
25	607	605	619	607	-
30	554	551	566	555	-
35	501	498	513	503	-
40	449	448	462	453	-
45	400	399	414	406	-
50	355	353	368	361	-
55	313	311	326	320	-
60	274	273	289	283	638
65	-	-	-	-	548
70	-	-	-	-	471
	Average Antenna Temperature	Average Phase Shifter Temperature	Ferrite Switch Temperature	Ambient Load Temperature	Reference Load Temperature

T_{CC} and δ as a function of the ferrite switch temperature (MUX 3) only and T_{AC} as a function of the ambient load temperature (MUX 4). Figures 4-21, 4-22, 4-23 show these values for the flight model of the ESMR.

With the radiometer calibrated, the antenna ohmic loss was measured by taking the unit to a high altitude (2.2 km) where it viewed the radiation coming from cold space. At this altitude the correction for atmospheric absorption is a manageable quantity.

The resulting loss is a function of beam position and the temperature of the phase shifters. Figure 4-24 shows that these two effects appear to be separable. In this figure the loss ratio, L, (defined as the reciprocal of the transmissivity) is shown for two beam positions. Note that only a bias separates them. Thus, the loss ratio of the antenna for the Jth beam position may be expressed as a sum $L(T_{ps}, J) = L(300°K, J) + F(T_{ps})$ where $F(T_{ps})$ is a function of the phase shifter temperature (MUX 2) only and is equal to 0 at $T_{ps} = 300°K$. Table 4-4 (data to be published in the first Nimbus 5 Data Catalog) will list L (300°K, J) for the flight model antenna and Figure 4-25 shows $F(T_{ps})$. If T_b is the brightness temperature at the radiometer input for the Jth beam position, then the temperature received by the antenna is $(T_A)_J = L(T_{ps}, J)(T_b)_J - [L(T_{ps}, J)-1]t$. An exact separation between the losses in the phase shifters and the array is not available, but the loss is roughly expected to be evenly divided; thus we use the average of the phase shifter and antenna array temperature, each of which is derived from a network of four strategically placed thermistors.

A further correction is needed to account for the effects of antenna sidelobes. The antenna measures a radiation intensity which is an average weighted by the gain functions

$$T_A = \frac{1}{4\pi} \int T_B(\theta, \phi)\, G(\theta, \phi)\, d\Omega , \tag{8}$$

where ϕ and θ are the conventional spherical polar coordinates and $d\Omega$ is a differential solid angle. Because of the separability of the gain function $G(\theta, \phi)$ into a product, $g(\alpha_x)g'(\alpha_y)$, and the extremely low sidelobe level in the α_x plane, this may be expressed as a one dimensional integral for the i th beam position

$$(T_A)_i = \frac{\int g_i'(\alpha_y)\, T_B(\alpha_y)\, d\alpha_y}{\int g_i'(\alpha_y)\, d\alpha_y} \tag{9}$$

T_B can be approximated by a sum of 78 functions

$$T_B(\alpha_y) \cong \sum a_j\, f_j(\alpha_y) \tag{10}$$

and the antenna temperature in matrix form is expressed as

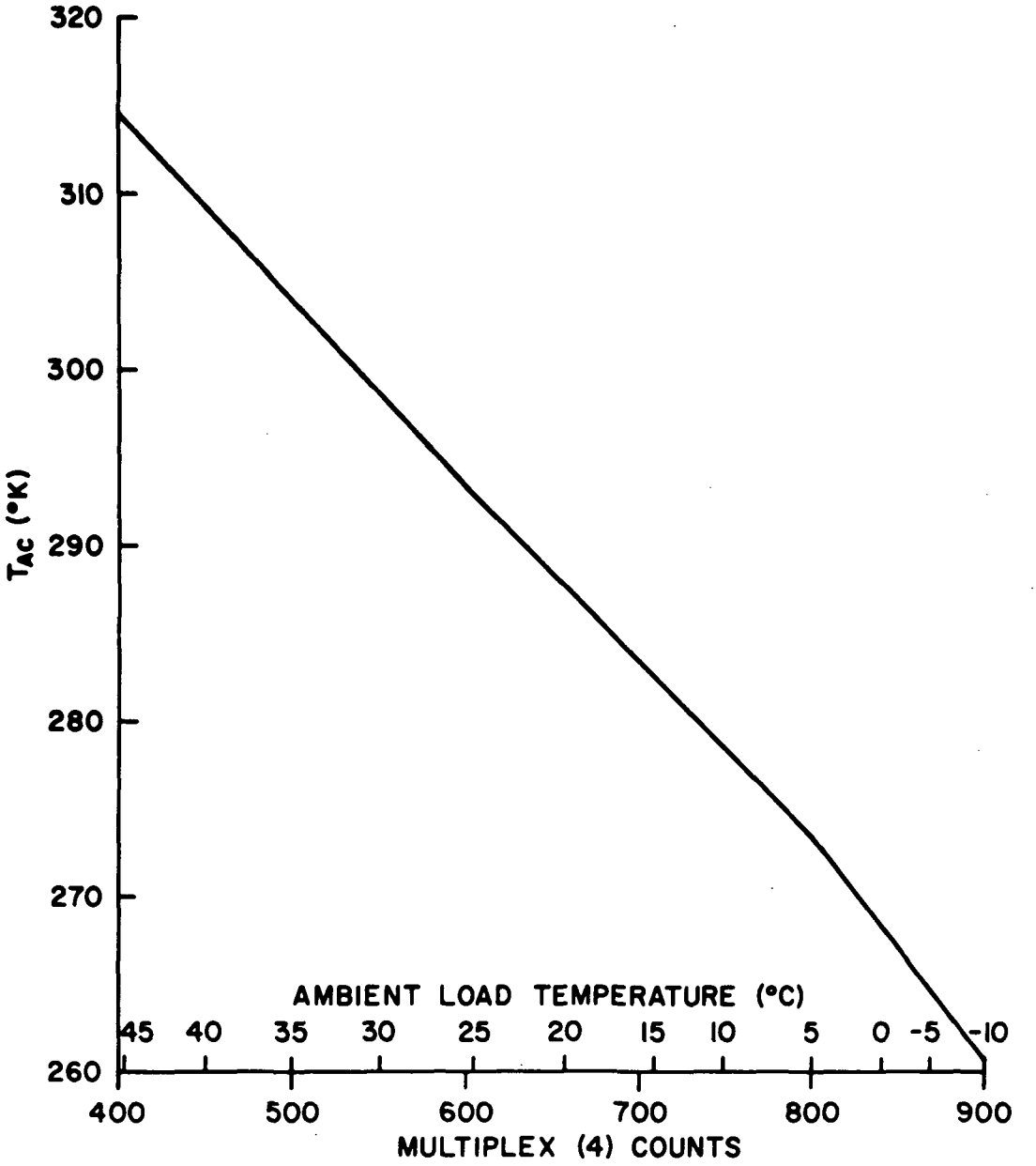

Figure 4-21. Ambient Temperature (T_{AC}) Calibration for ESMR Flight Model

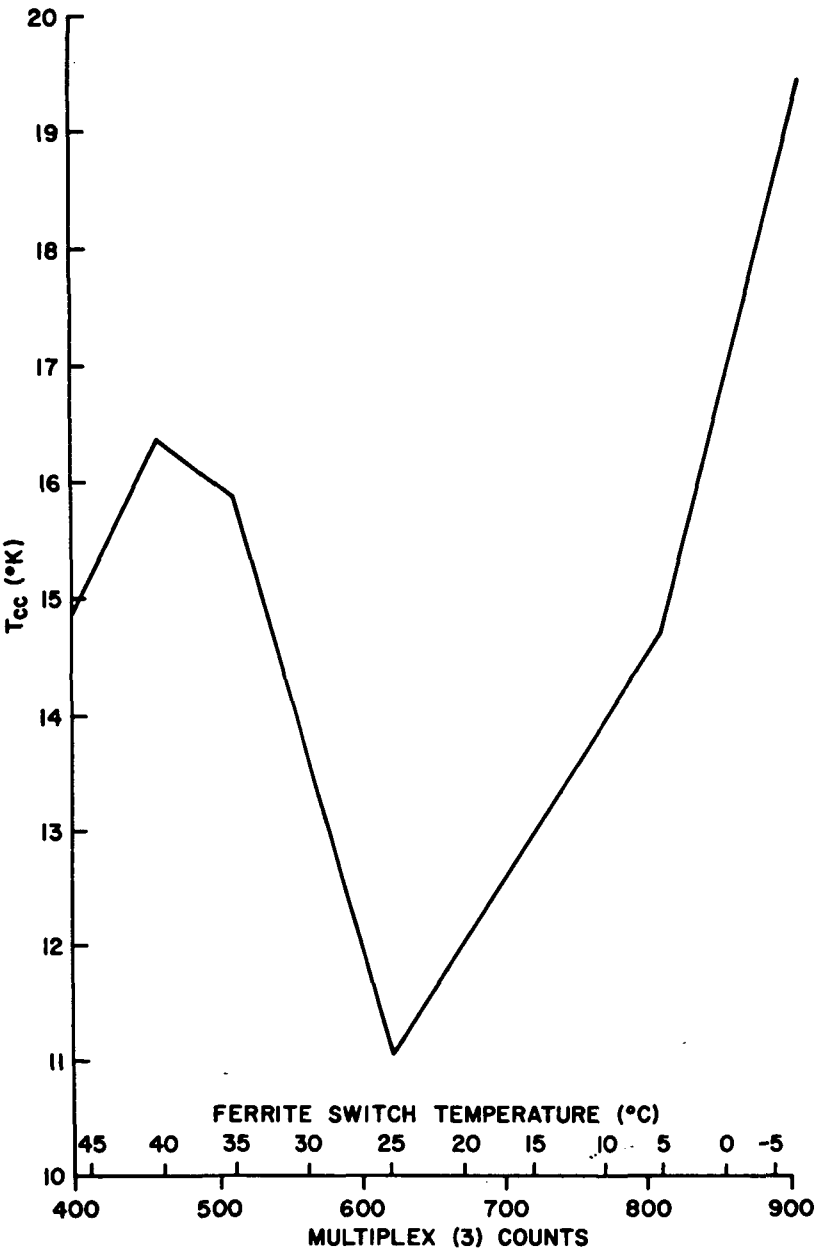

Figure 4-22. Cold Temperature (T_{cc}) Calibration for ESMR Flight Model.

C-2

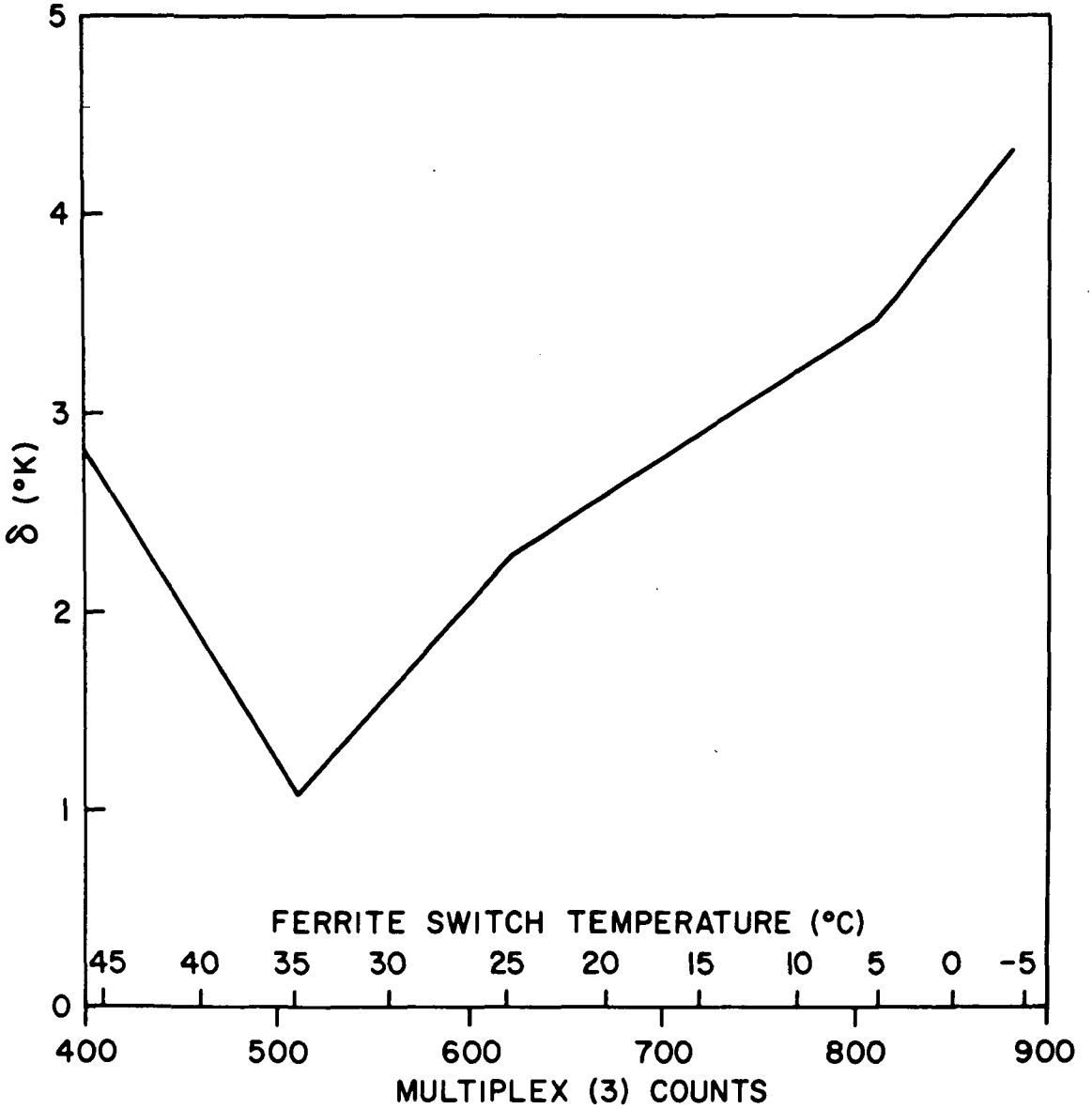

Figure 4-23. Even Scan (δ) Temperature Correction for ESMR Flight Model

$$(T_A)_i = \sum_j A_{ij}\, a_j \quad , \tag{11}$$

where $$A_{ij} = \frac{\int g'_i(\alpha_y)\ f_j(\alpha_i)\, d\alpha_y}{\int g'_i(\alpha_y)\, d\alpha_y} \tag{12}$$

The matrix A_{ij} may be inverted to

$$a_j = \sum_i A^{-1}_{ji}\ (T_A)_i \ ; \tag{13}$$

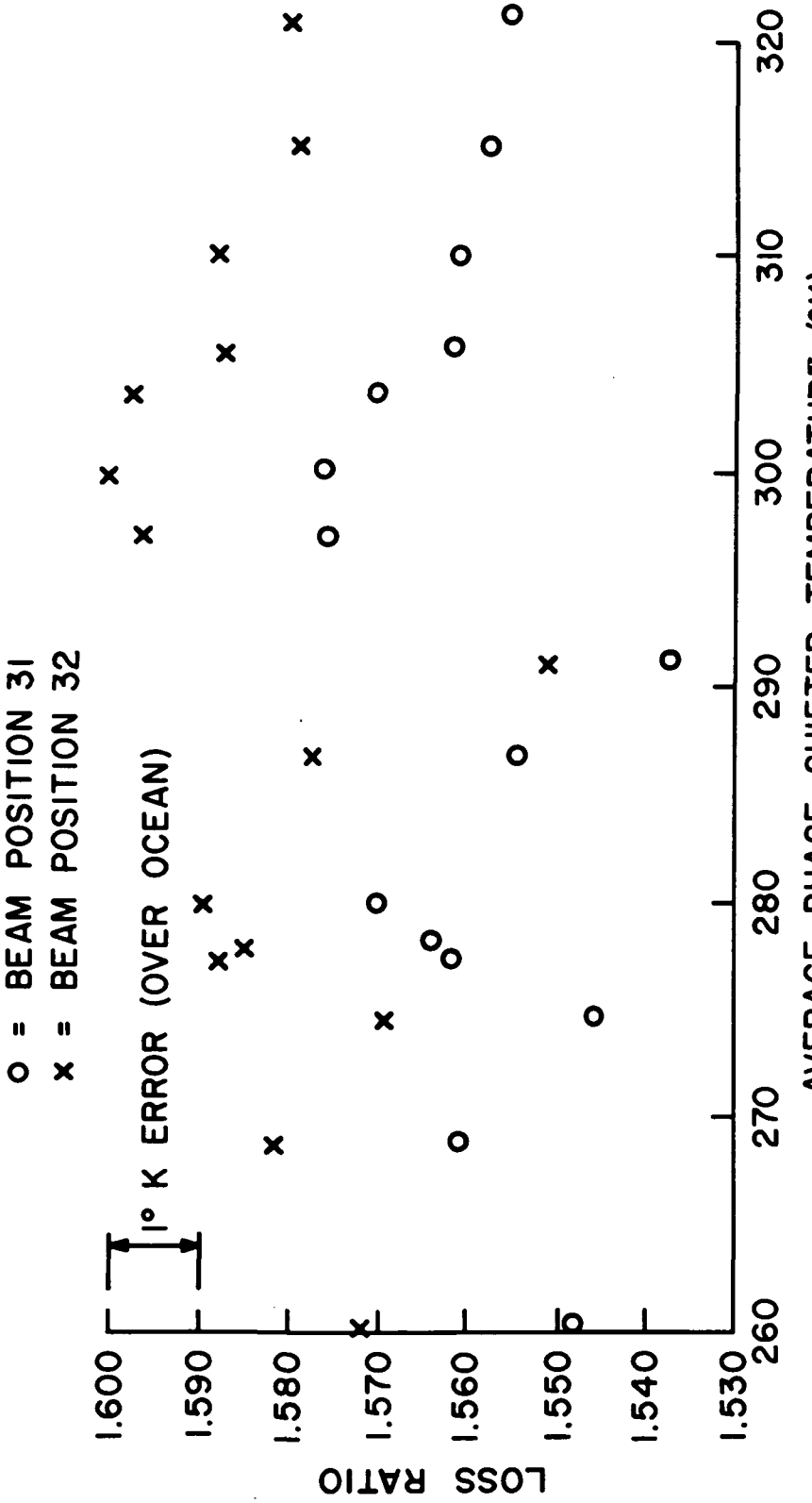

Figure 4-24. Measured Antenna Loss for Two Beam Positions

Table 4-4
ESMR Antenna Loss Ratio-Flight Model

To Be Included in the First
Nimbus 5 Data Catalog

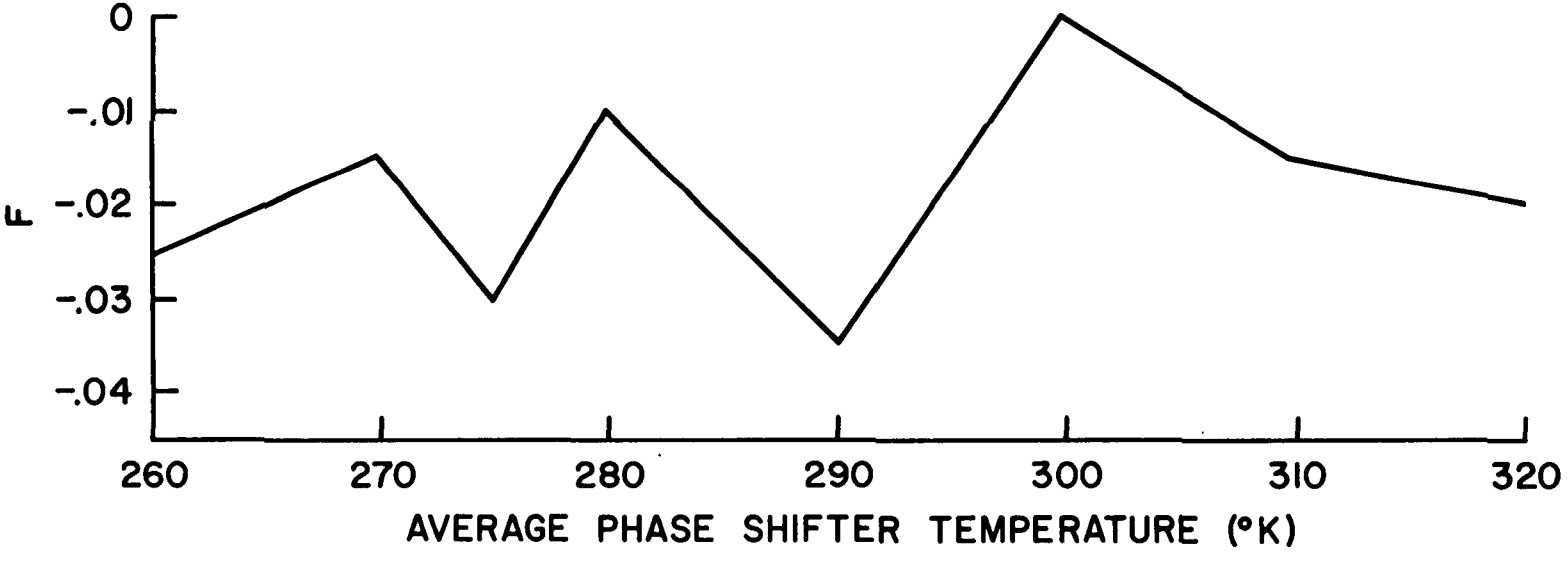

Figure 4-25. Temperature Dependence of Antenna Loss Ratio

thus, the expansion coefficients a may be obtained from the set of radiation intensity measurements made in one scan. If the set of triangular functions [f(j)] illustrated in Figure 4-26 is chosen, the a_j's are approximately the brightness temperatures in the direction of the corresponding beam center. A problem still remains. The noise amplification factor $N_i = \sqrt{\Sigma_j (A^{-1}{}_{ij})^2}$ of the resultant matrix is of the order of 2; that is, the radiometer noise makes the measurement of T_a, the gain function averaged brightness temperature, uncertain by about 2.2°K. This vector of T_a's is multiplied by the matrix A and, if the noise contributions are all independent, the noise of the resulting a's will be given by

$$(\delta a_i)_{rms} = 2.2^\circ K \sqrt{\Sigma_j (A^{-1}_{ij})^2} \qquad (14)$$

The source of this noise amplification is the large contribution from adjacent beam positions which is being corrected out. This contribution must be left uncorrected in order to keep N_i sufficiently low. We can define a matrix A' which is all zeros except for

$$A'_{j,\,j\pm1} = A_{j,\,j\pm1}$$

and $$A'_{jj} = (1 - A_{j,\,j+1} - A_{j,\,j-1})$$

and express a modified sidelobe correction matrix $B = A' A^{-1}$ which will correct for the sidelobe contribution, but not for the edges of the main beam. This reduces the noise amplification to the more reasonable range of 1.1 to 1.2°K.

The following is a summary of the calibration algorithm:

- Read two VIP major frames (eight scans) of data.
- Using the multiplex data, calculate the calibration temperatures T_{CC}, T_{AC} and δ.
- Average the four ambient and the four cold calibration numbers.
- Convert all the data for the 78 beam positions for all 8 scans to brightness temperatures at the radiometer input.
- Using the measured antenna thermodynamic temperature and the tabulated antenna losses as a function of beam position as corrected for phase shifter temperature, calculate the gain function for averaged brightness temperatures.
- Using matrix B, correct each scan for the sidelobe contribution.

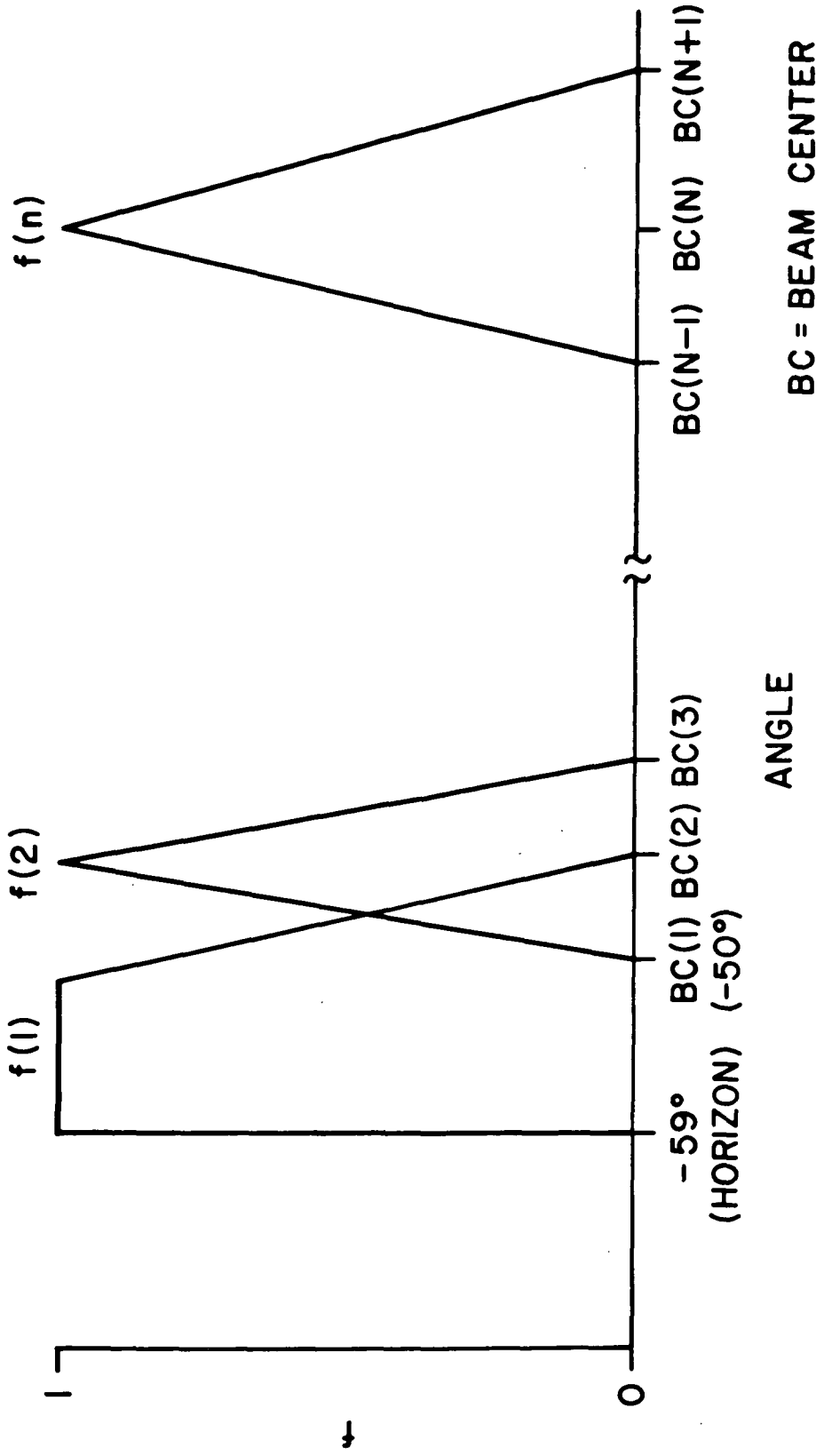

Figure 4-26. Brightness Temperature Expansion Functions

A summary of the ESMR flight model parameters is given in Table 4-5.

Table 4-5
ESMR Flight Model Parameters

Antenna	
Aperture Size (Linear Array Dimension)	83.3 cm (32.80 in.)
Aperture Size (Feed Array Dimension)	85.5 cm (33.66 in.)
Number of Linear Elements	103
Number of Slots per Element	81
Amplitude Distribution (Linear Array)	-40 db sidelobe Taylor distribution
Amplitude Distribution (Feed Array)	-35 db sidelobe Taylor distribution
Broadside Half Power Beamwidth	1.4°
Number of Beam Positions	78
Antenna Beam Efficiency	90 to 92.7%
Beam Scan Angle	±50°
Antenna Loss	1.7 db
Beam Squint Angle	-3.2° nominal
Polarization	Linear (E vector parallel to flight direction)
Cross Polarization	-25 to -36 db
Failsafe Angle (Non-Scanning Mode)	-13.7°
VSWR	<1.15
Radiometer	
Center Frequency	19.35 GHz
Bandwidth IF (Nominal)	50 - 150 MHz
Bandwidth RF (Nominal)	300 MHz
Local Oscillator	19.35 GHz
Mixer Noise Figure	6.5 db
ΔT_{rms}/47 ms	1.5°K
Absolute Accuracy	2°K
Dynamic Range	50 - 330°K
Calibration:	
Dicke Load	~338 ±0.1°K
Ambient Load	Local ambient
Sky Horn	<3°K

4.4 Data Processing, Format and Availability

4.4.1 Data Processing

All ESMR data will be acquired at the Rosman and Alaska data acquisition facilities and relayed to the MDHS at GSFC. MDHS will produce one Polaroid negative and positive of all ESMR data acquired from each interrogation orbit. MDHS will also produce and forward tapes containing raw ESMR data to LMES at GSFC. LMES will produce, from these tapes, calibrated brightness temperature tapes (CBTT).

4.4.2 Pictorial Format

The MDHS will produce a 4 inch x 5 inch Polaroid negative of all ESMR data acquired from an interrogation orbit. Six parallel strips of imagery and two geographic grids will be presented on each negative. Three strips and an adjacent grid will show one half of an orbit's data and, to the right, three strips with an adjacent grid will show the other half. Coverage in the first three strips of data will be identical but each strip will have a different dynamic range for its gray scale, with one presentation scheme corresponding roughly to 100-200°K, 190-270°K and 250-300°K. The other three strips of data will have the same format and cover the remainder of the orbit.

The exact ESMR image format schemes and selected ESMR imagery will be presented in the first Nimbus 5 Data Catalog.

4.4.3 Tape Format

The CBTTs produced by LMES will consist of the brightness temperature for each beam position, plus the earth location of each beam position and auxiliary data. There will be one file for each interrogation orbit.

Each logical record will consist of 1916 data words corresponding to 8 scans (32 seconds) of data. The format of this record is shown in Table 4-6.

4.4.4 Printout Format

Computer printouts of ESMR will give the complete radiometer data plus the satellite location at 16 second intervals. The printout format will be self-explanatory. Precision is needed in specifying the period to be covered by the data as one hour of data would fill about 30 pages of printout. A day's data would be a three inch stack of paper.

Table 4-6
ESMR-CBTT Data Record Format

Word Number	Quantity	Units	Scale	Remarks
1	Year	Year		Year associated with data in words 2-5; e.g., 1972.
2	Day	Days		
3	Hour	Hours		
4	Minute	Minutes		
5	Second	Seconds		
6	PGM ID			Unique identification number assigned to program that prepared tapes.
7	Pitch Fine Error	Degrees	E1	Pitch fine error at time specified in words 2-5.
8	Roll Fine Error	Degrees	E1	Roll fine error at time specified in words 2-5.
9	RMP Indicated Rate High		E1	
10	Latitude	Degrees	E1	Latitude of subsatellite point at time specified in words 2-5.
11	Longitude	Degrees	E1	Longitude of subsatellite point at time specified in words 2-5.
12	Height	Kilometers	E0	Height of spacecraft at time specified at words 2-5.

Table 4-6 (Continued)

Word Number	Quantity	Units	Scale	Remarks
13	Hot Load Mean		E1	
14	rms of Hot Load		E2	
15	Cold Load Mean		E1	
16	rms of Cold Load		E2	
17	MUX 1		E0	Average antenna temperature.
18	MUX 2		E0	Average phase shift temperature.
19	MUX 3		E0	Ferrite switch block temperature.
20	MUX 4		E0	Ambient load temperature
21	MUX 5		E0	Hot load temperature
22	MUX 6		E0	AGC
23	ANALOG 0			
24	ANALOG 1			
25	ANALOG 2			
26	ANALOG 3			
27	ANALOG 4			
28	ANALOG 5			

Table 4-6 (Continued)

Word Number	Quantity	Units	Scale	Remarks
29	ANALOG 6			
30	ANALOG 7			
31	ANALOG 8			
32	ANALOG 9			
33	ANALOG 10			
34	ANALOG 11			
35	ANALOG 12			
36	ANALOG 13			
37	ANALOG 14			
38	ANALOG 15			
39	DIGITAL B			Low order eight bits ($b_8 b_7 b_6 b_5 b_4 b_3 b_2 b_1$) b_8 - ephemeris 0 = estimated, 1 = data b_7 - radiometer power on/off b_6 - load power on/off b_5 - antenna scan on/off b_4 - AGC clear on/off b_3 - AGC inhibit on/off b_2 - temperature TLM power on/off

Table 4-6 (Continued)

Word Number	Quantity	Units	Scale	Remarks
39	Digital B (cont.)			b_1 - data cycle first half/ second half
40	Status Indicators			Low order fifteen bits (b_{15} b_{14} .....$b_2$$b_1$) b_{15} - primary comstor verify yes/no b_{14} - redundant comstor verify yes/no b_{13} - ITPR electronics on/off b_{12} - NEMS data unit on/off b_{11} - NEMS data chan 1 on/off b_{10} - NEMS data chan 2 on/off b_9 - NEMS data chan 3 on/off b_8 - NEMS data chan 4 on/off b_7 - NEMS data chan 5 on/off b_6 - ESMR radiometer power on/off b_5 - SCMR electronics on/off b_4 - THIR electronics on/off b_3 - S-Band A on/off b_2 - S-Band B on/off b_1 - SCMR S-Band on/off

Table 4-6 (Continued)

Word Number	Quantity	Units	Scale	Remarks
41	Status Indicators			Low order fifteen bits ($b_{15}b_{14}.....b_2b_1$) b_{15} - SCR power on/off b_{14} - SCR chopper MTR on/off b_{13} - ITPR chopper MTR on/off b_{12} - ESMR antenna scan on/off b_{11} - spare b_{10} - spare b_9 - spare b_8 - SCMR monitor on/off b_7 - Satellite day-night indicator 1 = day, 0 = night b_6 - ephermis data comp bit care input 1 = uncompensated, 2 = compensated b_5 - beacon XMTR A on/off b_4 - beacon XMTR B on/off b_3 - spare

Table 4-6 (Continued)

Word Number	Quantity	Units	Scale	Remarks
41	Data Source			b_2 and b_1 00 HDRSS A 01 HDRSS B 10 Real-Time
42	Beam Position 79			
43-46				Spare
47-124	Latitude	Degrees	E1	Latitude of the 78 scan spots.
125-202	Longitude	Degrees	E1	Longitude of the 78 scan spots.
203-280	Brightness Tempera-ture	°K	E1	Brightness temperature of the 78 scan spots.

At present, the feasibility of producing grid print maps of ESMR (similar to THIR grid print maps) is being investigated. If producing these maps is feasible, their format will be described in the first Nimbus 5 Data Catalog after they become available.

4.4.5 Data Availability

All 4 inch x 5 inch ESMR Polaroid negatives will be optically reduced to 70 mm film format by the NADUC and forwarded to the NSSDC. Upon request, the NSSDC will furnish a user with either positive or negative ESMR photographic products. All ESMR photographic data will be listed in the Nimbus 5 Data Catalogs.

In the course of the research to be carried on at LMES, false color images of portions of the data will be produced. The facilities and personnel are not available for the processing of user requests for special productions.

NSSDC will make available copies of those which have been produced and are considered suitable by the experimenter. Each data catalog will contain a list of color images available.

Seven track CBTTs (described in Section 4.4.3) will be available from NSSDC. The user may specify density (200,556 or 800 BPI), blocking factor (logical records per physical record) and time period desired. The data will be formatted as 16 bit 2's complement words which is FORTRAN readable on IBM System 360 Computers but may require special programming on others. NSSDC will also provide users with printouts of the radiometer data plus satellite location at 16 second intervals. The user should specify the data and time for which ESMR printouts are requested.

If it is found feasible for NSSDC to produce ESMR grid print maps, these may be requested from NSSDC. A Nimbus 5 Data Catalog will announce the availability and format of this product.

The address of the NSSDC and user ordering procedure are described in Section 1.7 of this report.

REFERENCES

1. Catoe, C., W. Nordberg, P. Thaddeus and G. Ling, "Preliminary Results from Aircraft Flight Tests of an Electrically Scanning Microwave Radiometer", NASA X-622-67-352, 1967.

2. Edgerton, A. T., F. Ruskey, D. Williams, A. Stogryn, G. Poe, D. Meeks and O. Russell, "Microwave Emission Characteristics of Natural Materials and the Environment", Microwave Division, Aerojet General Corp., ONR Contract NOOD 14-70C-0351, 1971.

3. Gunn, K. L. S. and T. U. R. East, "The Microwave Properties of Precipitation Particles", Quart. J. Met Soc., 80, 522-545, 1954.

4. Hollinger, J. P., "Passive Microwave Measurements of Sea Surface Roughness", Trans. IEEE Geoscience Electronics, GE-9, pp 165-169 (1971).

5. International Critical Tables of Numerical Data, Physics, Chemistry and Technology, Vol. IV, McGraw Hill, New York, 1928, pp 231-239.

6. Jackson, J. D., "Classical Electrodynamics", John Wiley & Sons, Inc., New York, 1962, p 216ff.

7. Lane, J. A. and J. A. Saxton, "Dielectric Dispersion in Pure Polar Liquids at Very High Radio Frequencies", Proc. Roy. Soc. London A, 214, pp 531-545, 1952.

8. Meeks, M. L. and A. E. Lilley, "The Microwave Spectrum of Oxygen in the Earth's Atmosphere", J. Geophys. Res. 68, 6, 1963.

9. Nordberg, W., J. Conaway, D. B. Ross, and T. Wilheit, "Measurements of Microwave Emission from a Foam-Covered Wind Driven Sea", J. Atmos. Sci., 28, 429-435, 1971.

10. Peake, W. H., R. L. Riegler, and C. A. Shultz, "The Mutual Interpretation of Active and Passive Microwave Sensor Outputs", Proc. 4th Symp. on Remote Sensing of Environment, Univ. of Mich., 1966.

11. Schmugge, T., P. Gloersen, and T. Wilheit, "Remote Sensing of Soil Moisture with Microwaves", NASA X-652-72-305.

12. Staelin, D. A., "Measurements and Interpretation of the Microwave Spectrum of the Terrestrial Atmosphere Near 1 Centimeter Wavelength", J. Geophys. Res., 71, 2875-2881, 1966.

13. Stogryn, A., "The Apparent Temperature of the Sea at Microwave Frequencies", Trans. IEEE Ant. and Prop., AP 15, 278-286, 1967.

14. Strong, A. E., "Mapping Sea-Surface Roughness Using Microwave Radiometry", J. Geophys. Res., 76, 8641-8648, 1971.

15. Wilheit, T., W. Nordberg, J. Blinn, W. Campbell, and A. Edgerton, "Aircraft Measurements of Microwave Emission from Arctic Sea Ice", to be published in Remote Sensing of Environment.

SECTION 5

THE INFRARED TEMPERATURE PROFILE RADIOMETER (ITPR) EXPERIMENT

by
W. L. Smith, H. B. Howell, J. C. Fischer, M. C. Chalfant and D. T. Hilleary
National Oceanic and Atmospheric Administration
National Environmental Satellite Service
Washington, D. C.

5.1 Introduction

The primary objective of the ITPR experiment is to describe the three-dimensional temperature field within the earth's atmosphere. The ITPR represents an improvement over previous satellite infrared radiometers because its higher spatial resolution allows more accurate determination of atmospheric temperature profiles in partly cloudy areas.

With a cross-course scan, described in Section 5.3.1, the ITPR will provide nearly contiguous coverage of the earth's surface over a 24-hour period. Figure 5-1 illustrates a typical 24-hour coverage of the Southern Hemisphere.

5.2 Description of the Experiment

The ITPR simultaneously measures the upwelling radiant flux in seven spectral intervals of the infrared spectrum:

- Two intervals in atmospheric "window" (low absorption) regions near 3.7 μm and 11 μm
- Four intervals in the carbon dioxide absorption band near 15 μm
- One interval in the rotational water vapor absorption band near 20 μm

A detailed description of these spectral intervals, and the spectral response functions for the ITPR are given in Table 5-1 and Figures 5-2 to 5-8 respectively.

Satellite observations of the earth's radiant flux in the seven spectral bands of the ITPR provide knowledge of the surface temperature (from the two window channels) as well as the temperature at a number of discrete levels in the atmo-

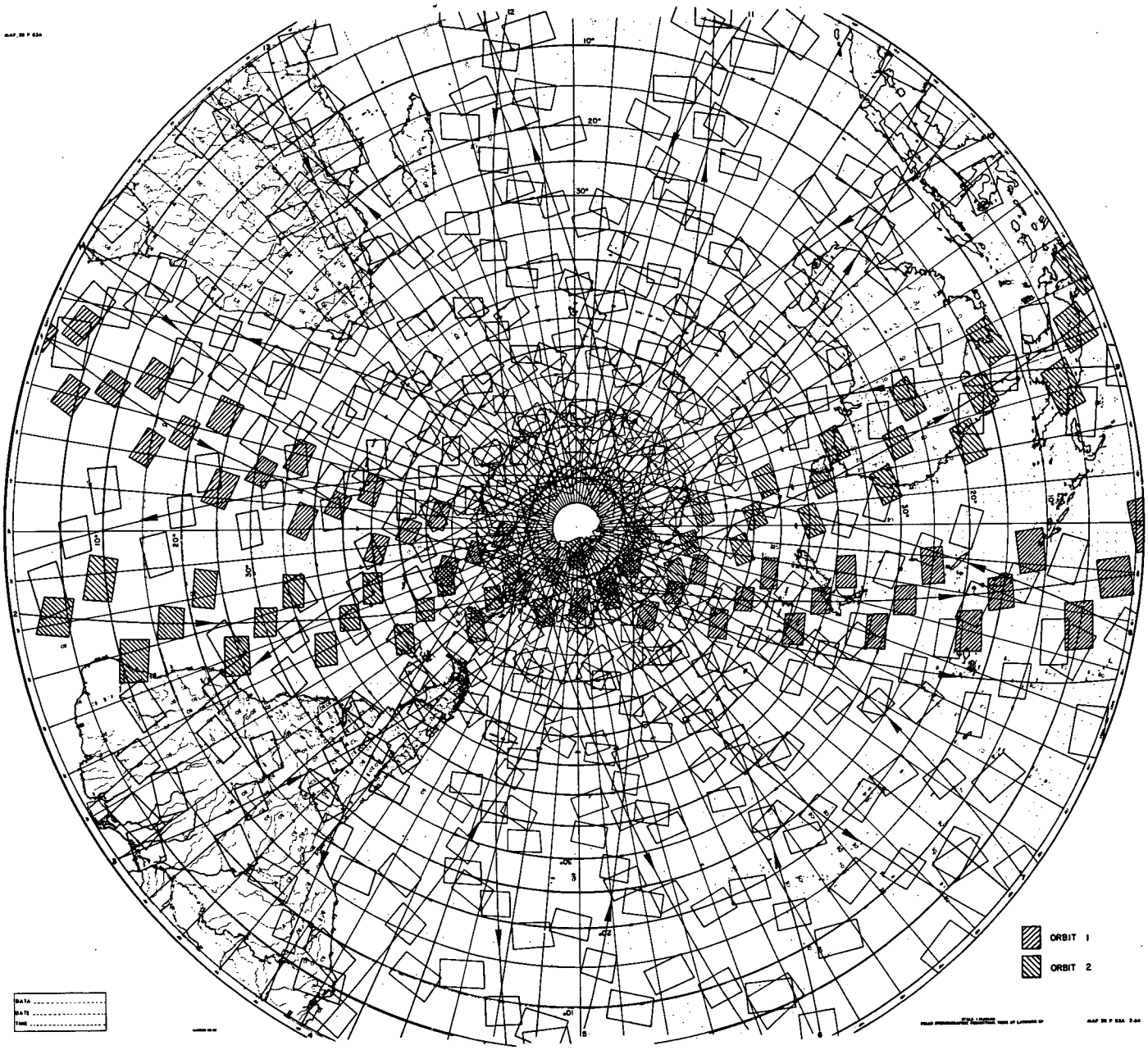

Figure 5-1. ITPR Grid Coverage of Southern Hemisphere During A 24-Hour Period

Table 5-1
ITPR Optical Unit Design Summary

Type of Instrument:	Multi-channel filter radiometer Cassegrainian before optics and refractive after optics.
Field of View:	Circular half power 1.45°, Circular 97% 1.84°; scans 35.1° each side of nadir.
Optical Design Summary:	Programmed object scan mirror 25 Hz earth-chopper reference reflective chopper. Cassegrainian fore optics, refractive aft optics. TGS pyroelectric detectors. Approximately 19.8 inches long, 10.25 inches wide and 10.75 inches high not including sun shields. Weight of 20 pounds.
Calibration:	Internal ambient blackbody reference surfaces and space.

ITPR Spectral Characteristics

Channel	Central Wave No. (cm^{-1})	Half Bandwidth (cm^{-1})	NEN ($mw/m^2\ sr\ cm^{-1}$)
1	2683	430	0.004
2	899.0	39.5	0.192
3	747.0	17.2	0.192
4	713.8	17.0	0.192
5	689.5	15.2	0.187
6	668.3	5.3	0.500
7	507.3	84	0.195

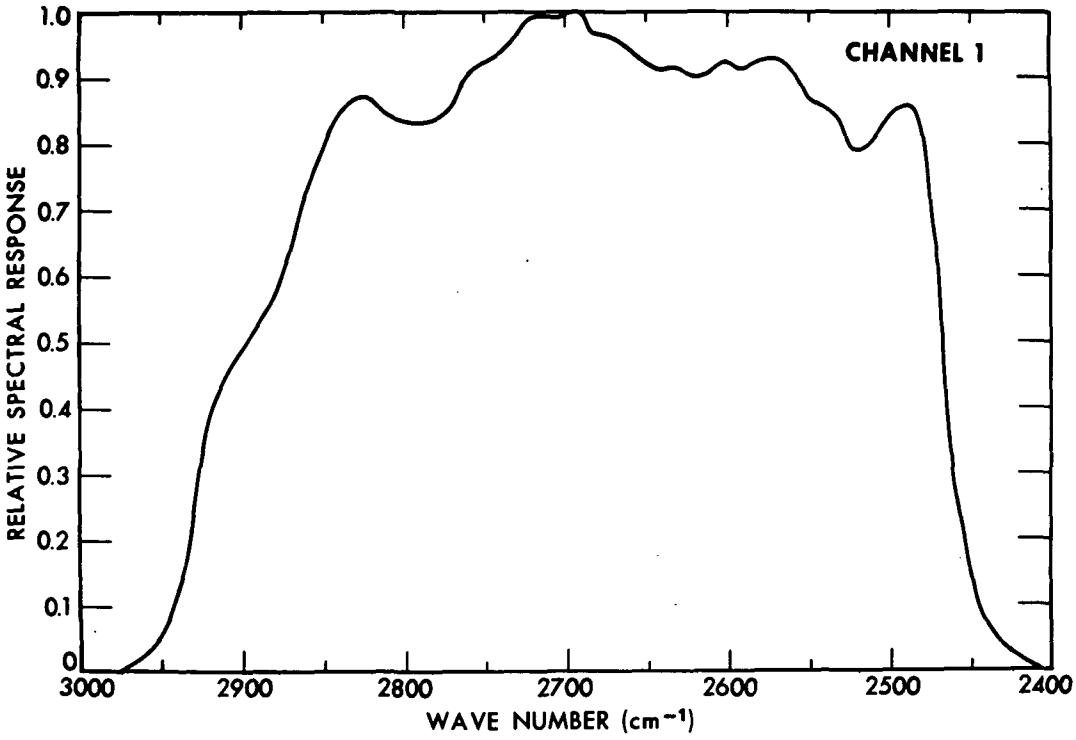

Figure 5-2. ITPR Channel 1 Spectral Response Function

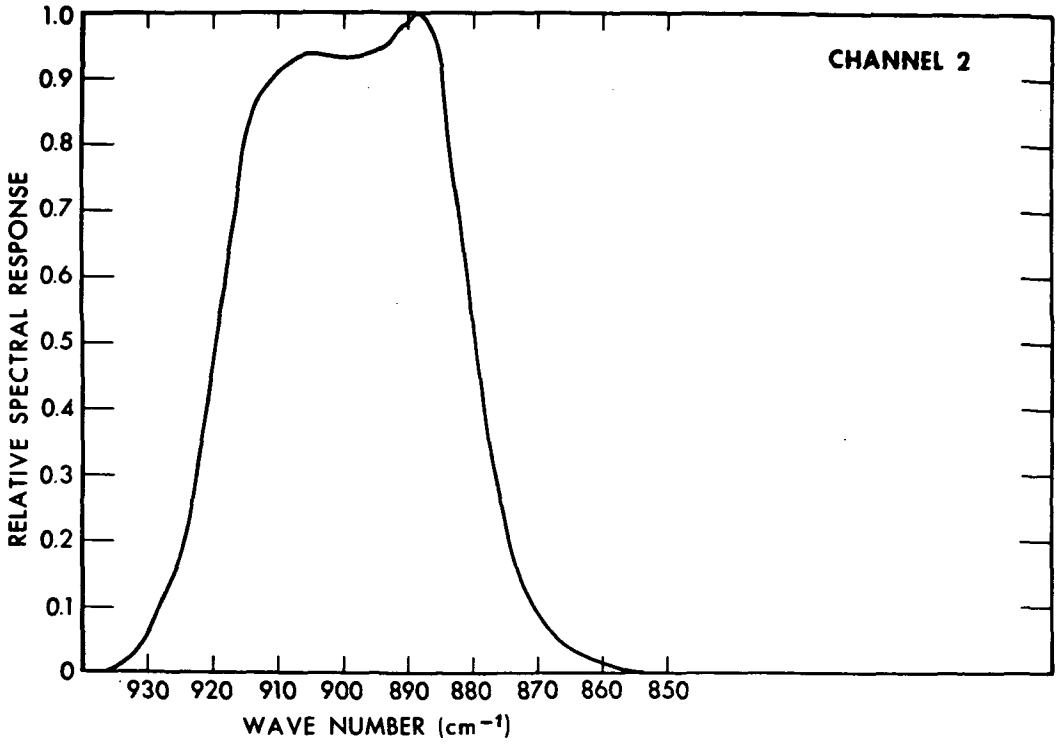

Figure 5-3. ITPR Channel 2 Spectral Response Function

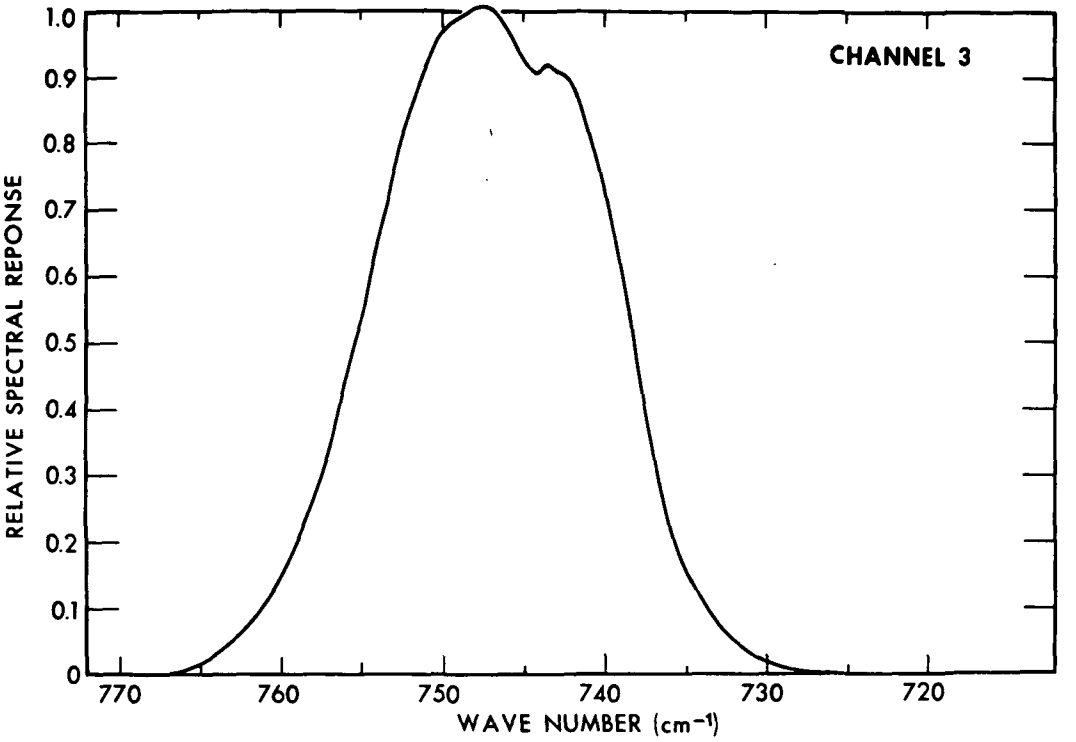

Figure 5-4. ITPR Channel 3 Spectral Response Function

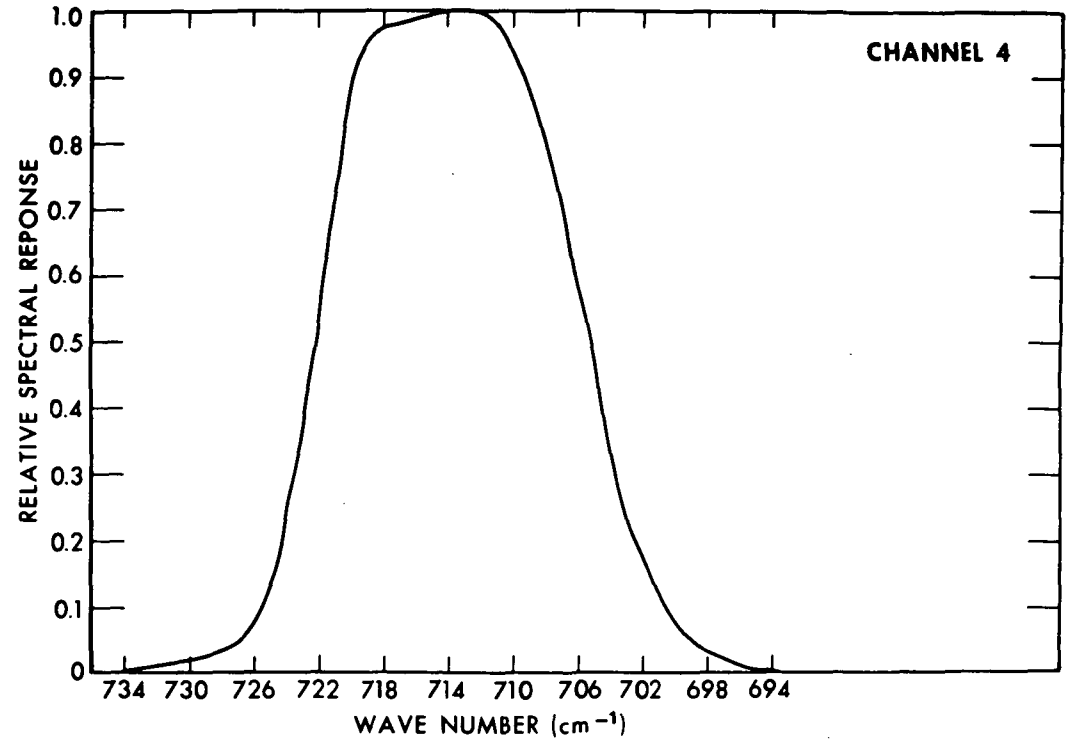

Figure 5-5. ITPR Channel 4 Spectral Response Function

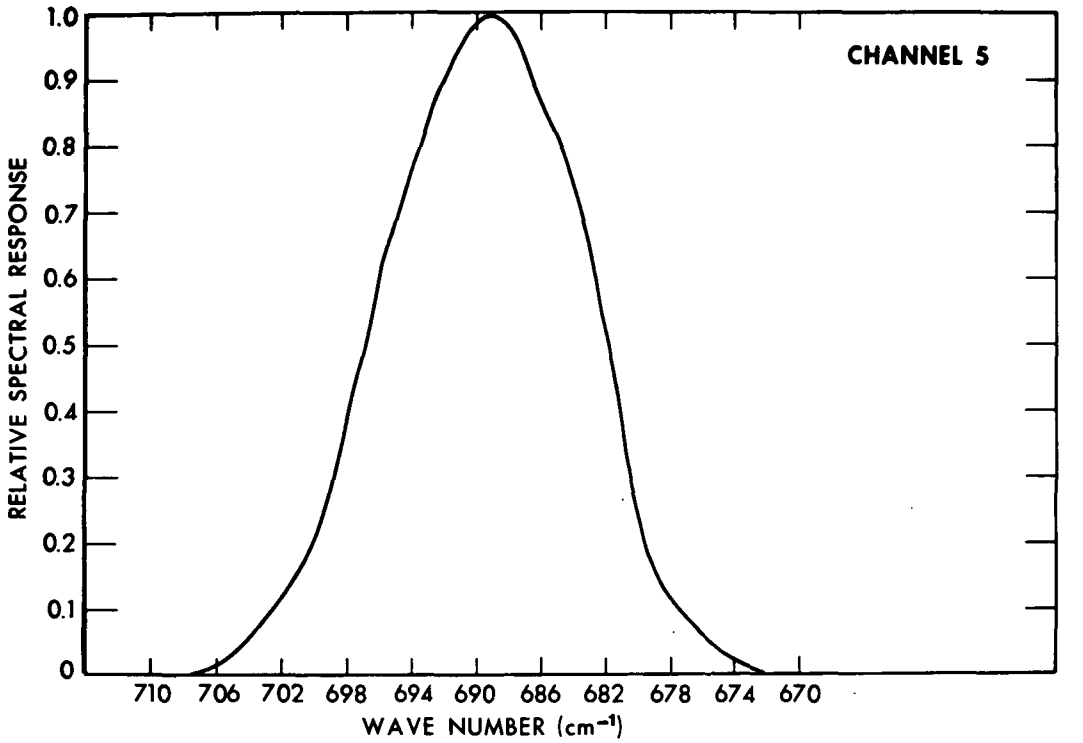

Figure 5-6. ITPR Channel 5 Spectral Response Function

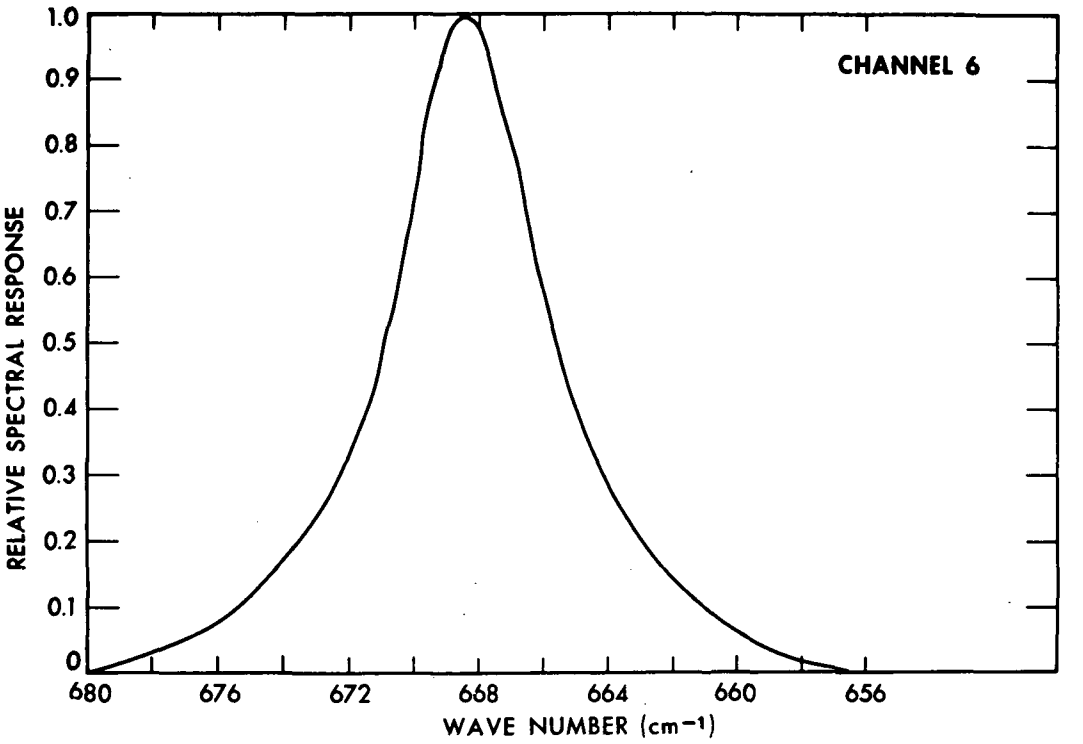

Figure 5-7. ITPR Channel 6 Spectral Response Function

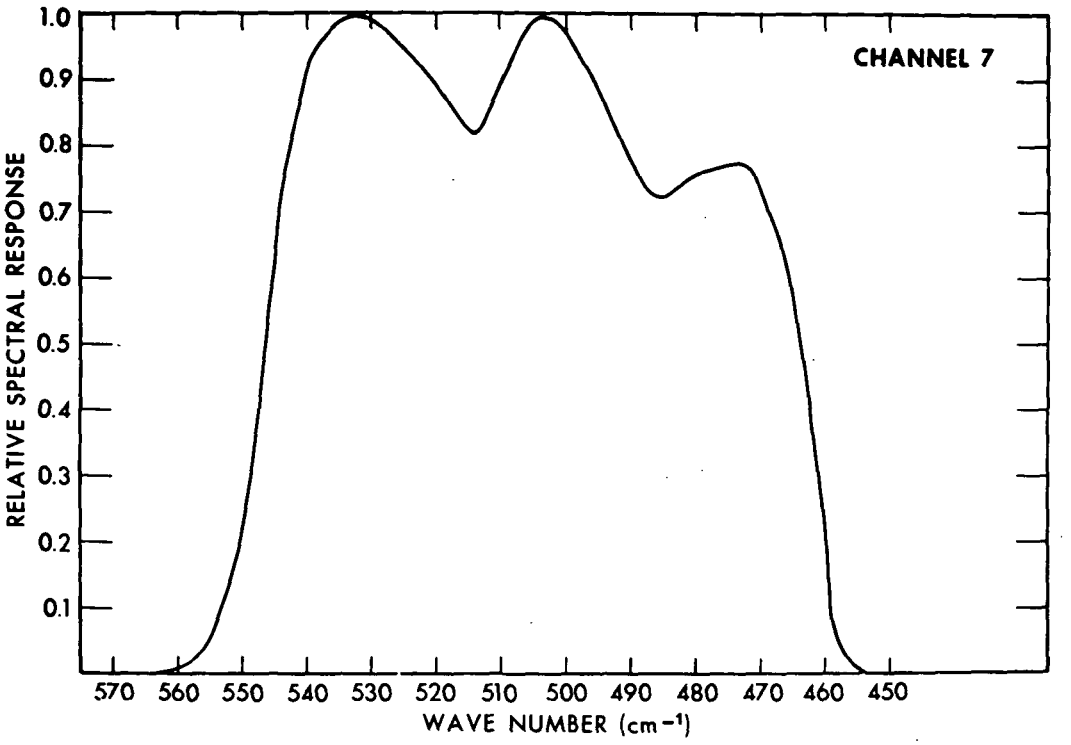

Figure 5-8. ITPR Channel 7 Spectral Response Function

sphere. The measured radiance $I(\nu)$ is related to the temperature profile T(p) by the integral form of the radiative transfer equation.

$$I(\nu) = B[\nu, T(p_s)]\, \tau(\nu, p_s) - \int_0^{p_s} B[\nu, T(p)] \frac{d\tau(\nu, p)}{d\ln p}\, d\ln p, \qquad (1)$$

where B is the Planck function, ν is the wave number of the radiation, and p is the atmospheric pressure, with subscript s referring to values at the earth's surface. The transmission of the atmosphere between pressure level p and the top of the atmosphere is expressed by $\tau(\nu,p)$. The more transparent spectral bands are more sensitive to the temperature variation lower in the atmosphere; the levels of primary sensitivity occur progressively higher in the atmosphere for the more opaque spectral intervals. The sensitivity of a given spectral interval to the temperature of a specific pressure level is proportional to the weight function $d\tau(\nu, p)/d\ln p$. The variation of this function with pressure is given in Figure 5-9 for the U.S. Standard Atmosphere. The more transparent ITPR channels are affected by the distribution of absorbing constituents in the atmosphere (e.g., water vapor, carbon dioxide, ozone) as well as the atmos-

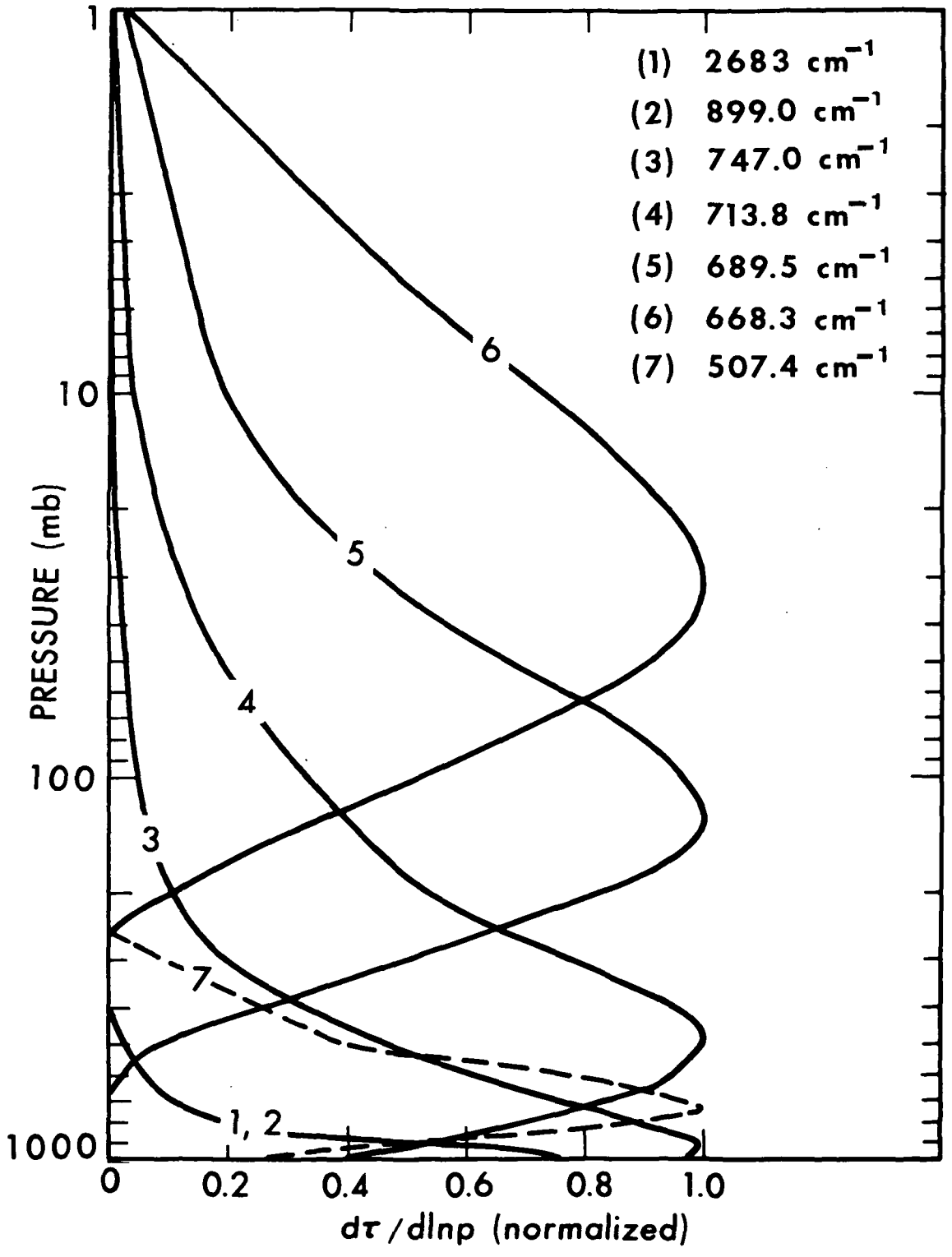

Figure 5-9. Atmospheric Weighting Functions for ITPR Spectral Channels

pheric temperature profile. The 20 μm interval provides a means of improving an estimate of the total precipitable water within a vertical column of the atmosphere, while the other channels are used in specifying the atmospheric temperature profile. A theoretical representation of atmospheric transmittance for the ITPR spectral intervals is described by Davis (Reference 1).

Successful inference of the vertical temperature profile down to the earth's surface depends on an accurate determination of the "clear column" radiance for each spectral interval. This, in turn, requires knowledge of the temperature of the earth's surface which can be obtained from the 3.7 μm and 11 μm window radiances measured from two adjacent fields of view (Reference 2).

Clouds generally exist within the fields of view of a sounding radiometer. In this case

$$I(\nu) = N\, I_{cd}\ (\nu) + (1 - N)\ I_c\ (\nu), \qquad (2)$$

where $I(\nu)$ is the observation, N is the fraction of the field covered by clouds, $I_{cd}(\nu)$ is the average radiance from the cloud covered portions of the field of view, and $I_c(\nu)$ is the average radiance from the cloud free portions of the field. The limitations imposed by clouds within the FOV are overcome with observations obtained from the spatially scanning ITPR which possesses sufficiently high spatial resolution (linear ground resolutions of about 30 km). With the ITPR measurements, it is possible to utilize the property that the scale of horizontal variability of clouds is much smaller than the scale of variability of the temperature profile. A numerical algorithm utilizing this property for determination of clear column radiance is presented by Smith (References 3 and 4).

Numerous temperature retrieval methods can also be used, such as described in Reference 7, and in the works listed in the Bibliography. Measurements of the water vapor profile will be obtained using radiance observations in the 20 μm band.

5.3 Description of the Instrument

The ITPR instrument consists of the following two components:

- Optical Unit

  This component measures the difference in IR radiation between the unknown scene and blackbodies on the satellite that are temperature controlled at 37.4°C. AC output voltages produced from the detectors are proportional to the radiance difference in each spectral interval. Each of these signals is amplified by its own amplifier before leaving the optical unit. The optical unit houses the telescopes, scan assembly, chopper and chopper motor, housing calibration radiation sources, and various electronics, including the amplifiers and detectors. Table 5-1 summarizes the design of the optical unit.

- Sensory Ring Module

  This component accepts the output voltages from the optical unit, synchronously demodulates, integrates, and converts these output voltages into ten-bit digital words for output into VIP. In addition to housing the synchronous demodulators, integrators, and A/D circuitry, the sensory ring module also houses the system power supply, command sequencer, scan logic, and temperature control circuitry. The sensory module is housed in a 3 over 3 module (6x6x13 inches) mounted in the sensory ring. Table 5-2 summarizes the design of the electronics.

Table 5-2
Electronics Design Summary

Analog Channel:	Gain: Variable, $2x10^4$ to $2x10^5$ Stability: 0.1%, 5°C to 55°C Demodulator: Full wave synchronous, timing derived from photo reference pickups on the chopper. Integrator Time: 240ms
A/D System:	Converts 7 IR Channels to a 10-bit plus sign digital word and 40 analog housekeeping channels to a 10-bit digital word. Samples the 7 IR channels every 400ms and the 40 housekeeping analog channels once every eight seconds. Provides sign, parity, scan mirror position, and various status bits information every 400ms.
Scan Control:	Sequence stepper scan motor to provide a three grid scan, each grid consisting of 140 discrete views. Operational programs include a calibration sequence at the end of each grid.
Commands:	14 commands are provided.
Temperature Control:	A closed loop temperature controller maintains the detectors, chopper reference blackbodies, and filters at 37.4° ± 0.2°C.

5.3.1 The Optical Unit

The ITPR sensor is a seven channel radiometer comprised of six Cassegrainian telescopes. Two of the channels are derived with a dichroic beam splitter located after one telescope. A photograph of the instrument's optical unit is shown in Figure 5-10. The ITPR FOV is positioned by the scan mirror. Exact scan mirror positioning is accomplished with a step-per-motor harmonic-drive encoder arrangement together with associated electronic logic. The scan sequence consists of three separate grids, each consisting of 140 individual observations obtained by cross-course scanning in step angles of 1.8°. Figure 5-11 illustrates a complete 3-grid ITPR scanning pattern. The first grid includes scan angles, referenced to the nadir, from 35.1° to the right of the subsatellite track to 11.7° to the right of the subsatellite track as viewed from the spacecraft. This grid will have surface dimensions of approximately 600 km (325 n.m.) perpendicular to the subsatellite track and 357 km (193 n.m.) paralled to the subsatellite track. The central grid will include scan angles from 11.7° to the left and right of the satellite track. Its surface dimensions are approximately 500 km (270 n.m.) perpendicular to the suborbital track and 357 km (193 n.m.) parallel to the subsatellite track. The third grid will be to the left of the subsatellite track and include the same scan angles and have the same surface dimensions as the first grid. Because of the spacecraft motion, the grids will be spaced along the subsatellite track, the first grid being to the lower right and the third to the upper left when looking downward and facing the direction of the spacecraft motion. The grids will be separated by a distance of approximately 99.2 km (53.6 n.m.) parallel to the subsatellite track due to the spacecraft motion during the time the scan mirror is positioned to view the internal (housing blackbody) calibration source and space.

Each channel sensing beam is alternately switched from the unknown scene input irradiance to an internal balckbody that is temperature controlled at 37.4° ±0.2°C. The optical switching is accomplished using a reflective chopper which produces a 25Hz chopping frequency. The chopper assembly includes an electrical pickoff arrangement for phasing as well as for furnishing control signals for the data processor demodulator-integrator.

The principal radiometer components are the scan mirror, optical chopper, telescopes and associated bandpass filters and detectors. These components have been optimized to obtain maximum sensitivity while maintaining the required radiometer characteristics. The average FOV of the optical channels is equivalent to a 1.46° right circular cone having a uniform spatial response. The half power FOV angular widths of channels 1, 3, 4, 5, 6, 7, are matched to within ±3% of that of channel 2. The half power edges of the fields of channels 1,3,4,5,6, and 7 are aligned with those of channel 2 within 0.05°.

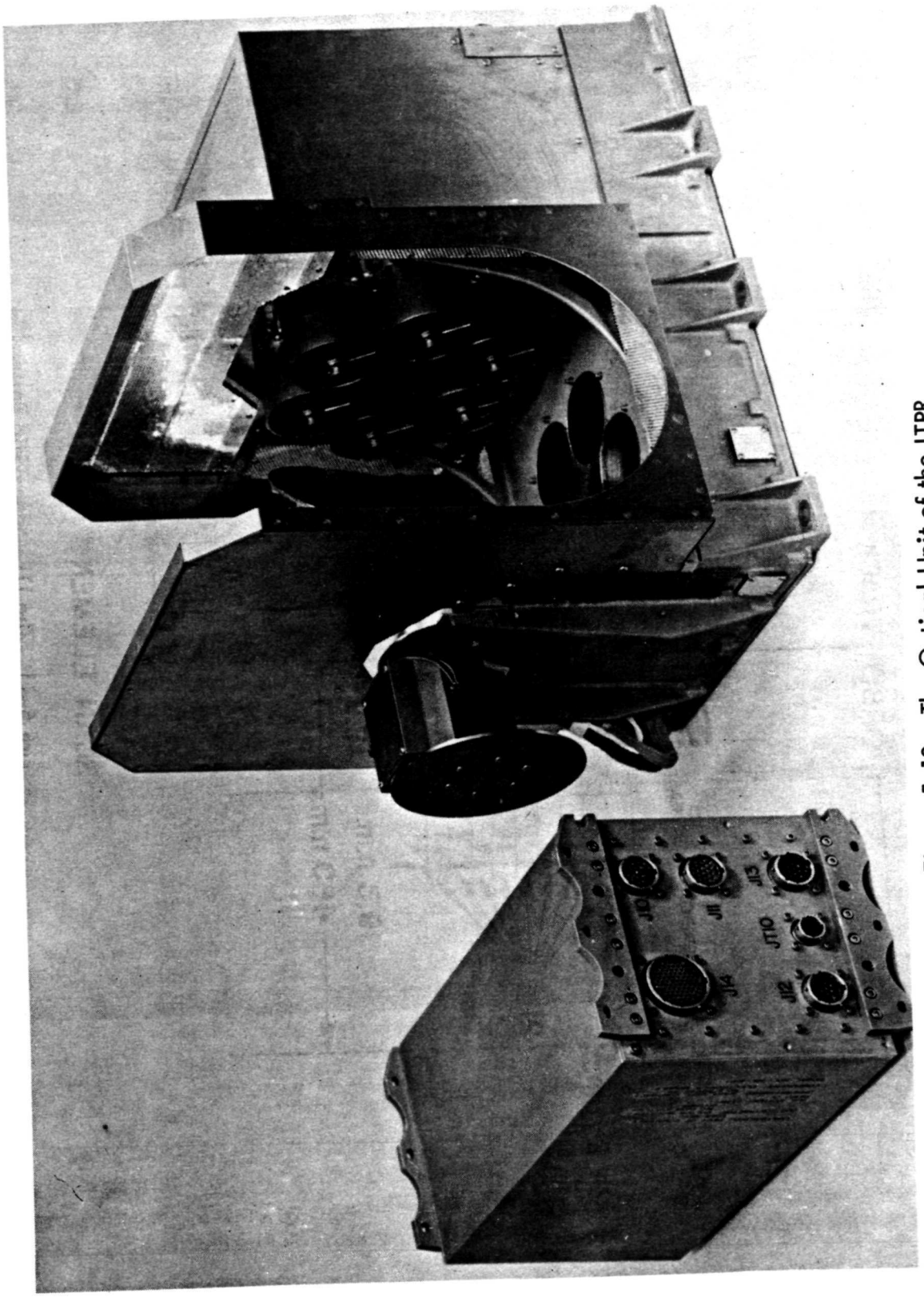

Figure 5-10. The Optical Unit of the ITPR

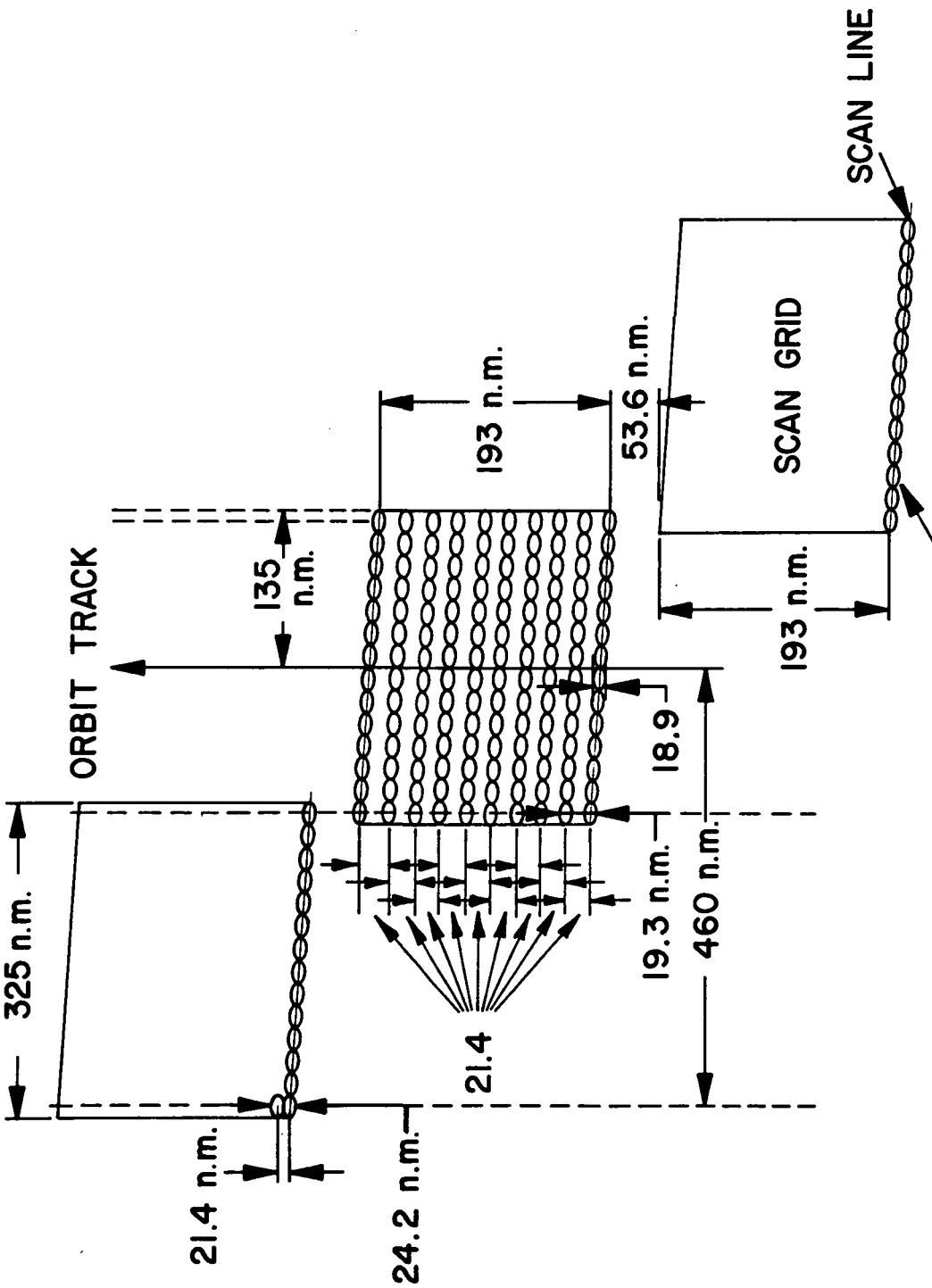

Figure 5-11. The ITPR Scan-Grid Pattern

The radiation in each selected spectral interval is detected by a Triglycine Sulphate (TGS) type pyroelectric detector element. Each detector element is placed at the image of a Cassegrainian telescope secondary. The output of each detector is amplified and processed through a full wave synchronous demodulator and integrated over a 240ms period during the mirror dwell period. The detectors are temperature controlled at 37.4° ± 0.2°C.

The amplifier is composed of a preamplifier and two ac-coupled gain stages. The preamplifier consists of a matched pair of low-noise field effect transistors (FET) used in a differential mode. The function of this circuit is to take very low level signals out of the pyroelectric detector and amplify them. To avoid stray capacitance and microphonism, one of the FETs of the matched pair and a two hundred gigaohm resistor are mounted inside the detector housing. The pair of FETs form the input drive for an integrated circuit amplifier. The preamplifier is composed of two feedback loops. One, made up of the pair of matched FETs and the integrated circuit amplifier, yields a stable closed loop gain. To keep small variations in the gate leakage of the input FETs from saturating the preamplifier output, a second feedback loop is employed. This feedback loop stabilizes the dc operating time of the input FET stage. The preamplifier is followed by two additional integrated circuit amplifiers. The purpose of these two stages is to establish the gain of the channel and to provide drive for the signal through the cable to the synchronous demodulator.

The synchronous demodulator is a full-wave demodulator whose output feeds a 240ms integrator. The integrator samples six cycles of the signal and then holds the signal until sampled by the analog-to-digital (A/D) converter. Each channel's six cycles of information is simultaneously taken and held in the integrator until sampled by the A/D. The seven data channels are sampled, encoded to ten binary bits, and sent along with sign and parity to the VIP telementry once every 400ms.

5.3.2 The Sensory Ring Module

The electronics in the sensory ring module provide the interface between the optical unit and the spacecraft power supply, clocks, and the VIP. This module contains seven synchronous demodulators and integrators for the signal channels, A/D system, scan control logic, temperature and voltage monitor circuits, command logic, and the system power supply.

The circuits of the sensory ring demodulate and integrate the outputs of the seven signal channels from the optical unit. This information is multiplexed with 40 channels of other analog information (temperature and circuit monitors) and converted into 10-bit digital words. A polarity bit is generated for the seven

signal channels. In addition to the analog data, five 10-bit digital words provide 50 bits for additional monitoring.

The 50 bits include encoder position, parity, sign, command verifications and other coded information. The seven signal channels and the five digital words are each sampled once every 400ms. The 40 various analog functions are sub-multiplexed and sampled twice each VIP major frame (every 8 seconds).

The sensory ring module contains the command circuitry necessary to control the instrument. Fourteen commands are utilized for this purpose.

5.3.3 Calibration

Flight calibration of the ITPR is achieved by turning the scan mirror to view a blackbody radiation source in the instrument housing for each of the six telescopes. A thermistor sensor in each radiation source senses the temperature. The calibration curves for the thermistors are shown in Figures 5-12 and 5-13. A second calibration point is taken by viewing space. Both points enable the noise of the system to be checked. A housing view and a space view are taken at the end of each scan grid, once every 80 seconds.

Pre-launch ground calibration of the ITPR is achieved by a special external radiation source. This source is varied in temperature from -180°C to + 70°C and thermocouples located in the source areas viewed by each telescope provide an accurate readout of the temperature. Calibration curves for the seven channels are defined by the constants given in Table 5-3. Up-to-date calibration constants will be derived after launch on the basis of in-flight calibrations.

5.4 ITPR Data Processing and Archiving

5.4.1 Data Processing

The ITPR data will be transmitted, via a DATRAN link from NASA/GSFC to NOAA/NESS as soon as the data can be extracted from the incoming VIP data stream. The data transmitted via DATRAN will be kept on magnetic tape at the NASA/GSFC for a one-month period.

The raw data will be routinely processed by NOAA/NESS and the data (including radiances, earth locations, in-flight calibration, and engineering data) will be stored on the master archival tapes. Compacted data archival tapes containing only the calibrated, located radiances and a minimum of auxiliary

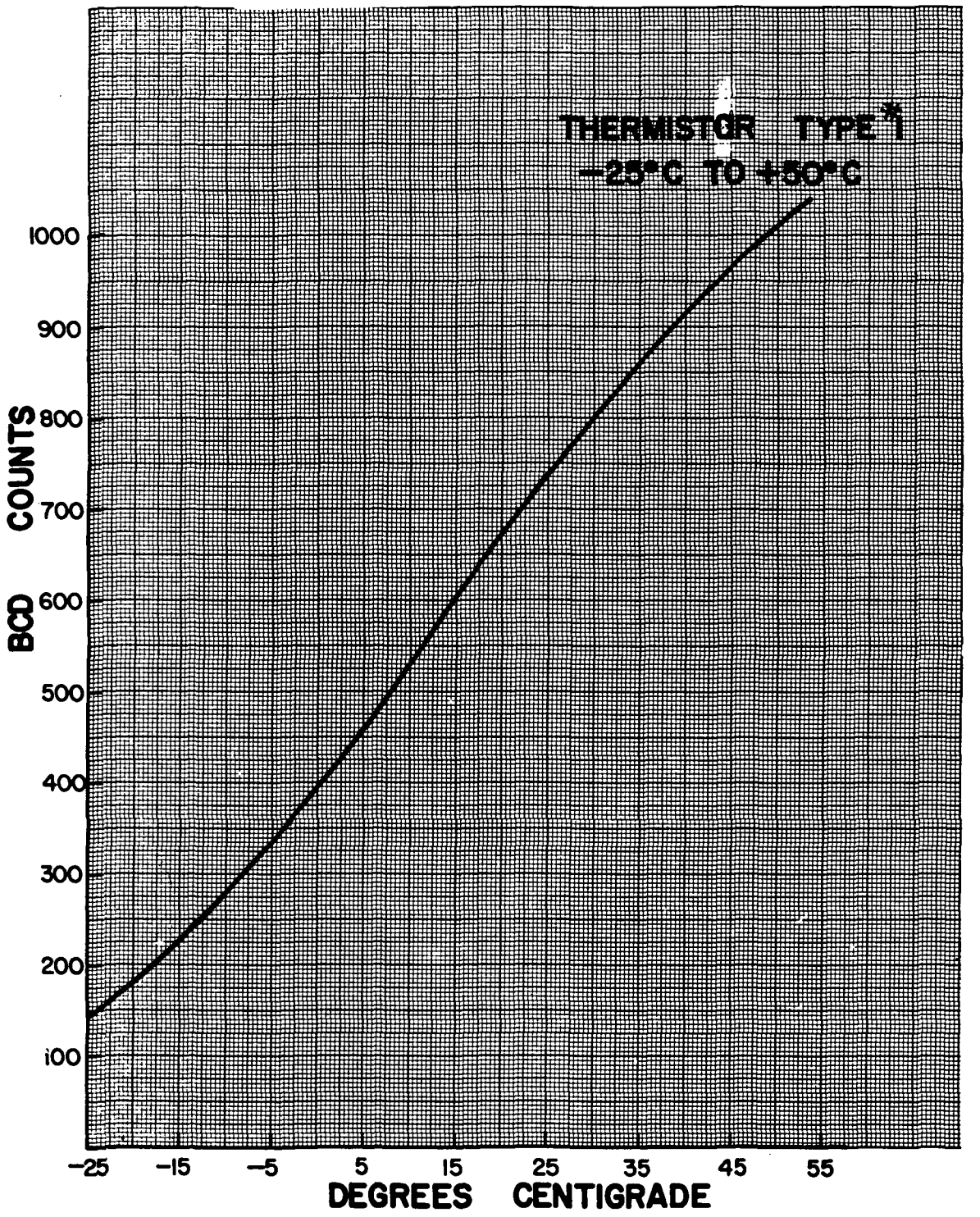

Figure 5-12. Calibration Curve for Type 1 Thermistors

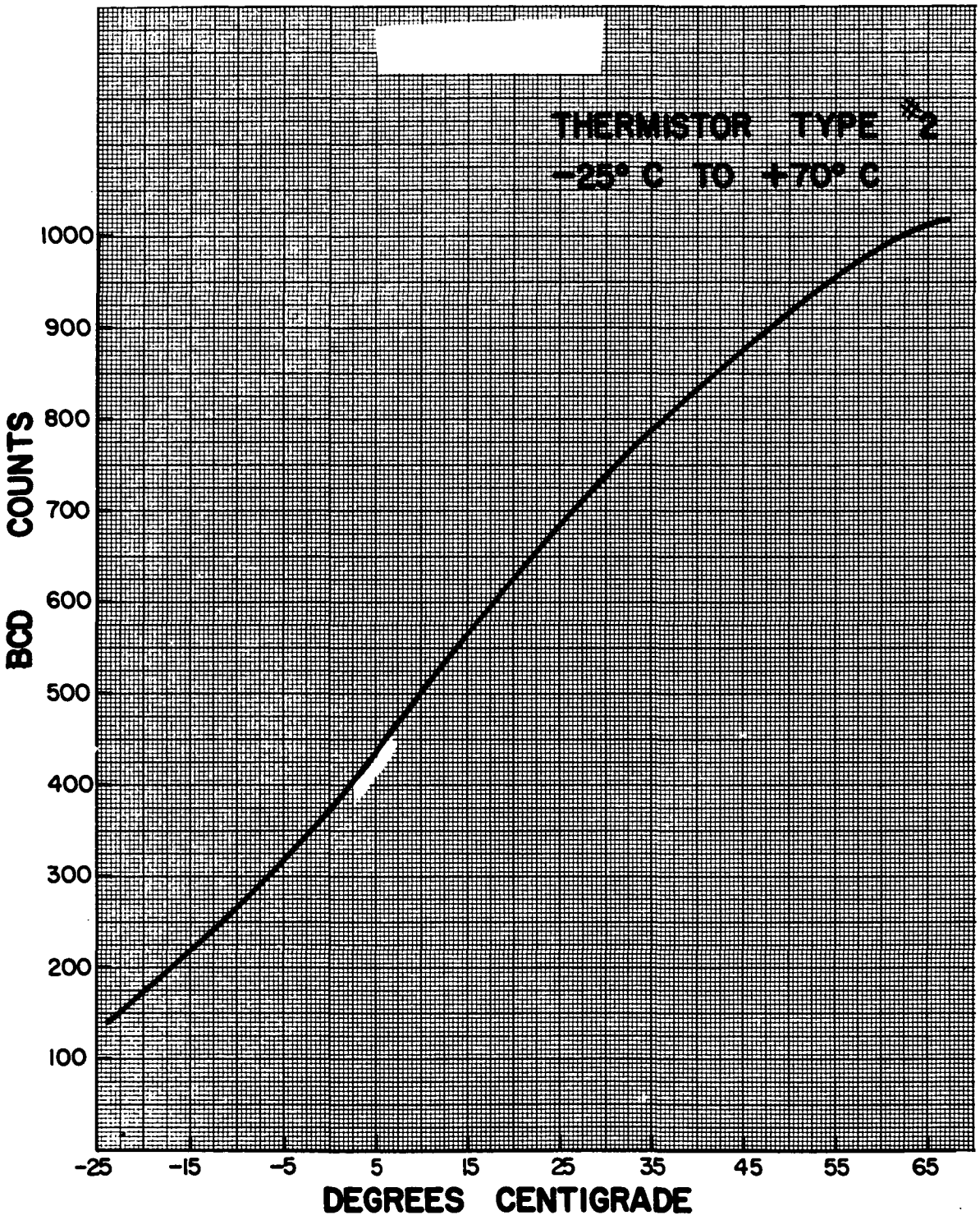

Figure 5-13. Calibration Curve for Type 2 Thermistors

Table 5-3
ITPR Calibration Constants*

$$R_S - R_C = a_0 + a_1 V$$

R_S = radiance of the scene (mw/m^2 sterad cm^{-1})

R_C = radiance of the chopper reference blackbody (mw/m^2 sterad cm^{-1})

V = digital counts

Channel	a_0	a_1
1	0.038	-0.001770
2	1.01	-0.1886
3	1.87	-0.1976
4	2.14	-0.1971
5	1.45	-0.1918
6	1.87	-0.1916
7	1.25	-0.1932

*These constants were derived from calibration data obtained during thermal vacuum tests in September 1972. Up-to-date calibration constants will be derived after launch on the basis of in-flight calibrations. These revisions in the calibration will be published in the Nimbus 5 Data Catalog.

information will be generated from the master archival tapes. The format of the compacted data tapes is described below:

Nimbus-5 Compacted Data Format

Word	Format	Description
1	I	GMT (seconds)
2	Spec 1	Julian Day & Year
3 - 146	Spec 2 (F1, F3)	Calibrated IR Data
147 - 164	F1	Latitude
165 - 182	F1	Longitude
183 - 200	F1	Zenith Angle

I This format stores data as right-adjusted integer in a 24-bit word.

F1 This format stores two data values as right-adjusted integers in the high and low order 12 bits of each 24-bit word. Negative numbers will be represented in one's compliment and the decimal point is understood to be to the left of the first decimal digit from the right for each 12-bit data value (i.e., after unpacking and extending the sign, multiply by 10^{-1}).

F3 This format stores data as a right-adjusted integer in a 24-bit word. The decimal point is understood to be to the left of the third decimal digit from the right (i.e., after unpacking multiply by 10^{-3}).

Spec 1 This format stores the Julian day as a right-adjusted integer in the high order 12-bits of word number 2 and the year as a two digit integer in the low order 12-bits of word number 2.

Spec 2 This format is a combination of the F1 and F3 formats. Data from channel 1 will be stored in word number 3 in F3 format. The next consecutive 12-bit bytes, which make up words numbered 4-6, will contain data from channels 2-7, respectively, in F1 format. This 4 word pattern will be repeated thru word 146, resulting in 36 sets of IR measurements.

Each data record will contain 6 major frames of 200 24-bit words for a total of 480 60-bit words. Because data frames will contain either 34 or 36 earth positions for each channel, it will be necessary to zero fill words 139-146, 163, 164, 181, 182, 199 and 200 when only 34 earth positions are available. It will also be necessary to zero fill if the number of major frames in a day is not a multiple of six.

The compacted tape will be written with a density of 556 6-bit bytes per inch, on seven track tape in odd parity (binary). There will be about 12 orbits per day at 320 major frames each. There will be about 640 records per day followed by an EOF. Each compacted tape will contain about 5 days of compacted ITPR data followed by a DEOF.

5.4.2 Data Archiving

Determinations of atmospheric temperature profiles and the corresponding radiances and earth locations will be archived at NOAA/NESS. Copies of these tapes will be available upon written request to:

Dr. W. L. Smith
NOAA/NESS
Suite 300
3737 Branch Avenue
Hillcrest Heights, Md. 20031

The first year's ITPR data, in compacted data tape format, will be furnished by NOAA/NESS to the NSSDC. The address and request procedure for these tapes are described in Section 1.7 of this report.

The ITPR derived temperature profiles used in the NMC operational forecasts will be available from the NCC, Asheville, North Carolina, as described in Section 1.7 of this report.

REFERENCES

1. Davis, P. A., "Universal Transmittance Representations For Application to ITPR Measurements", Final Report prepared for NOAA/NESS, Contract 2-35136, Stanford Research Institute, Menlo Park, California, May 1972, 45 pp.

2. Smith, W. L., and W. J. Jacob, "Multi-Spectral Window Determination of Sea Surface Temperature and Cloud Properties," (To be submitted to Monthly Weather Review).

3. Smith, W. L., "An Improved Method for Calculating Tropospheric Temperature and Moisture from Satellite Radiometer Measurements," Monthly Weather Review, Vol. 96, No. 6, June 1968, pp. 387-396.

4. Smith, W. L., "The Improvement of Clear Column Radiance Determination with a Supplementary 3.8μm Window Channel," ESSA Technical Memorandum NESCTM 16, 1969 (Available from the National Technical Information Service, 17 pp.).

5. Smith, W. L., Woolf, H. M., and W. J. Jacob, "A Regression Method for Obtaining Real Time Temperature and Geopotential Height Profiles from Satellite Spectrometer Measurements and Its Application to Nimbus III 'SIRS' Observations," Monthly Weather Review, Vol. 98, No. 8, Aug. 1970, pp. 582-603.

6. Smith, W. L., H. M. Woolf, and H. E. Fleming, "Retrieval of Atmospheric Temperature Profiles from Satellite Measurements for Dynamical Forecasting," Journal of Applied Meteorology, Vol. 11, No. 1, Feb. 1972, pp. 113-122.

7. Fleming, H. E., and W. L. Smith, "Inversion Techniques for Remote Sensing of Atmospheric Temperature", Proceedings of the Fifth Symposium on Temperature, Its Measurement and Control in Science and Industry, June 21-24, 1971, Washington, D. C.

BIBLIOGRAPHY

Chahine, M. T., "Recent Development in the Inversion by the Method of Relaxation", Mathematics of Profile Inversion, 1971.

Conrath, B. J., "Inverse Problems in Radiative Transfer: A Review", Proceedings of the Astronautical Congress, 339-360, 1968.

Gille, J. C., "Inversion of Radiometric Measurements", Bull. Am. Meteor. Soc., 49, 903-912, Sept. 1968.

Houghton, J. T., and S. D. Smith, Remote Sounding of Atmospheric Temperature from Satellite, Part 1. Introduction, Proc. Roy. Soc. London, A,320,23-33, 1970.

Kaplan, L., Jet Propulsion Lab., "Inference of Atmospheric Structure from Remote Radiation Measurements", Journal of the Optical Society of America, 49, October 1959.

Rodgers, C. D. ,"Satellite Infrared Radiometer, A Discussion of Inversion Methods", Memorandum No. 66.13 Clarendon Laboratory, Oxford University, 1966.

Rodgers, C. D., "Remote sounding of the atmospheric temperature profile in the presence of cloud," Quart. J. Roy. Meteorol. Soc., 96, 654-666, 1970.

Rodgers, C. D., "Statistical inversion techniques for sounding the meteorological structure of the atmosphere," in Mathematics of Profile Inversion, 1971.

Smith, W. L., and S. Fritz, "On the Statistical Relation Between Geopotential Height and Temperature-Pressure Profiles," ESSA Technical Memorandum NESC TM 18, 16 pp, 1969.

Smith, W. L., P. K. Rao, R. Koffler, and W. R. Curtis, "The Determination of Sea Surface Temperature from Satellite High Resolution Infrared Window Measurements", Monthly Weather Review, Vol. 98, No. 8, Aug. 1970, 604-611.

Smith, W. L., "Iterative Solution of the Radiative Transfer Equation for the Temperature and Absorbing Gas Profile of an Atmosphere". Applied Optics, Vol. 9, No. 9, 1993-1999, Sept. 1970.

Smith, W. L., and H. E. Fleming, "Statistical vs Non-Statistical Temperature Inversion Methods," Proceedings of the Workshop on the Mathematics of Profile Inversion, AMES Research Center, July 1971, Edited by L. Colin, NASA TMX-62150, 1972.

Strand, O. N., and E. R. Westwater, "Statistical Estimation of the Numerical Solution of a Fredholm Integral Equation of the First Kind", J. Assoc. Comp. Mach., 15, 100-114, 1968.

Twomey, S., "On the Numerical Solution of Fredholm Integral Equations of the First Kind by the Inversion of the Linear System Produced by Quadrature", J. Assoc. Comp. Mach., 10, 97-101, 1963.

Twomey, S., "The Application of Numerical Filtering to the Solution of Integral Equations Encountered in Indirect Sensing Measurements", J. Franklin Inst., 279, 95-109, 1965.

Twomey, S., "Indirect Measurements of Atmospheric Temperature Profiles from Satellites, II, Mathematical Aspects of the Inversion Problem", Mon. Wea. Rev., 94, 363-366, 1966.

Wark, D. Q., and H. E. Fleming, "Indirect Measurements of Atmospheric Temperature Profiles from Satellites, I, Introduction," Mon. Wea. Rev., 94, 351-362, 1966.

Wark, D. Q., and D. Hilleary, ESSA, "Atmospheric Temperature: Successful Test of Remote Probing", Science, 165, 1256-1258, September 1969.

Waters, J. W. and D. H. Staelin, "Statistical Inversion of Radiometric Data", Quart. Progress Report 89, Research Laboratory of Electronics, M.I.T., April 15, 1968.

Westwater, E. R., and O. Strand, "Statistical Information Content of Radiation Measurements Used in Indirect Sensing", J. Atmos. Sci., 25, 750-758, Sept. 1970.

SECTION 6

THE SELECTIVE CHOPPER RADIOMETER (SCR) EXPERIMENT

by
J. T. Houghton, Oxford University, England
and
S. D. Smith, Heriot-Watt University, Edinburg, Scotland

6.1 Introduction

The Selective Chopper Radiometer (SCR) for Nimbus 5 is a self-calibrating 16-channel radiometer for sounding the atmosphere beneath the satellite. The field of view (FOV) is 1.5° for 12 channels and 2.2° for the other four. The eight primary "temperature sounding" channels measure radiation in various spectral intervals within the 15μm band of carbon dioxide. The higher channels employ "selective chopping" of the incoming signal to determine the temperature profile up to 50 km. This is realized by changing the path of CO_2 inside the instrument and differencing the resultant signals. Support channels at long and short wavelengths measure cloud cover and water vapor parameters while three "window" channels at 11.6μm, 3.6μm and 3.3μm measure surface (or cloud top) temperatures. The channels' signal information is internally digitized to 10 bits. Motion in the FOV during sampling time is compensated. References 1 and 2 provide a description of the principles of atmospheric temperature sounding from satellites.

6.2 Optics and Radiometric Calibration

6.2.1 Optics

The 16 channels are detailed in Table 6-1 and Figure 6-1. They are subdivided into four filter wheel assemblies, each with its own light pipe/detector system. Channel B has four cells containing different amounts of carbon dioxide; A, C and D are straightforward filter changing.

Figure 6-2 shows the layout of the optical components. The radiation entering the earth port is diverted by the calibration mirror onto the off-axis paraboloid mirror at the left. The radiation is then directed toward a reflecting "bowtie" chopper set at 45° to the principal beams. As the chopper rotates, the earth radiation, in turn, reflects off the chopper onto a beam splitter, or passes through the chopper onto a second beam splitter. The A and D channel beam splitter is a piece of sapphire which reflects the A channels and transmits

Table 6-1
Channel Characteristics of SCR Flight Instrument

Channel Designation	Center cm^{-1}	Width at half transmission cm^{-1}	Filter type	path length mm	pressure CO_2 mb	Total pressure including He mb	*** f	Typical op for 21°C counts	rms noise	
									counts	(ΔT_n) °K **
A1	668.5	9.0	DHW					950	1.2	0.15
A2	688.5	9.0	DHW					741	0.7	0.11
A3	707.4	9.3	DHW					634	0.5	0.08
A4	726.5	12.6	DHW					626	1.2	0.2
B1	668.2	3.4	FP	3	0	13	1	447	1.2	0.3
B2	668.2	3.4	FP	3	40	49	0.89	442	1.0	0.2
B3	668.2	3.4	FP	3	95	103	0.81	483	1.4	0.3
B4	668.2	3.4	FP	3	310	325	0.64	390	1.4	0.4
C1	110*		MESH					686	1.8	0.6
C2	202	18	2nd order FP MESH					295	1.9	1.2
C3	536.4	13.3	DHW					895	0.7	0.1
C4	859	89	DHW					1232	TELEMETRY LIMITED	0.1
D1	3710	72	DHW					414	9	0.4
D2	3805	100	DHW					330	9	0.5
D3	4260(*10%)							113	9	1.5
D4	2817	50	DHW					283	9	0.7

* edge filter: number is position of edge.

** defined so that the rms noise at the output is equivalent to change in signal which would occur from a blackbody source near 250°K (channels A, B, C) or 291°K (channel D) if its temperature changed by ΔT_n K.

*** defined by equation (2).

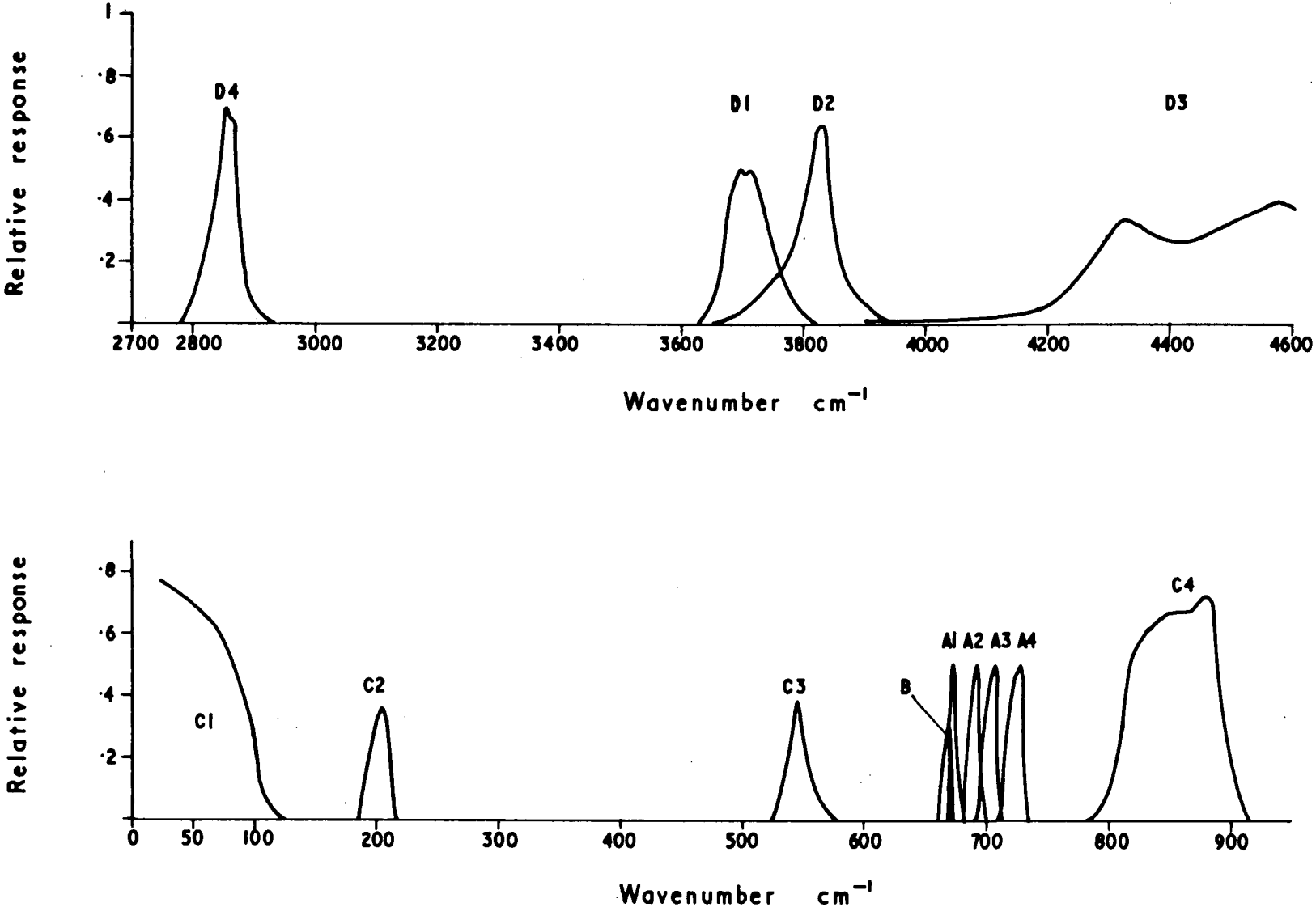

Figure 6-1. SCR Channel Spectral Response

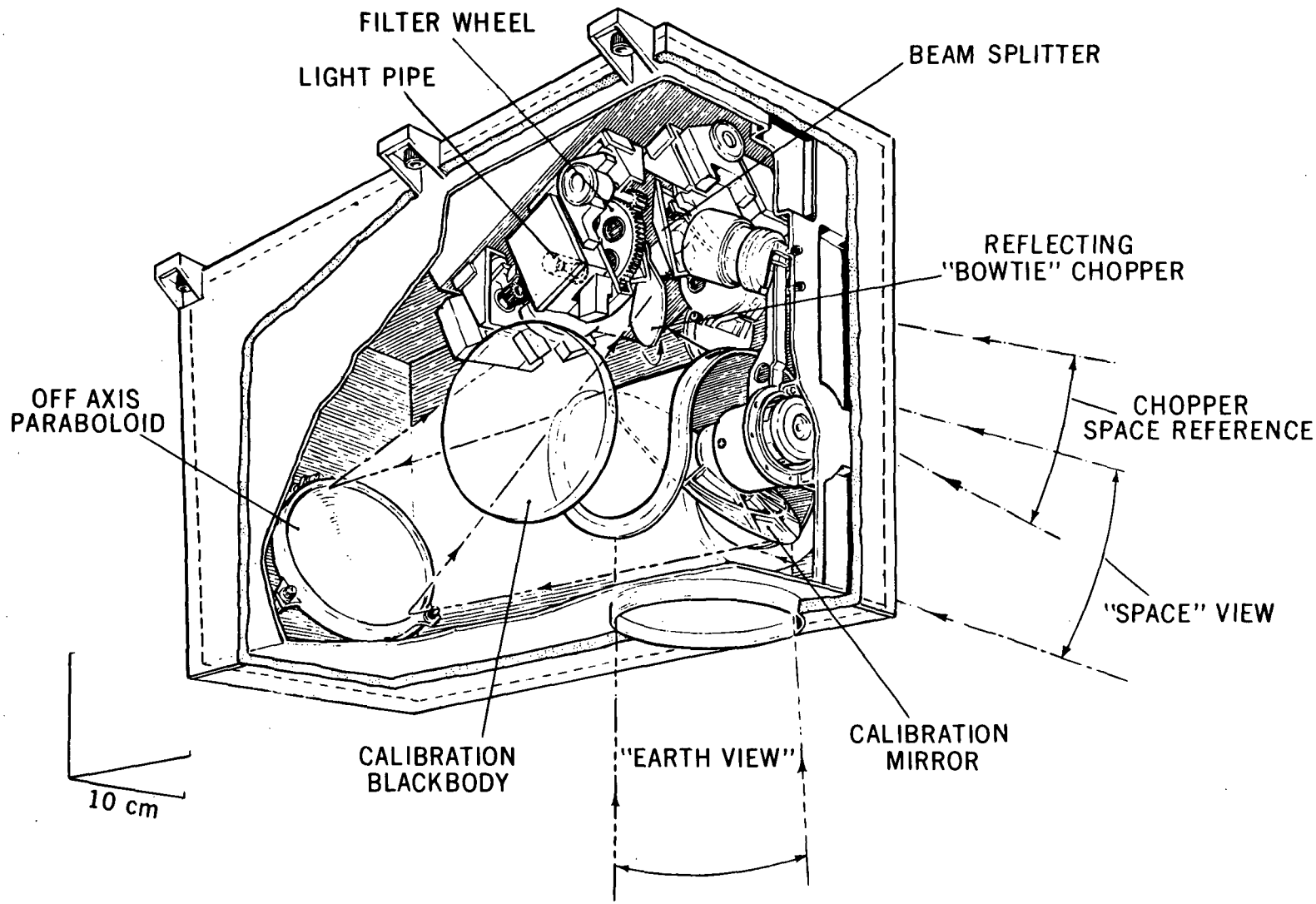

Figure 6-2. SCR Basic Optics

the D set. The B and C channel beam splitter is a multilayer component on a germanium substrate, which transmits the 15μm B channels and reflects the C channel wavelengths. The divided beams are then focused onto the entrance lenses of the four light pipes.

The FOV of each channel is defined by the diameter of the entrance to the light pipe and the focal length of the off-axis paraboloid. This is 1.5° for A, C, and D, and 2.2° for B.

6.2.2 Filter Stepping

The four filter wheels step synchronously with the leading edge of the 1 Hz spacecraft clock, the transition taking 150 ms. The wheel is then stationary for 850 ms. Associated logic circuitry ensures that a 4-1 transition of the filter wheels occurs with the VIP major frame pulse. Corrective drive pulses are supplied in case of mis-stepping. The filter wheels can be stopped in any selected position by command.

6.2.3 Field of View Compensation

To ensure that the 16 channels view the same vertical column, the calibration mirror is tilted linearily in time, back along the satellite path for 3.85 seconds with a return or a flyback time of 0.15 seconds. Thus the SCR earth viewing point remains "stationary" for four successive filter measurements, and "catches up" with the satellite during the 4-1 filter transition.

6.2.4 Inflight Calibration

The calibration mirror can rotate to view an internal blackbody, or it can view space through a port next to the chopper "space view." This sequence of mirror movements is initiated automatically every 128 major frames (31 minutes) as detailed in Table 6-2. This measures the overall gain of the system and offsets introduced by the emission of post-chopper optics. The temperature of the blackbody is monitored by three thermistors.

Thus the radiance R measured on channels A, B or C is given by

$$R^{A,\,B\text{ or }C} = \frac{R_B\,(T_B) \times [(EA - EZ) - (SP - EZO)]}{[(B - EZ) - (SP - EZO)]} \qquad (1)$$

where $R_B\ (T_B)$ is the radiance from blackbody within the channel spectral profile at the measured temperature of the internal blackbody. The other symbols are defined in Table 6-2, while EZ and EZO are explained in Section 6.3.3.

Table 6-2
SCR Calibration Sequence

Time (MFP units)	Function	Signal channel outputs		Digital B 54	77	78	79	80
0-1	Calibration imminent	Earth signal	(EA)	1	1	0	0	0
1-2	Mirror moves from earth to blackbody	Electrical zero	(EZ)	0	1	0	0	0
2-5	Mirror views blackbody	Blackbody	(B)	0	0	1	0	0
5-6	Mirror moves from blackbody to space view	Electrical zero offset	(EZO)	0	0	1	0	0
6-9	Mirror views space view	Space	(SP)	0	0	0	0	1
9-10	Mirror moves back from space view to earth view	Electrical zero	(EZ)	0	0	0	0	1
11-127	Mirror views earth	Earth view		0	1	0	0	0
	The cycle then repeats							

For the differenced B channels, radiances can be defined as

$$R_{B_1 - B_2} = \frac{R_{B_1} - f R_{B_2}}{1 - f} \tag{2}$$

where f is shown in Table 6-1.

The D channel radiances R^D are given by

$$R^D = \frac{R_B (T_B) \times G_D[(EA - EZ) - (SP - EZO)]}{[(B - EZ) - (SP - EZO)]} \tag{3}$$

where G_D is found from Table 6-3.

Table 6-3
Channel D Gain Change Compensation Factor (G_D)

Channel	Subsatellite point "day"	Subsatellite point "night"
	B64=0	B54=1
D1	14.4	1
D2	42.3	1
D3	2430	1
D4	1	1

The factor G_D compensates for the gain change made between viewing reflected sunlight and the much lower intensity internal blackbody. For "normal" automatic operation, D channels switch to low gain for "earth" view. This can be overridden by command.

6.2.5 Preflight Calibration

The typical response and noise figures for the unit are shown in Table 6-1. Large conical targets variable from LN_2 to + 40°C were used. The measurements showed equations 1 and 3 to be valid.

6.3 Signal Channel Electronics

6.3.1 Detectors

Channels A, B, and C use self-poling TGS pyroelectric detectors, while D uses a PbS detector. They are mounted with a source follower FET on the end of a nickel light pipe.

6.3.2 Amplifiers

A preamplifier of gain 50-200 is mounted with the light pipe in the filter wheel. The main amplifier gain is changed by logic using the filter position indication outputs. The output is divided and one part is inverted. A phase sensitive rectification provides a current source.

6.3.3 Output Ramp

The output current is fed into a true integrator to give a ramp output. The integrator is reset on the leading edge of the 1 Hz clock and held clamped to zero for 180 ms. (Compare filter wheel transit time of 150 ms + 30 ms for detector transients to decay.) Hence output waveforms for A channels are

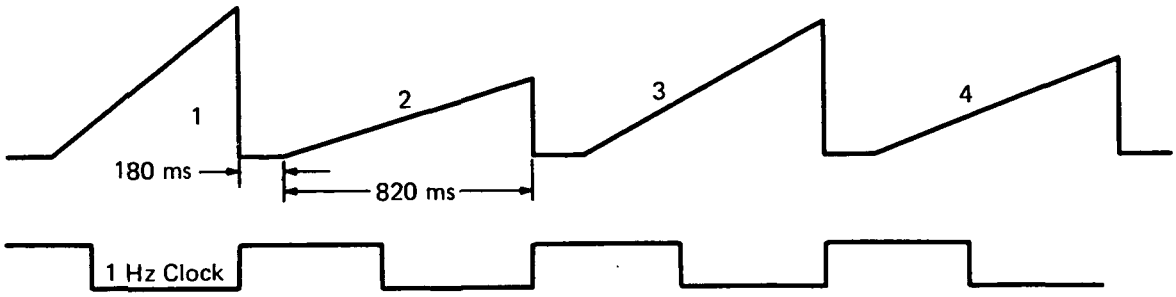

There is a bleed current of approximately 10% of full scale (EZ) to prevent "bottoming" on noisy low signal levels. A bleed current of half scale offset (EZO) is introduced when measuring in the space view. These offsets are measured during calibration mirror movements by reducing the preamplifier gain by a large factor.

6.3.4 The Digitizer

To measure the radiation to the required accuracy, it is necessary to digitize the output to 10 bits. A successive approximation digitizer is driven by the

VIP digital A clock pulses. Constraints on VIP slotting cause the ramp to be sampled 5 times a second at exact time differences of 200 ms. The digitizer is also used for measurement of blackbody temperature. It has a built in offset of 15 counts.

6.4 SCR Data Flow and Archiving

6.4.1 Data Flow

Housekeeping and sensory data from the SCR are sampled by the VIP system on the spacecraft and transmitted via the PCM 136.5 MHz beacon, and/or the HDRSS S-band transmitter to the Rosman or Alaska acquisition sites and then relayed to the MDHS at GSFC.

At the MDHS, the housekeeping and sensory data (including SCR) are formatted into the SET. From the SET, a CDC 160 computer extracts and formats the SCR data, which are sent via NASCOM circuit to the SCR experimenter at the Clarendon Laboratories, Oxford, England.

6.4.2 Data Archiving

The SCR experimenter will provide NSSDC with final SCR data tapes for archiving purposes. The data tapes will contain calibrated "declouded" radiances. The format and anticipated availability of the SCR tape sent to NSSDC will be published in the Nimbus 5 Data Catalog.

REFERENCES

1. Abel, P. G., Ellis, P. J., Houghton, J. T., Peckham, G., Rodgers, C. D., Smith, S. D. & Williamson, E. J. (1970). Remote sounding of atmospheric temperature from satellites: II. The selective chopper radiometer for Nimbus-D. Proc. Roy. Soc. Lond. A320, 35-55.

2. Houghton, J. T. & Smith, S. D. (1970). Remote sounding of atmospheric temperature from satellites: I. Introduction. Proc. Roy. Soc. Lond. A320, 23-33.

SECTION 7

THE NIMBUS E MICROWAVE SPECTROMETER (NEMS) EXPERIMENT

by
D. H. Staelin, Research Laboratory of Electronics
Massachusetts Institute of Technology
Cambridge, Massachusetts 02139
and
F. T. Barath, J. C. Blinn III, and E. J. Johnston
Jet Propulsion Laboratory
California Institute of Technology
Pasadena, California 91103

7.1 Introduction

The Nimbus E Microwave Spectrometer (NEMS) Experiment on the Nimbus 5 Satellite is the first step in the application of the microwave spectrum to global sensing of the atmospheric temperature structure. The instrument will also yield unique information about the atmospheric humidity and cloud water content over oceans, and about such parameters as snow cover, ice type, soil moisture, etc. (Reference 1, 2 and 3). The high-angular resolution and mapping capabilities of the 19.4 GHz ESMR (see Section 4) should complement the well-calibrated nadir spectral measurements of NEMS. The capabilities demonstrated at nadir by NEMS will be extended to global maps with 200 km resolution by the Scanning Microwave Spectrometer planned for the Nimbus F Satellite.

7.2 Scientific Objectives

The NEMS views nadir continuously with a resolution of approximately 100 nautical miles, and, at two-second intervals, measures microwave radiation at five wavelengths near the 5 millimeter oxygen resonances and the 1.35 cm water vapor resonance. The center frequencies are 22.235, 31.4, 53.65, 54.9, and 58.8 GHz. Each frequency is affected to a different degree by the terrestrial surface, clouds, precipitation, water vapor, and atmospheric temperature profile. Therefore, by appropriately interpreting a set of simultaneous equations, most of these meteorological parameters can be estimated separately.

The experiment can be considered as composed of two parts: 1) three channels near 5 mm wavelength which probe primarily the atmospheric temperature profile, and 2) two channels near 1 cm wavelength which are sensitive over

oceans to water vapor and liquid water, and which indicate land emissivity and temperature. Although these two parts could operate separately, the performance is superior when they are interpreted simultaneously. That is, the water vapor and liquid water estimates will improve the temperature profile measurements, and vice versa. The intensity of the microwave radiation is customarily expressed in terms of an equivalent brightness temperature T_B (°K), which is the temperature of a blackbody that would radiate the same power.

The brightness temperature perceived by the satellite has two components. The component contributed by the surface is equal to the average over the antenna beamwidth of the product of the surface emissivity ϵ, the surface temperature T_S, and the atmospheric transmissivity $e^{-\tau\nu}$. The other component of brightness temperature originates from the atmosphere. In the case of the oxygen channels, where the atmosphere is nearly opaque, this component can be expressed as the integral of the atmospheric temperature profile, T(h), weighted by the weighting function W(h,ν). The weighting function is weakly dependent upon atmospheric water content, temperature profile, and surface reflectivity. The brightness temperature at nadir is,

$$T_B(\nu) = \epsilon T_S e^{-\tau\nu} + \int_0^\infty T(h)\, W(h,\nu)\, dh. \qquad (1)$$

The experiment functions approximately as follows. The three channels near 5 mm wavelength are situated on the wing of the 5 mm complex of strong O_2 resonances. Each channel corresponds to a different weighting function W(h,ν), similar to those at infrared wavelengths, where h is altitude and ν is frequency. The weighting functions have half widths Δh of 8-12 km and will peak at altitudes near 4, 12, and 18 km, as shown in Figure 7-1. The temperature profile determinations should be nearly unaffected by cirrus clouds or clouds with less than 0.01 gm/cm^2 liquid water.

For more dense clouds, say 0.1 gm/cm^2, the error should normally be less than $\sim$ 2°K over land and 1°K over ocean. Since such clouds rarely fill the 200 km viewing zone, the error normally is much less. After calibration, the accuracy of the radiometer measurements should be approximately 1°K, and the accuracy of the inferred temperature profile should normally be 1-3°K, comparable to clear-weather profiles determined by infrared sensors. The absolute accuracy of the brightness temperature measurements will be reduced below 2°K by means of comparisons with many radiosondes after NEMS is in orbit.

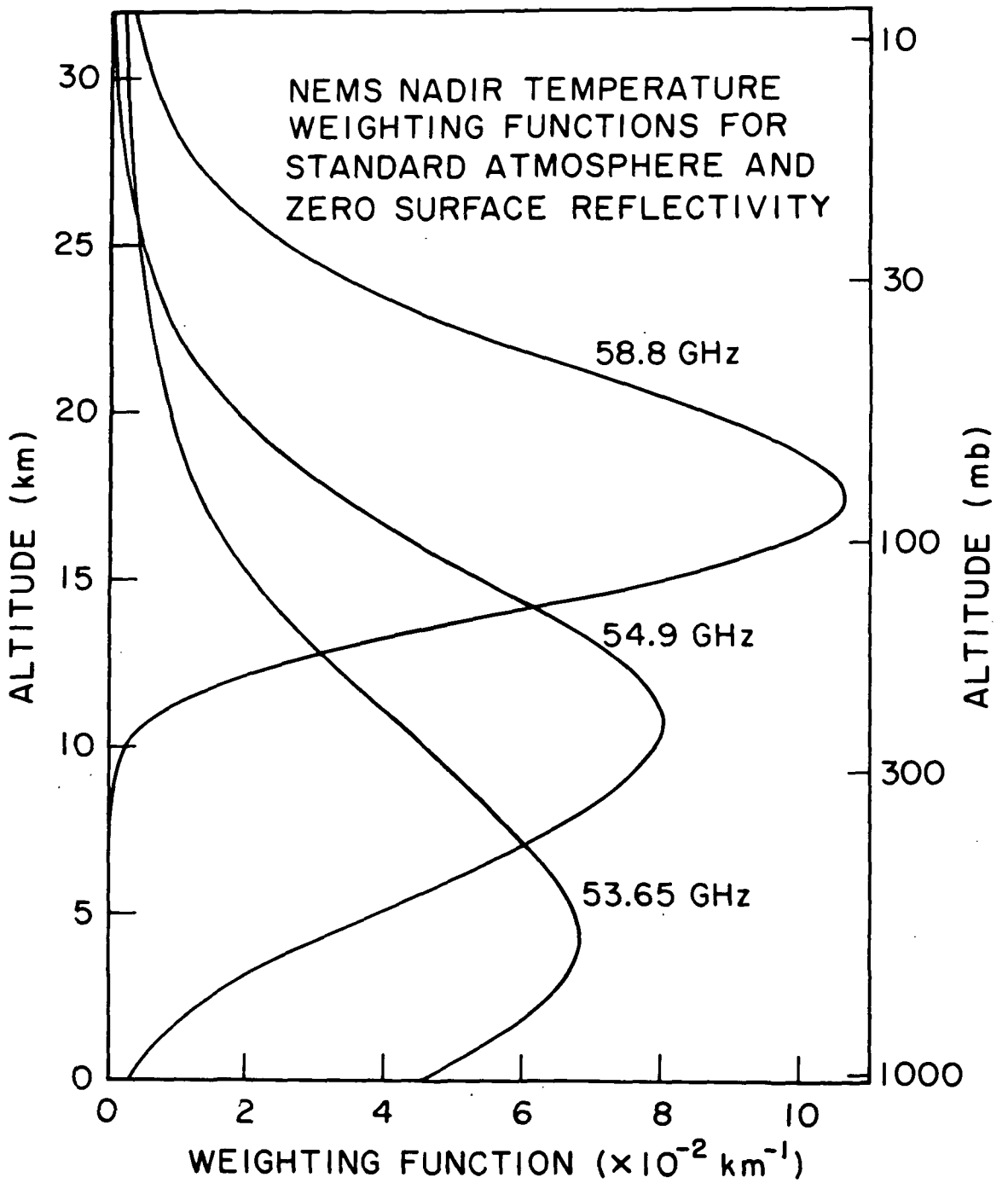

Figure 7-1. NEMS Nadir Temperature Weighting Functions

The two channels near 1 cm wavelength permit water vapor and cloud water content over the ocean to be estimated separately. This is possible because over the ocean the 9 mm channel is approximately twice as sensitive to clouds as the 13 mm channel, but is only 0.4 times as sensitive to water vapor. Water vapor may be estimated with approximately 0.1 gm/cm^2 accuracy, and clouds with approximately 0.04 gm/cm^2 accuracy. Significant sources of error include heavy seas with much foam, and the reflection of sunlight near the equator at noon. Over land, the two water channels will yield an estimate of surface temperature for regions where the surface emissivity has been calibrated by comparison of microwave and direct temperature measurements, and estimates of surface emissivity in those regions where surface temperature is known. Ice types, snow cover, and soil moisture are all properties which may be studied.

7.3. Description of the Instrument

7.3.1 Functional Block Diagram

The instrument is comprised of five functional units as shown in Figure 7-2. The first four of these are flight equipment, the fifth is ground support and calibration equipment. The five units are:

- The H_2O Radiometer Unit
- The O_2 Radiometer Unit
- The Data/Programmer Unit
- The Power Supply Unit
- The Bench Checkout Equipment

The five channels of the instrument are divided between the functional units and are identified as follows:

	Channel	Frequency (GHz)
H_2O Radiometers	R_1	22.235
	R_2	31.40
O_2 Radiometers	R_3	53.65
	R_4	54.90
	R_5	58.80

7.3.1.1 H_2O Radiometer Unit

The H_2O Radiometer Unit consists of channels R_1 (22.235 GHz) and R_2 (31.40 GHz). The two channels are completely independent, sharing no components in common. Each radiometer channel has separate components as

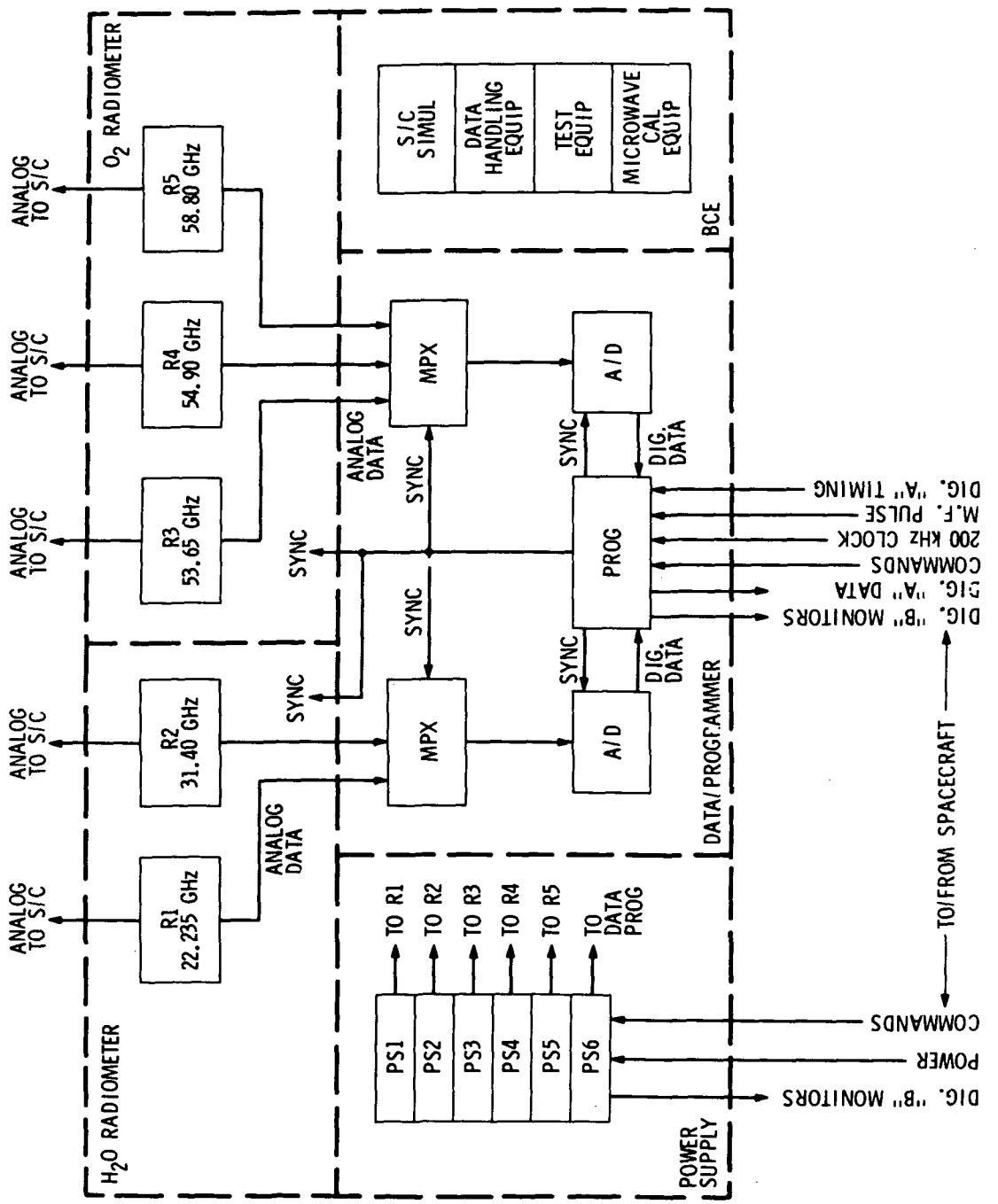

Figure 7-2. NEMS System Block Diagram

indicated by the blocks in Figure 7.2, and each channel is powered by its own separate power supply and ON/OFF commands. Both channels share a space radiator to cool their calibration loads, and the base and reference loads of both channels are physically linked to ensure they are at the same temperature.

7.3.1.2 O_2 Radiometer Unit

The O_2 Radiometer Unit consists of channels R_3 (53.65 GHz), R_4 (54.90 GHz). and R_5 (58.80 GHz), The channels are completely independent, sharing no components in common. A space radiator is shared by all three channels to cool their calibration loads. To ensure that the base and reference loads are at the same temperature, they are physically linked together.

7.3.1.3 Typical Radiometer Channel Operation

Since the five radiometer channels are functionally identical, the following description of one radiometer channel is applicable to any of the other channels. The major differences between the channels are the signal antennae, the local oscillator frequencies, and the reference oscillator frequencies for the Dicke switch drives. These differences are tabulated below:

Channel	Antenna/LO Frequency	Ref. Osc. Frequency
R_1	22.235 GHz	650 Hz
R_2	31.40 GHz	750 Hz
R_3	53.65 GHz	850 Hz
R_4	54.90 GHz	950 Hz
R_5	58.80 GHz	1050 Hz

The radiometer channel consists of the following components:

- Nadir viewing signal antenna
- Space-cooled calibration load
- Instrument ambient temperature base load
- Signal input switch
- Calibration input switch
- Dicke switch
- Reference (Dicke) load
- Mixer, IF Preamp
- Local oscillator
- IF amp, detector, video amplifier
- Video, phase detector, DC amplifier
- Reference oscillator, switch trigger and driver

Each channel is of the conventional Dicke switched, superheterodyne type with a two point calibration system as shown in Figure 7-3. The input network consists of the input and calibration switches which allow selection of one of the following inputs to the instrument:

- Nadir viewing signal antenna
- Space cooled "calibration load"
- Instrument ambient temperature "base load"

Normally, the experiment operates in an automatic sequence where the signal antenna is input to the instrument for 14 VIP major frames, followed by one major frame where the calibration load is input to the instrument, followed by one major frame where the base load is input to the instrument. This 16 VIP major frame sequence is repeated while the experiment is in the normal mode. Alternate modes may be commanded to lock the input switches into any one of the three positions to receive signals from that position only.

A two position Dicke switch follows the input switches, and switches (at the rate of the reference oscillator) between the signal from the input switches and a second instrument ambient temperature load identified as the reference load. The reference load is physically linked to the base load to maintain both loads at the same temperature.

The receiver portion of the channel is a conventional superheterodyne system isolated from the Dicke switch to minimize effects due to impedance modulation. The signal is routed to a low noise balanced mixer with a solid state local oscillator. An IF amplifier, video amplifier, phase detector and DC amplifier complete the radiometer channel, delivering a dc voltage proportional to the difference between the Dicke reference load and the signal presented to the signal input port of the Dicke switch. Since the Rayleigh-Jeans approximation is valid throughout the microwave region, the dc voltage will be a linear function of ΔT. The dc output is routed to the data system where it is processed prior to entering the Digital A data stream as prime data. It is also routed through a buffer circuit and output as an analog signal for "quick look" and prime data backup capability.

The instrument parameters are summarized in Table 7-1.

7.3.1.4 Data and Programmer Unit

This functional unit is the experiment data system which consists of the programmer and the data processing assemblies.

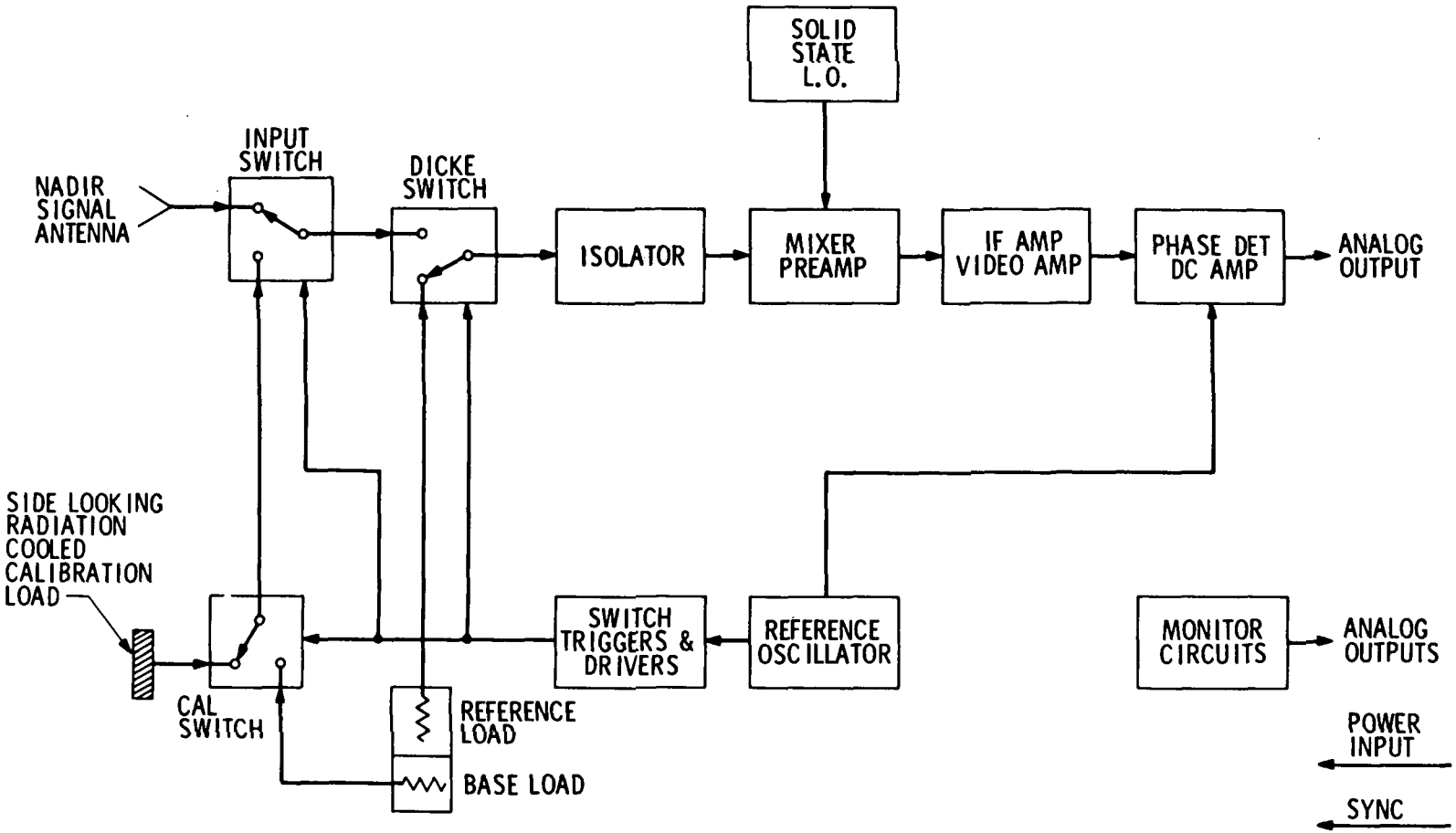

Figure 7-3. NEMS Channel Block Diagram

Table 7-1
NEMS Characteristics as of June, 1972

	SPEC	R 1	R 2	R 3	R 4	R 5
Frequency (MHz) (to be updated)	±5	22,235	31,400	53,650	54,900	58,800
RF Bandwidth (MHz)	220	250	250	250	250	250
Integration Time (sec)	> 1.9	1.9962	1.9962	1.9962	1.9962	1.9962
ΔT_{rms} (°K) (outside antenna)	< 1.0/1.5	0.24	0.23	0.29	0.29	0.24
Dynamic Range, Linearity (50-400°K) %	100-325°K < 0.1	< 0.05	< 0.05	< 0.05	< 0.05	< 0.05
Absolute Accuracy ($°K_{rms}$) Long Term	< 2.0	1 E	1 E	2 E	1 E	2 E
IF Frequency Range (MHz)	10-110	10-110	10-110	10-110	10-110	10-110
Antenna Beamwidth (deg)	10	10	10	10	10	10
Antenna Beam Efficiency, within 14° (%)	> 90	95	94	94	93	95
Cal Temperature Below Ambient (°C)	> 80/60	81-92	81-92	73-87	73-87	73-87

E = Estimated

The programmer synchronizes all periodic functions within the experiment. Specifically, it provides timing and control signals for:

- experiment sequencing
- baseload, antenna and calibration load switching
- integrate-hold-dump commands
- analog multiplexing
- power supply sync
- A/D conversion
- data formatting

These signals are derived from (and synchronous to) the spacecraft 200 Hz clock and VIP A_1, B_1 and C_1 signals, insuring the proper relationship between the NEMS readout and the spacecraft telemetry system.

The remainder of the data system consists of the integrate and dump, multiplexing, and A/D conversion functions. The primary radiometric data are integrated, then sequentially sampled by two primary multiplexers. The engineering and housekeeping data are sampled by submultiplexers and then routed to the two primary multiplexers. Two A/D converters are utilized, one in the O_2 module and one in the H_2O module, to minimize spacecraft noise by digitizing in the individual modules. One of the primary multiplexers accepts the radiometric data and monitor signals for channels R_1 and R_2 and commutates them in sequence onto the A/D converter in the H_2O module. The other primary multiplexer accepts the radiometric data and monitor signals for channels R_3, R_4, R_5 and commutates them in sequence onto the A/D converter in the O_2 module. The commutated digitized data are placed in a shift register and read out by the spacecraft telemetry system in the format described in 7.3.2. The sequencing and synchronizing signals for the multiplexers and the A/D converters are provided by the programmer which interfaces with the spacecraft clock and the VIP timing signals.

7.3.1.5 Power Supply Unit

The power supply unit consists of six independent power supplies, each providing several voltages to channels R_1 through R_5 and the Data Unit. The power supplies carry separate commons for maximum dc isolation between the channels.

The unit also contains the ON/OFF command relays which control the prime spacecraft power to the individual power supplies.

7.3.2 NEMS Data Format on VIP

The NEMS experiment data are monitored via a 5 sample per second Digital A channel. Each sample consists of a 10-bit digital word with the most significant bit read out first. The words are read out to the VIP subsystem 80 times per major frame and appear in column 73 of the VIP matrix. The full cycle of events for data readout is completed in one VIP major frame (16 seconds for 80 data words) and encompasses eight measurements of each of the five radiometric channel outputs.

The data format is as follows: The first 5 data words in the set of 80, i.e. VIP rows 00-04 (SM1-SM5) represent various submultiplexed engineering and housekeeping functions. The following 5 data words, in VIP rows 05-09, represent radiometric temperatures corresponding to the five radiometer channels read out sequentially, Channel 1 to Channel 5. This pattern (5 submultiplex channels followed by 5 radiometer channels) continues for the 16-second VIP major frame. Thus, the complete major frame contains 40 different engineering/housekeeping words and 40 radiometer channel data words. The net result is that the five radiometer channels are each read out once every 2 seconds, and the 40 separate engineering/housekeeping functions are read out once every 16 seconds. The engineering/housekeeping functions are listed in Table 7-2.

The data output is straight binary. The binary output for each radiometer channel is a function of the antenna temperature and is referenced to the other temperature inputs in the engineering/housekeeping data.

7.3.2.1 Submultiplex Data

A brief description of the submultiplex (SM) functions listed in Table 7-2 is provided below.

7.3.2.1.1 1777 Index (SM 1)

The 10 bits of the Index word are all digital ones. The word (1777 octal) identifies the beginning of a VIP major frame and is used as a sync word during ground data processing.

7.3.2.1.2 Instrument State (SM 2)

Word SM 2 is a digital representation of the instrument state at the beginning of a VIP major frame. It consists of 7 counter bits and 2 operating mode bits.

Table 7-2
NEMS Submultiplex Data Assignments

VIP Row	SM Number	Function Name	Purpose	Nominal Accuracy
00	1	1777 (Base 8) Index	Sync	--
01	2	Instrument State	Data	--
02	3	Ch. 1 Signal Input Switch Temp	Data	0.2°K
03	4	O_2 Signal Antenna Temp #1	Data	0.2°K
04	5	Ch. 2 Mixer-Preamp Monitor -	Housekeeping	1%
10	6	O_2 Cal Radiator Temp Fine	Data	0.1°K
11	7	Ch. 1 Mixer-Preamp Monitor +	Housekeeping	1%
12	8	Ch. 1 Cal Input Switch Temp	Data	0.2°K
13	9	O_2 Cal Radiator Temp Coarse	Data	0.2°K
14	10	Ch. 3 Mixer-Preamp Monitor +	Housekeeping	1%
20	11	O_2 Ref/Base Load Temp Fine #1	Data	0.1°K
21	12	Ch. 1 Mixer-Preamp Monitor -	Housekeeping	1%
22	13	Ch. 2 Signal Input Switch Temp	Data	0.2°K
23	14	O_2 Signal Antenna Temp #2	Data	0.2°K
24	15	Ch. 3 Mixer-Preamp Monitor -	Housekeeping	1%
30	16	O_2 Ref/Base Load Temp Fine #2	Data	0.1°K
31	17	Ch. 2 Mixer-Preamp Monitor +	Housekeeping	1%
32	18	Ch. 2 Cal Input Switch Temp	Data	0.2°K
33	19	Ch. 4 Cal Input Switch Temp	Data	0.2°K
34	20	Ch. 4 Mixer-Preamp Monitor +	Housekeeping	1%
40	21	Instrument Serial Number	Identification	--
41	22	H_2O Signal Antenna Temp #1	Data	0.2°K
42	23	Ch. 3 Signal Input Switch Temp	Data	0.2°K
43	24	Ch. 4 Signal Input Switch Temp	Data	0.2°K
44	25	Ch. 4 Mixer-Preamp Monitor -	Housekeeping	1%
50	26	H_2O Cal Radiator Temp Fine	Data	0.1°K
51	27	H_2O Cal Radiator Temp Coarse	Data	0.2°K
52	28	Ch. 3 Cal Input Switch Temp	Data	0.2°K
53	29	Ch. 5 Cal Input Switch Temp	Data	0.2°K
54	30	Ch. 5 Mixer-Preamp Monitor +	Housekeeping	1%
60	31	H_2O Ref/Base Load Temp Fine #1	Data	0.1°K
61	32	H_2O Signal Antenna Temp #2	Data	0.2°K
62	33	P/S Module Temp #1	Housekeeping	0.2°K
63	34	Ch. 5 Signal Input Switch Temp	Data	0.2°K
64	35	Ch. 5 Mixer-Preamp Monitor -	Housekeeping	1%
70	36	H_2O Ref/Base Load Temp Fine #2	Data	0.1°K
71	37	H_2O Ref/Base Load Temp Coarse	Data	0.2°K
72	38	P/S Module Temp #2	Housekeeping	0.2°K
73	39	O_2 Ref/Base Load Temp Coarse	Data	0.2°K
74	40	Data System Voltage	Housekeeping	1%

The SM 2 word format is indicated below where bit B10 is the most significant bit. Bit B10 is always a digital zero.

B10	B9	B8	B7	B6	B5	B4	B3	B2	B1

Digital "0" — Operating Mode — Major Frame Sequence Counter

The bits are decoded in the following manner, where bit B10 is ignored since it is always zero.

Bits B9 and B8 indicate the experiment operating mode as follows:

B9	B8	Operating Mode
0	0	Normal
0	1	Antenna
1	0	Calibration Load
1	1	Base Load

The sequence counter is synchronized upon receipt of the first VIP major frame pulse after power turn-on, but is not set to zero. Thereafter, it increments by one for every major frame pulse until bits B7 through B1 are all ones. The following major frame pulse will then set bits B7 through B1 to zero and the incrementing by one for every major frame pulse begins again. Thus, the sequence counter will initially indicate from a random number 1111111 binary (177 octal) and then repeatedly from 0000000 to 1111111 binary (000 to 177 octal) sequentially after power turn-on. This output is used to determine in which VIP frames the calibration load and base load data will appear in the channel outputs when the instrument is in the normal mode. In the normal mode, the calibration load data will appear at 16 major frame intervals, counting from the 15th major frame, and the baseload data will appear at 16 major frame intervals counting from the 16th major frame.

The sequence counter has no control over operating mode. Whenever the instrument is returned to the normal (automatic calibration) mode from any of its alternate modes, the calibration load and base load data will appear in the frames indicated by the sequence counter as if the instrument had always been in the normal mode.

7.3.2.1.3 Ferrite Switch Temperatures

Ch. 1 Signal Input Switch Temperature (SM 3)
Ch. 1 Calibration Input Switch Temperature (SM 8)
Ch. 2 Signal Input Switch Temperature (SM 13)
Ch. 2 Calibration Input Switch Temperature (SM 18)
Ch. 3 Signal Input Switch Temperature (SM 23)
Ch. 3 Calibration Input Switch Temperature (SM 28)
Ch. 4 Signal Input Switch Temperature (SM 24)
Ch. 4 Calibration Input Switch Temperature (SM 19)
Ch. 5 Signal Input Switch Temperature (SM 34)
Ch. 5 Calibration Input Switch Temperature (SM 29)

These words indicate the temperatures of the ferrite devices which select antenna, calibration load, or base load inputs to the respective radiometer channels. The temperatures are to be computed on the ground.

7.3.2.1.4 Antenna Temperatures

O_2 Signal Antenna Temperature #1 (SM 4)
O_2 Signal Antenna Temperature #2 (SM 14)
H_2O Signal Antenna Temperature #1 (SM 22)
H_2O Signal Antenna Temperature #2 (SM 32)

These words represent the outputs from four platinum temperature sensors selectively placed on the radiometer modules to indicate the temperatures in the vicinity of the two antennas of the H_2O module and the three antennas of the O_2 module.

7.3.2.1.5 Radiator Temperatures

O_2 Calibration Radiator Temperature Fine (SM 6)
O_2 Calibration Radiator Temperature Coarse (SM 9)
H_2O Calibration Radiator Temperature Fine (SM 26)
H_2O Calibration Radiator Temperature Coarse (SM 27)

7.3.2.1.6 Reference/Base Load Temperatures

O_2 Ref/Base Load Temperature Fine #1 (SM 11)
O_2 Ref/Base Load Temperature Fine #2 (SM 16)
O_2 Ref/Base Load Temperature Coarse (SM 39)
H_2O Ref/Base Load Temperature Fine #1 (SM 31)
H_2O Ref/Base Load Temperature Fine #2 (SM 36)
H_2O Ref/Base Load Temperature Coarse (SM 37)

The reference load for every channel is physically linked to the baseload for that channel. In addition, the reference and base loads for Channels 3, 4 and 5 in the O_2 module are thermally tied to one another. The words above indicate the outputs from sensors selectively placed (3 in each module) to indicate the temperatures of the ref/base loads. Since these temperatures are critical in data evaluation, two "fine" monitors are provided for redundancy.

7.3.2.1.7 Power Supply Temperatures

Power Supply Module Temperature #1 (SM 33)
Power Supply Module Temperature #2 (SM 38)

These words represent the temperature at two locations in the power supply module.

7.3.2.1.8 Instrument Serial Number (SM 21)

Word SM 21 is a digital readout of the instrument serial number. The NEMS instruments will have the following serial numbers:

Model	Serial Number
Engineering	1
Prototype	2
Flight	3

The 10 bits of Word SM 21 are decoded as follows:

	B10	B9	B8	B7	B6	B5	B4	B3	B2	B1
Ser. No. 1	0	0	1	X	X	X	X	X	X	X
Ser. No. 2	0	1	X	X	X	X	X	X	X	X
Ser. No. 3	1	X	X	X	X	X	X	X	X	X

7.3.2.1.9 Mixer-Preamp Monitors

Ch. 1 Mixer-Preamp Monitor + (SM 7)
Ch. 1 Mixer-Preamp Monitor - (SM 12)
Ch. 2 Mixer-Preamp Monitor + (SM 17)
Ch. 2 Mixer-Preamp Monitor - (SM 5)
Ch. 3 Mixer-Preamp Monitor + (SM 10)
Ch. 3 Mixer-Preamp Monitor - (SM 15)
Ch. 4 Mixer-Preamp Monitor + (SM 20)
Ch. 4 Mixer-Preamp Monitor - (SM 25)

Ch. 5 Mixer-Preamp Monitor + (SM 30)
Ch. 5 Mixer-Preamp Monitor - (SM 35)

These words represent the Schottky barrier mixer diode currents. The currents are read as a voltage drop across a 1000 (O_2 channels) or 500 ohm (H_2O channels) resistor, amplified 5 times and presented to the multiplexer input as a voltage between 1 and 6 volts.

7.3.2.1.10 Data System Voltage (SM 40)

This word monitors the status of +5 volt output from power supply number 6 which is common to most of the data system functional units.

7.4 Data Processing and Archiving

All NEMS signals are recorded by the VIP system on a HDRSS tape recorder for playback at a data acquisition station or, alternately, transmitted real-time with the spacecraft beacon transmitter. At GSFC, a SET is generated containing data from most of the experiments. This tape will be processed at MIT to yield the NEMS Output Tape (NEMSOT), which will contain basic spacecraft data, the raw NEMS data, inferred NEMS antenna temperatures, inferred brightness temperatures, selected data from other experiments, NEMS atmospheric and surface determinations, and NOAA atmospheric verification data. The NEMSOT will be archived and available at the NSSDC as described in Section 1.7 of this report. The format for NEMSOT will be published in a Nimbus 5 Data Catalog.

REFERENCES AND BIBLIOGRAPHY

1. D. H. Staelin, "Passive Remote Sensing at Microwave Wavelengths," Proc. I.E.E.E., 57, pp. 427-439, 1969.

2. P. W. Rosenkranz, F. T. Barath, J. C. Blinn III, E. J. Johnston, W. B. Lenoir, D. H. Staelin, and J. W. Waters, "Microwave Radiometric Measurements of Atmospheric Temperature and Water from an Aircraft," J. Geophys. Res., in press, 1972.

3. A. Ye. Basharinov, A. S. Gurvich, and S. T. Yegorov, "Determination of Geophysical Parameters from Measurements of Thermal Microwave Radiation by the Satellite 'Cosmos-243'," Doklady AN SSSR, 188, 6 pp. 1273-1276, 1969.

SECTION 8

THE NIMBUS 5 DATA CATALOG

Nimbus 5 Data Catalogs will be published periodically to provide a relatively current source of information required to obtain Nimbus 5 data. Each Catalog will be divided into five main sections described below:

- Summary of Operations
  Section 1 will contain significant highlights of the satellite operation during the period of the catalog including any required post-launch changes in experiment description and archival tape formats as contained in preceding sections of this Guide. Performance of the various sensory systems and the spacecraft will be described, particularly when significant deviations from normal operations have been experienced.

- Orbital Elements and Daily Sensors On-Off Table
  Section 2 will give the Nimbus 5 satellite orbital elements valid for the catalog period. This section will also have a daily Sensors On-Off Table recording the times the experiments (except SCMR) were on for the period of the catalog. The table will include ascending and descending node times and longitudes. To assist the user in determining the sensor coverage on the earth each volume will include a Subsatellite Tracks Vellum Overlay with its accompanying World Map. The subsatellite Tracks Overlay contains 14 correctly spaced tracks with the time annotations ending at the approximate day/night transitions.

- THIR Montages
  This section pictorially documents the data from the Temperature Humidity Infrared Radiometer subsystem. The montages represent the 11.5 μm channel and the 6.7 μm channel data obtained for each day (UT) and are arranged in chronological order in a world montage format. Key latitudes can be read from the superimposed grids. Grid points are identified where each swath crosses 60°N, 30°N, EQUATOR, 30°S and 60°S.

  THIR transparent grid overlays (Location Guides), one for daytime montages and another for nighttime montages, will be provided as inserts to each Nimbus Catalog for general orientation with the latitude and longitude of the data presented. A THIR Time Scale, to be used for measuring time on the data strips in the daytime or nighttime montages, will be included adjacent to each montage.

- ESMR Pictorial Data
  This section will contain selected pictorial examples of ESMR data. Each picture will contain sufficient geographic and time information to locate and reference the data.

  A list of all available ESMR pictures generated in a pseudo-color mode will be included in this section.

  Complete ESMR coverage documentation will be listed in Section 2 by the Sensor On-Off Table.

- Summary of Revisions and Changes to the User's Guide and Sensor Anomalies will be presented in this section with the information cumulatively carried forward from catalog to catalog.

APPENDIX A

ABBREVIATIONS

A/D	Analog to Digital
AC	Alternating Current
AGC	Automatic Gain Control
ARA	Allied Research Associates, Inc.
ATS	Applications Technology Satellite
BCD	Binary Coded Decimal
bps	Bits per second
bpi	Bits per inch
CBTT	Calibrated Brightness Temperature Tapes
dc	Direct Current
DEOF	Double End of File
EIS	Electronic Image System
EOF	End of File
ERTS	Earth Resources Technology Satellite
ESMR	Electrically Scanning Microwave Radiometer
FET	Field Effect Transistor
FM	Frequency Modulation
FOV	Field of View
GARP	Global Atmospheric Research Program
GHz	Gigahertz
GMT	Greenwich Mean Time (UT)
GSFC	Goddard Space Flight Center
HDRSS	High Data Rate Storage System
Hz	Hertz (cycles per second)
IFOV	Instantaneous Field of View
IR	Infrared
ITPR	Infrared Temperature Profile Radiometer
kbs	Kilobits per second
kHz	Kilohertz
LMES	Laboratory for Meteorology and Earth Sciences
MDHS	Meteorological Data Handling System
MHz	Megahertz
MIT	Massachusetts Institute of Technology
mr	Milliradian
ms	Millisecond
μm	Micrometer
MUX	Multiplexer
NADUC	Nimbus/ATS Data Utilization Center
NASA	National Aeronautics and Space Administration

NASCOM	NASA Communications
NCC	National Climatic Center
NEMS	Nimbus E Microwave Spectrometer
NEMSOT	NEMS Output Tape
NESS	National Environmental Satellite Service
n.m.	Nautical Miles
NMC	National Meteorological Center
NMRT	Nimbus Meteorological Radiation Tape
NOAA	National Oceanic and Atmospheric Administration
NSSDC	National Space Science Data Center
PCM	Pulse Code Modulation
PIP	Position Pulse
rms	Root Mean Square
SCMR	Surface Composition Mapping Radiometer
SCR	Selective Chopper Radiometer
SET	Stacked Experiment Tape
SIRS	Satellite Infrared Radiometer
SSP	Subsatellite Point
STDN	Spaceflight Tracking and Data Network
TGS	Trigylcine Sulphate
THIR	Temperature Humidity Infrared Radiometer
UT	Universal Time (GMT)
VCO	Voltage Controlled Oscillator
VDC	Volts Direct Current
VIP	Versatile Information Processor

* U.S. GOVERNMENT PRINTING OFFICE: 1972—735-963/259